POLYURETHANE ADHESIVE SYNTHESIS USING LINGIN-BASED BIO-POLYOLS

eman ta zabal zazu

Universidad del País Vasco

Euskal Herriko Unibertsitatea

Fabio Hernández Ramos

January 2023

“Hello there”

Obi-Wan Kenobi

Polyurethane adhesive synthesis using lignin-based bio-polyols

A dissertation presented by

Fabio Hernández Ramos

In fulfilment of the requirements for the degree

Doctor of Philosophy by the University of the Basque Country

in the program Renewable Materials Engineering

Under the supervision of

Dr. Jalel Labidi & Dr. Xabier Erdocia

Chemical and Environmental Engineering Department

DONOSTIA – SAN SEBASTIÁN

2023

“No, try not. Do or do not. There is no try”

Master Yoda

Agradecimientos

Sinceramente no se ni por dónde empezar. Tengo que admitir que esto nunca entró dentro de lo que yo me imaginaba que sería mi futuro, pero he aquí que a mis 35 encontré mi vocación. No porque no me gustara, sino porque la falta de seguridad en mí mismo no me dejaba creer que fuera capaz de hacerlo. Sin embargo, lo he hecho, lo he disfrutado y lo he sufrido, lo he odiado y lo he amado y sobre todo me lo he trabajado, día a día, metiendo horas, leyendo "peipers", ensuciando la bata, rompiendo algún que otro vidrio y equipo, y pasando un sinfín de horas en la fregadera. Sin embargo, considero que, en esta aventura, he tenido, igual que tuvo Frodo Bolsón, a gente maravillosa apoyándome y azuzándome para que todo llegará a buen puerto. Por ello, no puedo más que darles mis más sinceros agradecimientos.

En primer lugar, quiero agradecer a mi director el Dr. Jalel Labidi por darme la oportunidad de realizar esta tesis en la que tanto he aprendido, no solo sobre lignina y los poliuretanos, si no también sobre mí mismo. Al Dr. Xabier Erdocia, por ser un apoyo incondicional durante este lustro, porque sé que lo ha sufrido casi igual que yo y porque ha aprendido conmigo, que al final todo sale bien, por ello, mi más profundo agradecimiento y respeto. Hay otra persona a la que le debo estar aquí, por toda la ayuda que me ha brindado desde mi época de estudiante hasta el día de hoy, siempre con una sonrisa y una palabra amable, porque así es la Dra. María González Alriols, por ello gracias. Quisiera agradecer también al Dr. Bruno Miguel Morais por ayudarme y guiarme durante mi estancia en el Instituto Politécnico de Viseu.

A toda mi cuadrilla, en especial a Imanol, Mikel, Luis y el Dr. Iñigo Calvo, es decir, a los ¨Brothers of Metal", por todas esas noches de Metal.

A Aintzane de la Clínica Osasun Sport Clinic, por las mañanas de entreno y las risas que nos echamos, te deseo lo mejor, porque sin duda lo mereces. A

Sergio y Lucía, por no daros por vencidos. Algún día conseguiré seguir todos y cada uno de vuestros sabios consejos.

A todos mis compañeros del grupo BioRP, tanto nuevos como antiguos, por la ayuda y apoyo que en algún momento hayáis podido ofrecerme. Pero en especial a aquellas que habéis compartido estrechamente conmigo este largo camino, ya no sois solo compañeras de trabajo, os habéis convertido en grandes amigas a las que puedo recurrir en busca de consejo, consuelo y apoyo, y porque no decirlo, en busca de fiesta, mojitos y tontería, mucha tontería. Gracias a las Dras. Rut, Leyre (mi esposa de congresos) Izaskun y Patricia y por supuesto también a Farida. Y no, no me olvido de ti Dra. Amaia, que, aunque tú tampoco me caíste en gracia en un primer momento, puedo decir que te has convertido en una de mis personas favoritas.

Gracias a Julen Vadillo por tus sabios consejos, a Izaskun, Tamara, Kizkitza, Joseba, Iratxe, Mireia y Nerea por vuestro tiempo y ayuda. Y a Loli, que, aunque nunca la encuentro siempre está ahí.

A mis padres, por hacerlo lo mejor que han sabido incluso en mis etapas más sombrías. A mis hermanos Ingrid y Christian, por lo mismo. A mis suegros Marisa y Manolo, y a Marce, Pedro, Jessica, Hugo, David y Dosi por acogerme en la familia.

Finalmente, a ***Cris***, mi ***AMORE***. Nos conocimos de pequeños, jugando en el barrio y la vida separo nuestros caminos por un tiempo, aunque solo para volver a encontrarnos cuando los dos más lo necesitábamos. Juntos hemos decidido recorrer un camino, el más importante, el de la vida y estoy seguro de que sabremos sortear los baches que se nos pongan por delante, como estos últimos meses locos. Gracias por aguantarme durante esta etapa.

Y por supuesto, a ***Luka***, por ser mi sol y mis estrellas.

Nomenclature

Acid number	A_n
Activation Energy	E_a
(3-aminopropyl)trimethoxysilane	APTMS
Attenuated Total Reflection-Fourier Transformed Infrared	ATR-FTIR
Automated bonding evaluation system	ABES
Average molecular weight	M_W
Bio-polyols formulated with CG for elastic PUs from *Eucalyptus globulus*	$EOPE_{CG}$
Bio-polyols formulated with CG for elastic PUs from *Pinus radiata*	$POPE_{CG}$
Bio-polyols formulated with CG for rigid PUs from *Eucalyptus globulus*	$EOPR_{CG}$
Bio-polyols formulated with CG for rigid PUs from *Pinus radiata*	$POPR_{CG}$
Black Liquor	BL
Box-Benkhen Design	BBD
Carbon	C
Crude Glycerol	CG
Derivative Thermogravimetric	DTG
Dimethyl Carbonate	DMC
Equivalent Weight	EW
Eucalyptus globulus organosolv black liquor	EOBL
Eucalyptus globulus organosolv lignin	EOL
Eucalyptus globulus organosolv lignin after ultrasound treatment	EOUL
Eucalyptus globulus organosolv Polyol for Elastic PU	EOPE
Eucalyptus globulus organosolv Polyol for Rigid PU	EOPR
Eucalyptus globulus organosolv Polyol for Elastic PU	EOPE
Eucalyptus globulus organosolv Polyol for Rigid PU	EOPR
Eucalyptus Organosolv Polyol	EOP
Fatty Acids Methyl Esters	FAMEs

Free Fatty Acids	FFA
Functionality	*f*
Gas chromatography-Mass spectrometry	CG-MS
Gel Permeation Cromatography	GPC
Hexamethylenediamine	HDMA
Hard Segment	HS
Hard Segment weight fraction	HS_W
Hydroxyl number	I_{OH}
Isocyanate group	NCO
Ixocyanate to OH ratio	NCO:OH
Kissingr-Akahira-Sunose	KAS
Lignin-based polyurethane adhesive	LPA
Lignin-based NIPU adhesive	LNA
LNA with the silane coupling agent	CLNA
Maximum mass fraction of the rigid segment mixed in the soft segment	W_H
4,4'-Methylene diphenyl diisocyanate	MDI
Non-isocyanate polyurethane	NIPU
Number Average Molecular Weight	M_n
Ozawa-Flyn-Wall	OFW
Pine organosolv Polyol	POP
Pinus radiata organosolv black liquor	POBL
Pinus radiata organosolv lignin	POL
Pinus radiata organosolv Polyol for Elastic PU	POPE
Pinus radiata organosolv Polyol for Rigid PU	POPR
Pinus radiata organosolv lignin after ultrasound treatment	POUL
Polydispersity Index	PDI
Polyethylene Glycol	PEG
Polyethylene glycol/Glycerol weight ratio	PEG/Gly
Polyurethane	PU

Preexponential factor	A
Response Surface Methodology	RSM
Soft Segment	SS
Soft segment weight fraction	SS_W
Theoretical Hard Segment	HS_t
Thermogravimetric Analysis	TGA
Weight fraction of H-bonded urethane groups	X_{HB}
Weight fraction of the mixed phase	MP_W

Table of Contents

1st PART INTRODUCTION

1.1. Once upon a time 1

1.2. Humankind and Climate Change 3

1.3. Polyurethanes 6

1.3.1. Polyols 10

1.3.2. Isocyanates 10

1.3.3. Types of polyurethane 11

1.3.3.1. PU adhesives 11

1.3.4. Greener alternatives for PU synthesis 12

1.4. Biorefineries for a bio-based future 13

1.4.1. Biorefineries and biomass 14

1.4.1.1. Biorefinery 11

1.4.2.1. Biomass 11

1.5. Lignocelullosic biomass 16

1.5.1. Cellulose 17

1.5.2. Hemicellulose 17

1.5.3. Lignin 18

1.6. Lignin based polyurethanes 21

1.6.1. Lignin based polyols 21

1.6.2. Lignin based non-isocyanate polyurethanes 24

1.7. Lignin based polyurethane adhesives 25

1.8. Objectives of the thesis 27

1.9. References 30

2nd PART METHODOLOGY

2.1. Raw materials and chemicals 51

2.2. Delignification of raw material and sonication process of black liquors 52

2.3. Synthesis procedure of bio-polyols 53

2.3.1. Scale-up of the liquefaction reaction 55

2.4. Transesterification of vegetable oil to obtain crude glycerol 55

2.5. Synthesis procedure of lignin based polyurethane adhesive 55

2.6. Synthesis procedure of lignin based non-isocyanate polyurethane adhesive 56

2.7. Characterisation methods 57

3rd PART RESULTS AND DISCUSSION

OBTAINING AND SYNTHESIS OF BIO-POLYOLS

Publication I

Renewable bio-polyols from residual aqueous phase resulting after lignin precipitation

ABSTRACT 67

1. MATERIALS AND METHODS 67

1.1. Materials 67

1.2. Delignification of raw materials and sonication treatments of the black liquors 68

1.3. Black liquor characterisation 68

1.4. Bio-polyol obtaining 68

1.5. Bio-polyol characterisation 68

2. RESULTS AND DISCUSSION 68

2.1. Black liquors 68

2.2. Bio-polyol 69

3. CONCLUSIONS 80

REFERENCES 81

Publication II

Organosolv lignin-based bio-polyols for polyurethane production: Process optimisation through response surface methodology

ABSTRACT 87

1. MATERIALS AND METHODS 88

1.1. Materials 88

1.2. Lignin obtaining procedure 88

1.3. Lignin characterisation 88

1.4. Experimental design of microwave assisted lignin liquefaction 89

2. RESULTS AND DISCUSSION 91

2.1. Lignin characterisation 91

2.2. Optimisation of the conditions for obtaining suitable bio-polyols for PU applications 93

3. CONCLUSIONS 112

REFERENCES 113

Publication III

Valorisation of crude glycerol in the production of liquefied lignin bio-polyols for polyurethane formulation

ABSTRACT 119

1. MATERIALS AND METHODS 120

1.1. Materials 120

1.2. Lignin obtaining procedure 120

1.3. Transesterification of vegetable oil to obtain crude glycerol 120

1.4. Synthesis of bio-polyols through microwave assisted liquefaction 120

1.5. Characterisation of crude glycerol 121

1.6. Characterisation of the obtained bio-polyols 121

2. RESULTS AND DISCUSSION 122

2.1. Crude glycerol characterisation 122

2.2. Characterisation of the bio-polyols 124

2.3. Effect of crude glycerol in bio-polyols parameters 133

3. CONCLUSIONS 138

REFERENCES 139

SYNTHESIS OF POLYURETHANE AND NON-ISOCYANATE POLYURETHANE WOOD ADHESIVES

Publication IV

Synthesis, characterisation, and thermal degradation kinetic of lignin-based polyurethane wood adhesives

ABSTRACT 149

1. MATERIALS AND METHODS 150

1.1. Materials 150

1.2. Lignin obtaining procedure 150

1.3. Crude glycerol obtaining procedure 150

1.4. Synthesis of bio-polyols through microwave assisted liquefaction 150

1.5. Synthesis of lignin-based polyurethane adhesives 151

1.6. Characterisation of the obtained bio-polyols 151

1.7. Characterisation of lignin-based polyurethane adhesives 152

2. RESULTS AND DISCUSSION 152

2.1. Bio-polyols characterisation 152

2.2. Lignin-based polyurethane adhesive characterisation 153

2.3. Characterisation of LPA employing bio-polyols formulated with CG 162

3. CONCLUSIONS 173

REFERENCES 174

Lignin-based non isocyanate polyurethane adhesives. Synthesis and determination of adhesion properties and thermal degradation kinetic

ABSTRACT 181

1. MATERIALS AND METHODS 182

1.1. Materials 182

1.2. Lignin obtaining procedure 182

1.3. Crude glycerol obtaining procedure 182

1.4. Lignin based bio-polyols 182

1.5. Synthesis of lignin based non-isocyanate polyurethane adhesives 183

1.6. Characterisation of the obtained non-isocyanate polyurethane adhesives 183

2. RESULTS AND DISCUSSION 184

2.1. Characterisation of the synthesised lignin based non-isocyanate polyurethane adhesives 184

2.2. Characterisation of the synthesised lignin based non-isocyanate polyurethane adhesives with silane coupling agent 196

3. CONCLUSIONS 207

REFERENCES 208

4th PART CONCLUSIONS AND FUTURE WORK

CONCLUSIONS 217

FUTURE WORKS 219

LIST OF FIGURES & TABLES 240

APPENDIX 237

APPENDIX I. Procedure for black liquor characterisation 239

I. pH determination 239

II. Density determination 239

III. Total Dissolved Solids (TDS) 239

IV. Inorganic and Organic Matter (IM, OM) 240

***V.* Lignin content** 240

APPENDIX II. Procedure for bio-polyols and polyurethane characterisation 242

I. Chemical composition 242

II. Chemical structure 242

III. Molecular weight distribution 244

IV. Elemental analysis 244

V. Hydroxyl number (I_{OH}) and acid number (A_n) determination 245

VI. Rheological behaviour 246

VII. Thermogravimetric analysis (TGA) 247

VIII. Thermal degradation kinetic and lifetime estimation 248

IX. Adhesion test of PUs and NIPUs with ABES 249

REFERENCES 250

APPENDIX III. Publications & Conferences 251

Contributions included in this thesis 251

Contributions not included in this thesis 253

Contributions to conferences 256

1st PART

INTRODUCTION

“You can’t stop change any more than

you can stop the suns from setting”

Shmi Skywaker

1.1. Once upon a time

The Solar System, located in the Orion Arm of the Milky Way, was formed about 4.57 billion years ago probably in a star cluster, after the collapse of a dense cloud of interstellar gas and dust into a solar nebula [1]. Due to gravity, the centre of the nebula gradually accumulated more and more material until the pressure was able to fuse hydrogen atoms into helium, giving rise to the birth of a star, called the Sun. After the Sun's birth, the remaining material clumped together to form first the gaseous planets (Jupiter, Saturn, Uranus, and Neptune), then the rocky planets (Mercury, Venus, The Earth and Mars) and dwarf planets (Pluto, Ceres, Haumea, Makemake, Eris, Sedna and Phattie). Finally, when the nebula dissipated, the solar system was formed by its central star (the Sun), planets and their moons, dwarf planets and debris. The latter are located mainly in the asteroid belt, the Kuiper belt and the Oort cloud. Since its creation, the Solar System has completed about 27 orbits around the galactic centre [2] in which the planet Earth has been transformed from a barren wasteland of fire and rock to a planet plentiful of life.

The earliest forms of life, bacteria, appeared probably in submarine-hydrothermal environments more than 3770 million years ago [3]. Later, a new type of cell called prokaryotes appeared, giving rise to a new milestone of life on Earth with the evolution of oxygenic phototrophic prokaryotes, in particular Cyanobacteria from which chloroplasts evolved, paving the way for the evolution of other organism such as algae and plants. [4,5]. With the emergence of Cyanobacteria, the level of atmospheric oxygen increased around 2450-2220 million years ago, leading to an event called the Great Oxidation Event [6].

The presence of oxygen led to one of the most important processes of life on Earth, the evolution of eukaryotic cells [7]. Eukaryotic cells are complex cells

containing a nucleus and different organelles that are well compartmentalised within a plasma membrane. Due to their great complexity compared to bacteria and archaea, eukaryotic cells led to the formation of new and more complex systems, which eventually evolved into the animal, plant, fungi, and protista kingdoms [8].

The colonisation of terrestrial land by plants probably began around 500 million years ago, when the algal ancestors of the first land plants were constantly washed up and deposited on marine and freshwater shores, initiating an adaptive process that eventually led to the conquest of land. However, it was not until 50 million years later, in the late Ordovician, when the first land plants appeared [9].

These early land plant had to face different evolutionary challenges to adapt to the new conditions in which they thrived. Amongst others, they had to adapt to the UV-B exposure and to the lack of structural support previously provided by the aquatic environment. They also had to develop new strategies to avoid desiccation and protection mechanisms against other species such as herbivores and pathogens [10]. Although all adaptations were essential for the development of these new terrestrial plants, the evolution of the so-called phenylpropanoid metabolism was certainly one of the most important. In fact, this enables the plant to accumulate phenylpropanoid units capable of protecting the plant from the action of UV-B in the 280-320 nm range [11]. However, it was not until roughly 10 million years later, with the emergence of tracheophytes, that plants developed the ability to deposit these phenylpropanoid units into the cell wall forming the lignin molecule. Lignin provided plants not only with the structural reinforcement to grow erect complementing the tensile strength of cellulose [12], but it also allowed the development of the vascular systems [11]. Finally, all these adaptations gave rise to a series of characteristics features of all terrestrial vascular plants, such as the possession of xylem, cuticle,

stomata, intercellular air spaces, phloem, endodermis and alternation of generations required to survive and colonise the terrestrial ecosystem [13].

On the other hand, as mentioned above, eukaryotic cells evolved into countless animal species, including *Homo Sapiens*. *Homo Sapiens* can know and understand his environment rationally and is able to perform highly complex conceptual and symbolic operations such as language, abstract reasoning and the capacity for introspection and speculation. Therefore, the human being can be considered as the pinnacle of animal evolution up to the present day. However, this great intelligence could become a double-edged sword that could lead humans to their own extinction.

1.2. Humankind and Climate Change

As mentioned above, probably the pinnacle of animal evolution up to the present day could be humankind. However, humans and their ability to shape the environment around them has led to serious environmental disruptions. Such alteration has resulted in the extinction of many animal and plant species and could eventually lead to climatic changes that would make the survival of the human species itself extremely difficult. Although humankind has had the capacity to transform the environment for thousands of years, it was not until the late 18th century that human activity began to visibly alter the climate. This milestone coincided with one of the greatest inventions that would change the future of humanity, the steam engine [14]. Developed by James Watt in 1784, this invention catapulted humankind into a period of technological development never seen before, called First Industrial Revolution (FIR), which changed the production method from manual to mechanical production, which led to a great improvement in productivity [15]. Nevertheless, this new device used coal as fuel, which rapidly increased anthropogenic CO_2 emissions, among other gases, such as NO_x and SO_x. Just as carbon was the main raw material for energy production during the FIR,

oil was the driving force in the development of the Second Industrial Revolution, (SIR), not only as a fuel for energy production and transport, but also as a raw material for a large number of commodities. Such has been the importance of oil in our society that the 20th century is considered the century of oil, with 7 of the 20 largest companies in the world being oil companies in 2009 [16]. Nonetheless, this over-dependence on fossil fuels, such as coal, oil, gas and others, has had a direct impact on the environment. On the one hand, the concentration of greenhouse gases over the last 200 years has increased due to the increase in anthropogenic emissions [17]. Figure I.1 shows the evolution of CO_2 concentration over the last 2000 years. Note that until the middle of the 19th century the concentration of atmospheric CO_2 remained almost constant and began to increase as the century progressed. It was in the second half of the 20th century that emissions skyrocketed due to increased energy requirements and consumption of goods as a result of population growth [18].

However, despite the existence of policies to reduce dependence on fossil fuels, the targets set are far from being met. In fact, by 2021, global primary energy demand increased by 5.8% and world oil production increased by 1.4 million barrels per day [21], and on the other hand the controversial decision of the European Union to consider natural gas as green energy [22] could jeopardise the EU's zero emissions target for 2050. However, in addition to air pollution, the uncontrolled use of oil as raw material generates other types of environmental disasters. Among others, one of the most problematic is the pollution generated by the indiscriminate use of plastic materials derived from oil.

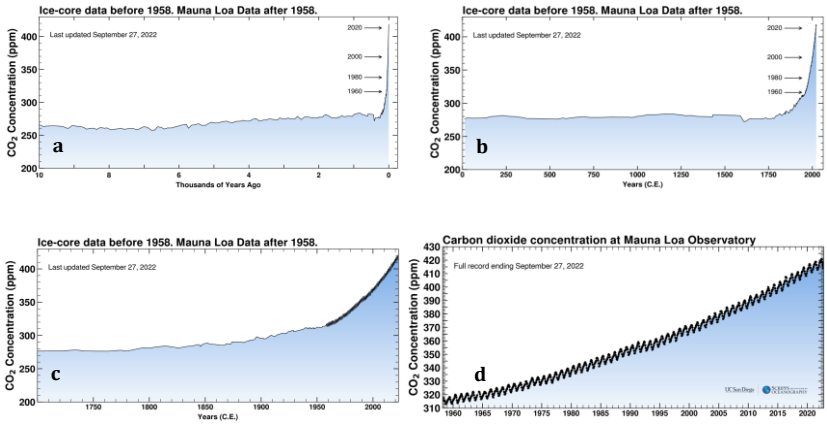

Figure I. 1. a adapted from [19], b and c adapted from [17], d is courtesy of the Scripps Institution of Oceanography, University of California, San Diego [20]

The first synthetic plastic, called celluloid, was developed by John Wesley Hyatt in 1869. This material was developed with the noble aim of replacing the ivory used to make billiards balls to save elephants from certain extinction [23]. Since then, synthetic plastics have become part of daily life and a key element in the development of human activity [24]. Indeed, global virgin plastic production has increased year by year, from 1.5 Mt in 1950 to 364 Mt in 2020 (Figure I.2) [25].

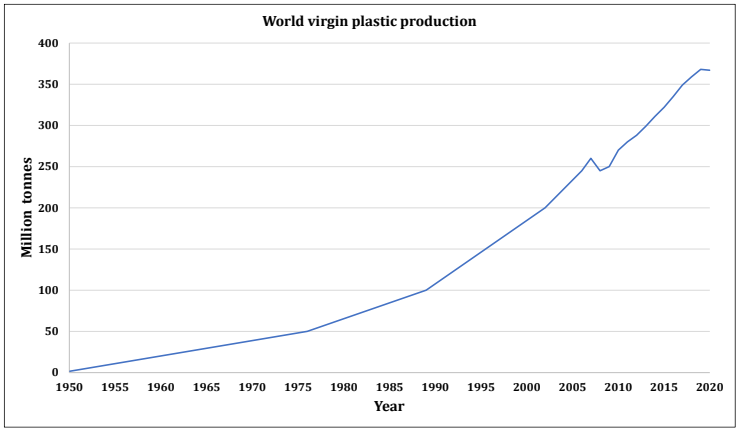

Figure I. 2. World virgin plastic production. Includes Thermoplastics, Polyurethanes, Thermosets, Elastomers, Adhesives, Coatings and Sealants and PP-fibres. Not Included PET, PA and Polyacryl-Fibres. Data obtained from [25]

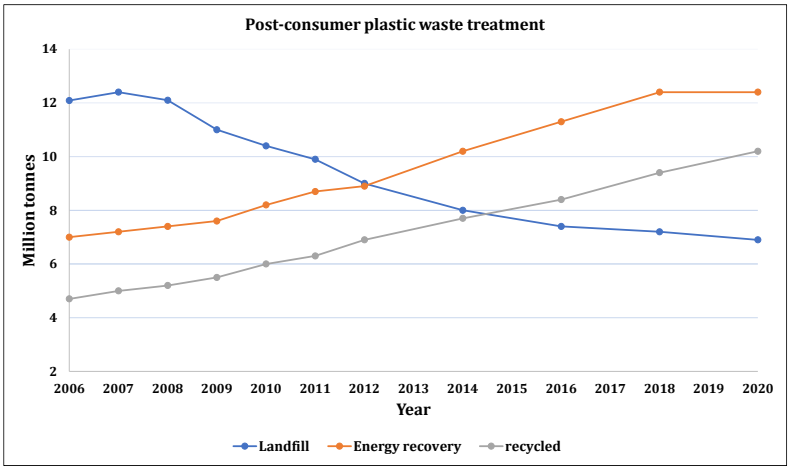

Figure I. 3. Plastic Post-Consumer Waste treatment in EU27+3. Adapted from [26]

However, only a small fraction of plastic waste is collected, which means that a large part of post-consumer plastic waste is dumped into the environment. Indeed, in the European Union, although the amount collected has increased from 23.79 Mt in 2006 to 29.5 Mt in 2020, these quantities are still insufficient to mitigate the serious environmental damage. Nevertheless, it is worth noting, as shown in Figure I.3 that over this period, the option landfilling has decreased by 46.4% while recycling and the use for energy recovery have increased by 117.7% and 77.1% respectively.

1.3. Polyurethanes

Within the large family of plastic materials, polyurethanes (PU) are of great importance for the industry, as they are the most versatile polymers due to their tuneable mechanical properties and huge range of applications such as thermoplastics, foams, elastomers, adhesives, coatings and sealants [27–29].

Since Dr. Otto Bayer first synthesised the first PU in 1937, the worldwide production of PUs grew to 20 million tonnes [30] and reached a market of $69.2 billion net worth in 2019 and is expected to growth of around 5.0-5.6% per year by 2025 [31].

PUs are formed by polyaddition reactions of hydroxyl containing components, mainly polyester or polyether polyols, isocyanates and chain extenders. The addition reaction of a hydroxyl and isocyanate functional groups leads to the formation of a urethane group (Figure I.4). Therefore, PUs are usually synthesised from the condensation reaction between polyols, low molecular weight chain extenders, and a diisocyanate molecule to produce a repeating urethane bond [32]. Other compounds such catalysts can also be used in the reaction, as well as other additives such as emulsifiers, stabilisers, pigments, fillers, and plasticisers.

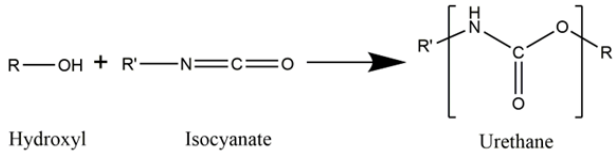

Figure I. 4. Addition reaction between hydroxyl and isocyanate group to form urethane group

The polyol, the isocyanate and the chain extender are linked through covalent bonds to form a repeating unit creating the main chain which is the primary structure of the polymer [33] (Figure I.5).

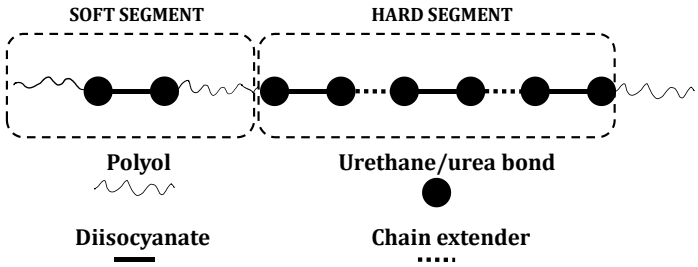

Figure I. 5. Primary structure of PU

The polyol forms the so-called soft segment (SS), while the isocyanate and the chain extender form the hard segment (HS) (Figure I.6). Due to their thermodynamic incompatibility a phase separation is generated in the PU

structure, creating microdomains known as soft block (SB) and hard block (HB) [34]. The former provides the flexibility while the latter is the responsible of the stiffness of the material [35].

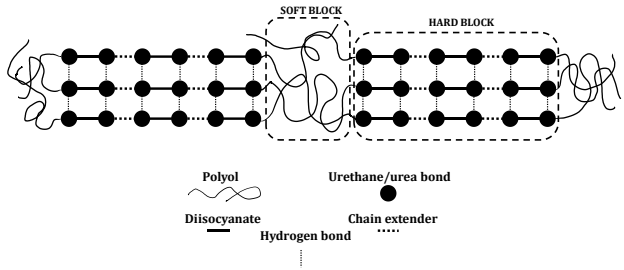

Figure I. 6. Secondary structure of PUs formed by HS and SS

The way these compounds (polyols, isocyanate and chain extender) are bonded to each other can be controlled depending on the synthesis method used. Polyurethanes are mainly synthesised by two methods called one-shot and prepolymer processes [36].

- One-shot method

  In this method all the components are mixed at the same time. Thus, the isocyanate is free to react with any component of the system forming hard blocks of random length, therefore, very dispersed domain sizes are obtained through the one-shot method [37]. A schematic of the molecular structure of a PU synthesised by this method is provided in Figure I.7.

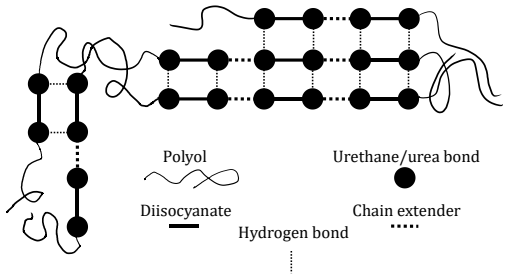

Figure I. 7. Schematic of the molecular structure of a PU synthesised by the one-shot method

❖ Prepolymer method

The prepolymer method consist essentially of two reaction steps. In the first step, the isocyanate is reacted with the polyol to form a prepolymer with a low concentration of NCO at the chain extremities [38]. This prepolymer is then reacted with the chain extender and finally the remaining NCO groups are reacted with a capping agent, which is usually a monofunctional alcohol. Thus, relatively small and uniform HS blocks tend to be formed, usually consisting of two isocyanate units and one chain extender unit, resulting in improved mechanical properties [37]. The molecular structure of a PU synthesised by the prepolymer method is shown in the scheme shown in Figure I.8.

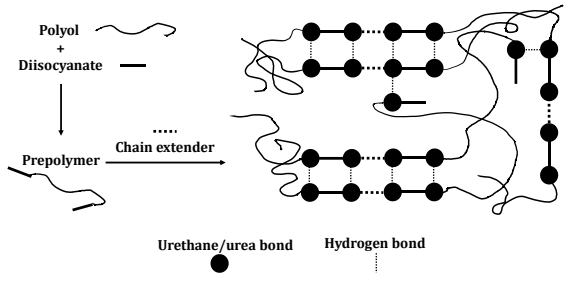

Figure I. 8. Scheme of the molecular structure of a PU synthesised by the prepolymer method

1.3.1. Polyols

As mentioned above, the PU industry is of great relevance today. Therefore, considering that polyols are one of the fundamental components of these compounds, its market is equally relevant. In fact, in 2019 the polyol industry generated roughly $26.2 billion per year and is expected to grow to $34.4 billion by 2024 [39]. Polyols, which are commonly petroleum derived, are defined as chemicals which contain two or more hydroxyl groups or amine groups per molecule [40]. Polyols can be classified into two main categories according to their molecular weight: low molecular weight or monomeric polyols and high molecular weight or polymeric polyols, also called oligopolyols. The former, which may have two or more hydroxyl groups, are usually employed as chain extenders when having two hydroxyl groups (diol), or as crosslinkers in the case of polyols with more than two hydroxyl groups (triols, tetraols, etc) [41]. The latter, are polymers with molecular weight up to 10000 Daltons with a maximum number of hydroxyl groups of eight [42] and can be subclassified into two main categories, viz. polyether and polyester polyols. Depending on the final application, polyether or polyester polyol is preferable. For instance, the former offer better chain flexibility and better dispersibility in aqueous media but lower resistance to light and ageing if compared to polyester polyols.

1.3.2. Isocyanates

Isocyanates are produced by the phosgenation reaction of a primary amine as shown in Equation I.1.

$$R - NH_2 + COCl_2 \rightarrow R - NCO + 2HCl \qquad \text{Equation I.1}$$

Isocyanates can be classified as aromatic and aliphatic depending on their structure, being the aromatic the most employed for PU production since they are more reactive and less hazardous [36]. Among other aromatic

isocyanates 4,4-Dipheny methane diisocyanate (MDI) and Toluenediisocyanate (TDI) are the most employed isocyanates, however both are classified as carcinogenic, mutagenic and reprotoxic, representing an important health risk for workers of the PU industry [43]. PU based on aromatic diisocyanates present good thermal and mechanical behaviour, however, if low oxidation and good ultraviolet stabilisation is desired, aliphatic diisocyanates are recommended [36].

1.3.3. Types of polyurethane

PUs offers a wide variety of products that can be classified in different ways. According to Karak (2017) [36] and Akindoyo et al. (2016) [33] this classification could be done taking into account their structure, thermal behaviour, origin and application as shown in Table I.1.

Table I. 1. Main PU types based on the different existing criteria

PU classification			
Structure	Origin	Thermal behaviour	Product application
Linear	Synthetic	Thermoplastic	Foams Fibres
Branch-chained Crosslinked	Bio-sourced	Thermosetting	CASE (coatings, adhesives, sealants and elastomers) Smart materials (ionomers)

1.3.3.1. PU adhesives

An adhesive is a material which, when applied to two surfaces, is capable of permanently joining them by a process of adhesive bonding [44]. Adhesives derived from natural products such as bones, skins, fish, milk, and plants have been used for thousands of years. However, since the mid-1940s, when

synthetic adhesives were permanently introduced into industry, their usability has increased and nowadays it is difficult to imagine an article that does not contain adhesive [45].

Among the variety of adhesives available in the industry, such as epoxies, acrylics, polyimides, silicones, polysulphides, urea, melamine, and phenol-formaldehyde [46], PU adhesives are considered as the most versatile and high performing adhesives due to their high shear and tensile strength. This is due to their ability to wet surfaces, form H bonds on different substrates, allow the permeation through porous substrates and form covalent bonds with substrates which contain active H atoms or functional groups [36,47]. In addition, PU adhesives cause fewer environmental and health problems when compared with the most common adhesives, such as urea, melamine, and phenol-formaldehyde, as PU adhesives do no emit volatile organic compounds during the lifetime of the PU [48]. Moreover, besides higher strength and the absence of formaldehyde emissions, PU adhesives generally require shorter pressing times, and they are also moderately flexible. This type of adhesive is capable of bonding different substrates such as wood, metal, glass, plastic, rubber, ceramics and textile fibre [49]. Nevertheless, it should be considered that their properties are highly impacted by the nature of its constituents i.e., isocyanate and polyol. PU adhesives are commonly used in engineered wood product due to their excellent properties.

1.3.4. Greener alternatives for PU synthesis

As mentioned above the chemicals required for PU production are usually obtained from petrochemical industry, therefore the environmental impact of this industry is an unfinished business for the chemical industry if it wants to comply with the regulations that are becoming more and more restrictive. To tackle this challenge PU industry can adopt two courses of action. The firs one is to remove from the equation the most environmentally harmful

component, isocyanate, by synthesising non isocyanate polyurethanes (NIPUs).

There are four different pathways to synthesise NIPUs (Figure I.9). Among them, the most promising and the most environmentally desirable option is the polyaddition reaction between cyclic carbonates and polyamines. However, the polycondensation route using dimethyl carbonate (DMC) could also be a good strategy since the DMC can be obtained from glycerol through different processes that do not require phosgenation and is considered as a green non-cyclic carboxymethylating agent [50]. In fact, since Enichem Co. from Italy synthesised in 1970 DMC from the oxidative carbonylation of methanol using metal catalyst, DMC has become a commonly used solvent in coatings, adhesives, and aerosols formulations, among others [51].

The second course of action is to replace petroleum-based polyols, isocyanates, and chain extenders with bio-based ones. In fact, the possibility of obtaining them from biomass is a reality that is being studied over the last decades, being vegetable oils [52], fatty acids [53,54], fatty acid methyl esters (FAME) [55,56], crude glycerol [57] and lignocellulosic biomass derived compounds [58] are some of the most studied raw materials.

1.4. Biorefineries for a bio-based future

The European Union (EU) is engaged in an ambitious process to build a sustainable future by developing different strategies such as the European Green Deal, which aims to reduce greenhouse gas emissions (GHG) in the EU by 55% by 2030 and to zero net emissions by 2050, the Circular Economy Action Plan, the Biodiversity Strategy, and the Farm to Fork Strategy. In this future that EU proposes, biorefineries have an important role to play contributing to the fulfilment of the established objectives.

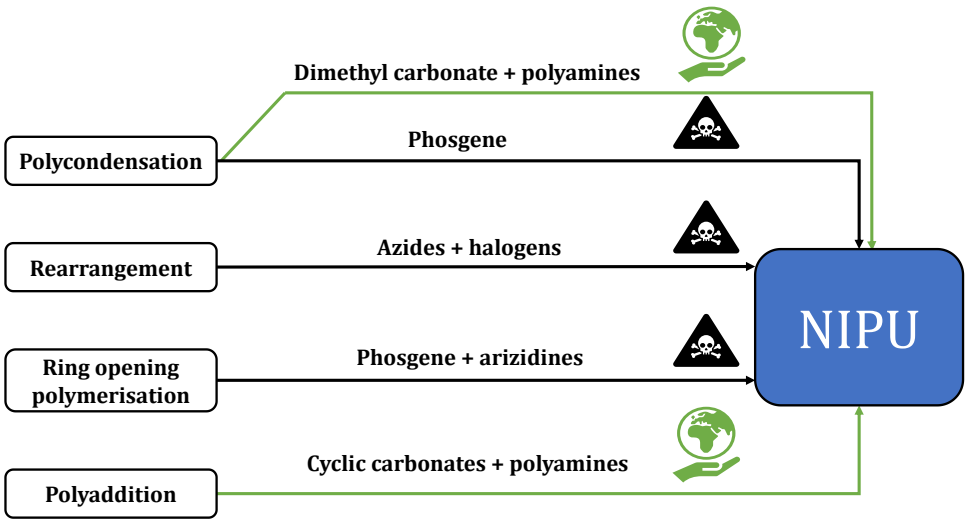

Figure I.9. Different synthesis routes to produce NIPUs

1.4.1. Biorefineries and biomass

1.4.1.1. Biorefinery

The biorefinery concept is similar to conventional oil refining, but instead of using crude oil as feedstock, different types of biomasses are used, which can be employed in liquid, solid or gas form. Thus, biorefinery can be defined as a set of economical, environmentally and socially beneficial processes for transforming biomass into a portfolio of marketable bio-based products, which could include co-production of food and feed, chemicals, materials and bioenergy [59] Biorefineries can be classified according to different parameters [60–62] such as the degree of integration, the processing route and the raw material used in the process (Figure I.10).

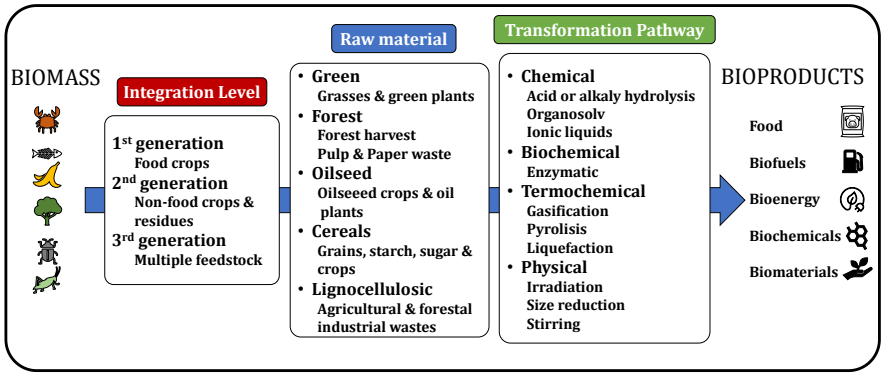

Figure I.10. Diagram with the different classification parameters of a biorefinery

First and second generation biorefineries use a single type of feedstock in the process. However, while the former use sugar or oil-rich feedstocks to produce only biofuel, the latter can use raw materials from different sources to produce multiple products. Furthermore, it should be noted that first generation biorefineries generally use food crops that compete with food prices, while second generation ones elude this problem by avoiding the use of food crops. Finally, third generation biorefineries represent an important technological improvement, being the most ambitious since it is possible to use almost any organic waste employing different technologies, thus broadening the range of products which can be obtained.

1.4.1.2. Biomass

Several definitions of biomass are available, of which the following is perhaps the most widely accepted: “Biomass is a group of renewable energy products and feedstocks that originate biologically from organic matter”. It should be noted that this definition excludes biologically derived compounds such as coal, oil, or gas. Thus, all biodegradable fractions from waste products and residues from agriculture, aquiculture, forestry, and related industries as well as the biodegradable fraction of industrial and municipal waste are considered as biomass, including lignocellulosic biomass. As a result,

biomass is one of the most abundant and renewable resource and has an enormous potential to produce both fuels and high value-added materials and chemicals.

1.5. Lignocelullosic biomass

One of the main renewable resource distributed all over the world is lignocellulosic biomass which is abundant, inexpensive and environmentally friendly feedstock with huge potential for the production of biofuels, chemicals, and materials [63,64].

Lignocellulosic biomass can be defined as a composite matrix made up of cellulose, hemicellulose, and lignin [65] which are distributed as a complex network within the plant cell walls (Figure I.11) [66].

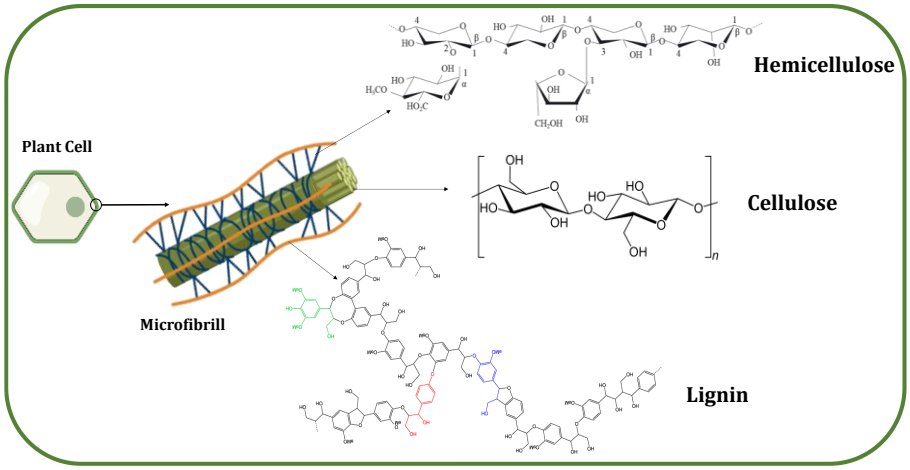

Figure I.11. Representation of the structural constituents of the plant cell wall

The percentage composition of these three different components could vary significantly based on the source of the biomass feedstock and environmental factors [67], as shown in Table I.2. In addition to these three structural compounds, lignocellulosic biomass also contains other non-structural compounds such as proteins, pectins, extractives and ash [68].

Table I.2. Chemical composition of different lignocellulosic biomass types (Adapted from [67]

Feedstock	Cellulose (%)	Hemicellulose (%)	Lignin (%)
Hardwood	45-55	24-40	18-25
Softwood	45-50	25-35	25-35
Grass	25-40	25-50	10-30

1.5.1. Cellulose

Cellulose is the most widely available renewable biopolymer on Earth and is the main component of lignocellulosic biomass comprising around 30–50% of the total weight [69].

Cellulose is packed in the cell wall as follows: the elementary unit is the β-D-glucopyranose which is linked together by *β*-1-4-glycosidic linkages to form a linear structure called fibril [70]. These linear structures are linked to each other through hydrogen bonds via the hydroxyl groups of the β-D-glucopyranose units, thus forming macrofibrils which are organised into crystalline and amorphous domains [71]. Finally, macrofibrils are packed with other structural component into the so-called walls.

Cellulose exhibits a number of desirables properties, such as hydrophilicity, chirality, biodegradability or the versatility to link different functional groups, which make it an excellent candidate for using in different applications such as hydrogels, aerogels, films, membranes and others. [72]

1.5.2. Hemicellulose

Hemicelluloses can be defined as amorphous branched polysaccharides from the plant cell walls that can be composed of different structural units such as xyloglucans, xylans, mannans and glucomannans, and β-(1,3 and 1,4)-glucans [73]. They account 20–35% of the lignocellulosic biomass [74] and

acts as a binding agent between the cellulose and lignin fractions adding rigidity to the overall biomass matrix [75]. Although their applicability is more limited than that for the other structural component of the cell wall, hemicelluloses have demonstrated a great potential to produce high value-added product such as oligosaccharides for the food industry and organic acids for the chemical industry.

1.5.3. Lignin

Finally, lignin is the second most abundant natural polymer and the main source of aromatic structures on earth [76]. It comprises 15-40%wt. of the total lignocellulosic biomass and it protects cellulose and hemicelluloses from microbial degradation providing also strength and hydrophobicity to the plant cell walls [77]. The structure of native lignin is still relatively unknown since it cannot be isolated without altering its native structure [78]. There are many different methods for lignin extraction with their own characteristics and particularities which provide very diverse lignin types. Among the main lignin producers worldwide are pulp and paper factories with a production of 97% of total lignin, of which 88% are lignosulphonates and 9% is Kraft lignin [79]. These two types of lignin have between 1.5-5%wt. of sulphur content in their structure and are usually employed for low-added value applications, such as heat and electricity generation [80]. Other lignin extraction processes from which lignin can be isolated, are several sulphur-free alternative methods, such as alkaline processes, organosolv processes, steam explosion, dilute acid hydrolysis or more recently developed ionic liquids or deep eutectic solvent extraction processes [81–86]. These type of lignins have in general higher purity and more adequate properties than lignosulphonates or Kraft lignin to be further valorised in high-added value applications.

Despite all the different kind of lignins that can be isolated depending on the

extraction method and type of lignocellulosic biomass, it is well accepted that lignin has a rigid polymer cross-linked 3D irregular structure. It is constituted through an enzyme-mediated dehydrogenative polymerization of p-coumaryl, coniferyl and sinapyl aromatic alcohols (Figure I.12).

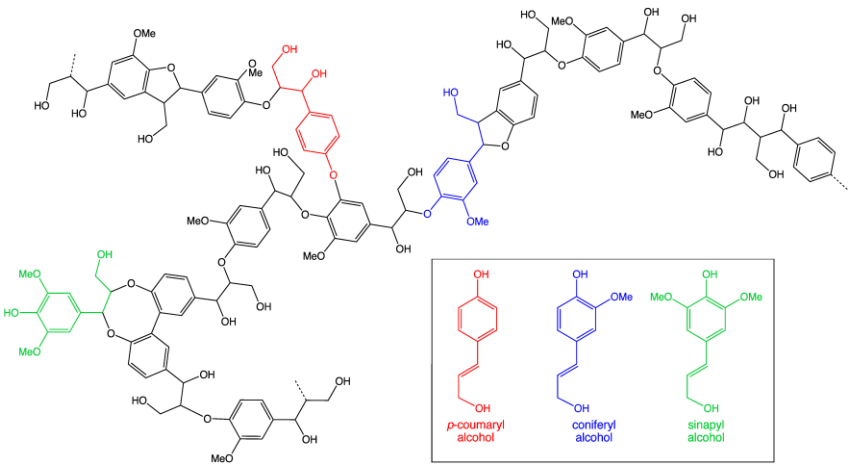

Figure I.12. Structure of lignin molecule and the aromatics alcohols from which it is synthesised (Adapted from [87])

These aromatic alcohols eventually synthesise the respective polymer units, forming p-hydroxyphenyl (H), guaiacyl (G) and syringyl (S) phenolic units (Figure I.13) [88,89]. These phenolic units appear in different proportion depending on the plant species. Therefore, lignin from softwood mostly contains coniferyl alcohol, around 90-95%, whereas lignin from hardwood typically is made up by 25-50% of coniferyl and 50-75% of sinapyl alcohols, while lignin from grass is composed by all three monomer alcohols [90,91].

The H, G and S phenolic units are linked together by ether bonds, such as β-O-4, α-O-4 and 4-O-5, and carbon-carbon bonds, such as 5-5, β-5, β-1 and β-β which contents vary depending on the feedstock [92]. However, the most frequent linkage in lignin is the β-O-4 bond, which varies from 43% to 65% [93].

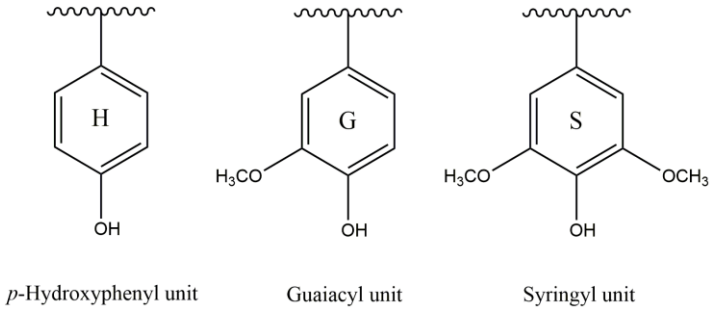

Figure I. 13. Lignin phenolic units

Lignin has many different functional groups including hydroxyl, carbonyl, methoxy, and carboxyl groups that have an effect on lignin's reactivity [94]. The proportion of these functional groups in lignin molecule depends not only on the type of biomass but also on the lignin extraction method employed. The percentage of the main functional groups present in lignin is showed in Table I.3.

Table I.3. Percentage (%wt.) of functional groups in lignin [95]

Functional group	Percentage (%wt.)
Methoxy	8.7-19.3
Phenolic hydroxyl	2.2-4.5
Aliphatic hydroxyl	3.1-10.1
Carboxyl	2.9-7.1
Carbonyl	2.1-4.5

Lignin chemical structure and its high functionality have contributed to the study of lignin as an ideal candidate for the development of new bio-based materials such as, carbon fibres, engineering plastics, asphalt binder modifier, membranes, polyols and polyurethanes as well as a variety of fuels and chemicals [96]. In addition, as mentioned before, lignin has high aromatic content with both aromatic and aliphatic hydroxyl groups which makes it a potential raw material for polyurethane production [29]. However, the

complex structure and the lack of repeatability of lignin as well as the still insufficiently developed technologies makes difficult its practical application [80].

1.6. Lignin based polyurethanes

As mentioned above, lignocellulosic biomass is an interesting feedstock to substitute fully or partially the petrolleum-based components required to synthesise PUs [49]. Among the components of this raw material, lignin is, due to its phenolic nature and its large amount of phenolic and aliphatic hydroxyl groups, the most promising candidate. In fact, lignin can be used to synthesise PUs through different routes, e.g. by using it without any modification as a filler in PUs formulations [97], or by modifying it to synthesise bio-based isocyanates [98], cyclic carbonates [99], polyamines [100], non-isocyanate polyurethanes (NIPUs) [101] and polyols [39]. Of the above methods, synthesis of NIPUs and bio-based polyols are the two most promising approaches for the use of lignin in PU formulations.

1.6.1. Lignin based polyols

The unique characteristics of the lignin molecule, previously discussed, make it an outstanding resource for synthesising bio-based polyols useful for industry [39]. Unfortunately, these characteristics are responsible for the low reactivity of the molecule [102]. To overcome this setback, different strategies have been developed, always with the aim of increasing the reactivity of the molecule. These processes can be classified into three main families: fragmentation or depolymerisation of lignin, modification creating new chemical active sites and functionalization of hydroxyl groups [103]. Among all the existing techniques encompassed in these three routes, liquefaction with polyhydric alcohols is one of the most widely studied strategies to synthesise polyols from lignin [103,104].

1.6.1.1. Liquefaction process

Liquefaction is a thermochemical conversion technology where biomass, or concretely lignin, is degraded to small molecular fragments by the application of heat in the presence of a liquid-phase and at mild temperatures (200–400 °C) [73]. Depending on the solvent used, liquefaction technology can be classified in two main groups: hydrothermal liquefaction (HTL) and solvothermal liquefaction (STL) [105]. In HTL water is the main solvent used while in STL non-aqueous solvents such as, phenol, tetralin γ-valerolactone or polyhydric alcohols, such as PEG or glycerol can be employed [106,107].

The STL of lignin with polyhydric alcohols is the main process to obtain bio-polyols for PU production. Normally, the solvents used in the liquefaction process are PEG, glycerol or 1-4 butanediol, and the catalysts are strong acids, mainly sulphuric acid or in some studies bases, such as sodium hydroxide [104,107]. The reason of employing sulphuric acid as the principal catalyst, is the lower temperature requirement of the process (110-180 °C), while for base catalyst the needed temperature to obtain similar polyol yields is around 250 °C [108]. Raw material to solvent ratio, solvent type, catalyst concentration, liquefaction temperature and time have great influence on acid and hydroxyl numbers and yield of the polyols [109].

The STL process is usually carried out in atmospheric pressure reactors heated by heating mantle at high temperatures (240 °C) and for long residence times (3 h) [110]. However, these high temperatures and prolonged residence times could decrease the yield of the polyols [111]. Therefore, as an alternative to the classical heating in the liquefaction processes, microwave irradiation technology has been proposed [112]. Using the microwave irradiation, the heating is faster and more homogeneous so the time needed for completing the liquefaction is reduced to only few minutes [104,108,113,114].

1.6.1.2. Crude glycerol for the liquefaction process

As mentioned above, the glycerol employed in the lignin liquefaction process is usually petro-based; however, a more sustainable alternative is available: crude glycerol from the biodiesel industry. This type of glycerol is generated in high quantity due to the booming of the biodiesel industry, in fact, one tonne of crude glycerol is generated as a by-product for every 10 tonnes of biodiesel. Once purified, crude glycerol is suitable for using in different industries such as food, pharmaceuticals, and cosmetics among others [115]. Nevertheless, due to the growing of the biodiesel industry, which has increased the production by more than 21 billion tonnes in Europe between 2000 and 2019 (Figure I.14), there is a large surplus of crude glycerol.

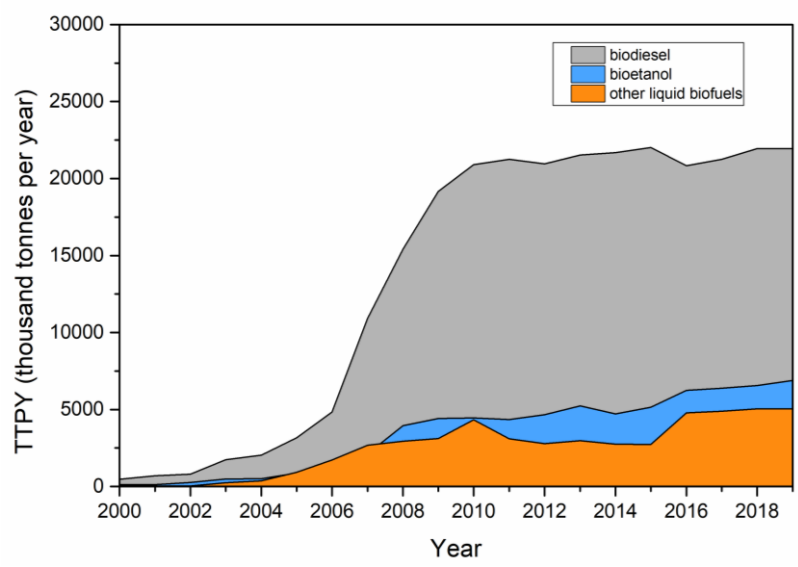

Figure I.14. Liquid biofuels production capacities in Europe between 2000 and 2019. Data obtained from [116]

As a result of this enormous excess of crude glycerol, it is economically unprofitable to refine it, and it is therefore necessary to find an industrial use for it [117]. One industrial application for this residue could be as solvent in the production of polyols by liquefaction of lignin [104,118–121].

1.6.2. Lignin based non-isocyanate polyurethanes

Among others, lignin and certain of its derivatives have been employed for the synthesis of non-isocyanate PU. The polyaddition route employing lignin as precursor has been used to synthesise different thermoplastic and thermosets. Of these, thermosets are the most reported compounds. In this way, Sternberg and Pilla (2020) processed a foam by reacting a lignin based cyclic carbonate with a diamine. The resulting foam had a high bio-based content, shape memory and good thermal and mechanical properties. In other work, soda lignin was used to prepare a thermoset resin through the reaction between a lignin derived cyclic carbonate with a diamine in the presence of poly(ethylene glycol) bis cyclic carbonate [123]. Enzymatic hydrolysis lignin from corncob was employed in other study to produce a thermoplastic composite with excellent mechanical and thermal properties, high reprocessability and recyclability, shape memory and self-healing properties, which could be used in a wide range of applications [124]. Lignosulphonate lignin is also a viable raw material to produce NIPUs, even though the application areas may differ from those of Kraft or Organosolv lignin. This is due to the special properties of lignosulphonate lignin, e.g. SO_3H content, water solubility and relatively high hydrophilicity [125]. In addition, lignin derivatives such as ferulic acid, syringaresinol and creosol were also employed in NIPU production. Ménard et al., (2017) [126] were able to synthesise different NIPU employing ferulic acid as a precursor of cyclic carbonates, which were reacted with different amines resulting in various thermoplastic and thermoset materials. Similarly, but utilising syringaresinol as the precursor of the cyclic carbonates and using different amines, a new set of thermoplastic and thermoset compounds were synthesised [127]. In another study, creosol based bis(cyclic carbonate) was employed to produce NIPUs with a great content of amorphous region [128].

1.7. Lignin based polyurethane adhesives

The incorporation of lignin as a polyol in a PU adhesive enhances the final aromatic content of the polymer increasing the glass transition temperature and the thermal stability of the adhesive since, due to its structure, lignin remains stable at high temperatures and behaves like a thermosetting [129]. Moreover, though lignin is used as a soft segment, usually act as a network former, its aromatic structure acts as rigid segment improving the mechanical strength of the adhesive [49]. Nevertheless, lignin due to its structure acts by increasing the phase separation between the HS and the SS of the PU, which can worsen the mechanical properties of PU adhesives [130]. Therefore, it is necessary to find the lignin isocyanate ratio that provides adequate phase separation.

It should be highlighted that lignin for PU adhesives is employed in both its pristine state and after modification. The former case is the simplest solution for the incorporation of lignin into the adhesives formulation. Nevertheless, in most of the cases, it needs from a previous solubilization of the lignin with organic solvents such as tetrahydrofuran (THF) [131]. Moreover, due to the excessive stiffness that lignin can impart to the polymer, it is often used in combination with other polyols such as PEG, castor oil and glycerol among others [97]. In the latter case, the modification is used as a procedure for the improvement of the reactivity of the lignin and its dispersion into the rest of the components. For instance, Chen et al., (2020) [132] confirmed the increase of the lignin reactivity after demethylation, provided by the conversion of methoxy moieties of the aromatic groups to phenolic hydroxyls. In respect to the components, it is again observed that additional secondary polyols are added into the adhesive formulations. The reason for that is the reduction of the brittleness derived from lignin incorporation (especially at high percentages) and the increase of the ductility of the PU

adhesives [133]. Finally concerning the impact of the lignin in the PU adhesive formulations, it can be highlighted that the great improvement of both thermal [134,135] and mechanical [136] properties. Moreover, a high degree of adhesion to different substrates is achieved by the incorporation of lignin into the PU adhesives, which can be even higher to that of standard PU adhesives [137]. Regardless of whether lignin is used as a filler or modified, PU adhesives are generally synthesised with toxic diisocyanates, being MDI and TDI the most commonly used [130].

The formulation of NIPU adhesives offers a more environmentally friendly alternative. In addition, one of its potential niche market is the wood panel industry, where the most commonly used adhesive is formaldehyde-based which produce emissions during manipulation, manufacture and use [138]. As mentioned above, DMC is a widely used solvent in the formulation of different materials, including NIPUs through polycondensation reaction with hexamethylenediamine (HDMA).

Synthesis of NIPUs through this type of reaction consists in two clearly differentiated steps [139]. Firstly, lignin is functionalised by a carbonation reaction, which can be carried out employing DMC creating an intermediate that is reacted in the second step by adding a diamine, usually hexamethylene diamine (HDMA), creating urethane bonds [140].

In recent years, several studies have been carried out to formulate bio-based NIPUs through polycondensation reactions using DMC and HDMA as solvents, together with different raw materials from lignocellulosic biomass such as glucose [50,141], non-furanic humins [142], tannins [141,143] and lignin [140,144]. A study performed by Arias et al., (2022) [139] proved that at laboratory scale and employing LCA methodology as an environmental impact assessment tool, a NIPU adhesive synthesised through polycondensation reaction between organosolv lignin, DMC and HDMA

proved to be a viable alternative to synthetic adhesives with a fully optimised and implemented production process.

1.8. Objectives of the thesis

The main objective of this thesis was to synthesis polyurethane wood adhesives, with and without isocyanate, by using bio-polyols based on the liquefaction of different types of lignin, from hardwood (*Eucalyptus globulus*) and softwood (*Pinus radiata*) with polyhydric alcohols as solvents. For this purpose, the reaction conditions for the liquefaction of the lignins were first optimised through a Box Behnken experimental design using response surface methodology and microwave irradiation technology. Afterwards, the resulting polyols were used to synthesise the different polyurethane wood adhesives employing isocyanate and through polycondensation reaction with DMC and HDMA. In Figure I.15 a schematic explanation of the experimental procedure is represented, which is briefly summarised below.

Publication I: In this part of the work, the two raw materials were delignified and lignins were obtained, which were used in the following parts of the work. In addition, a bio-polyol was obtained from the aqueous residue that remains after lignin precipitation.

Publication II: In this second part, the reaction conditions to produce bio-polyols were optimised using technical grade solvents. For this purpose, a Box-Behnken experimental design was performed employing the response surface methodology.

Publication III: Using the previously optimised reaction conditions, bio-polyols were synthesised by replacing the technical grade glycerol with an unpurified crude glycerol obtained from used vegetable cooking oil residue.

Publication IV: Employing the reaction conditions optimised in Publication II, a scale-up of the reaction was performed using both technical grade solvents and crude glycerol. The obtained bio-polyols were used to synthesise polyurethane wood adhesives.

Publication V: In this last part of the work, the bio-polyols obtained in the scale-up carried out in Publication IV were used to synthesise different non isocyanate polyurethanes through a polycondensation reaction with DMC and HDMA.

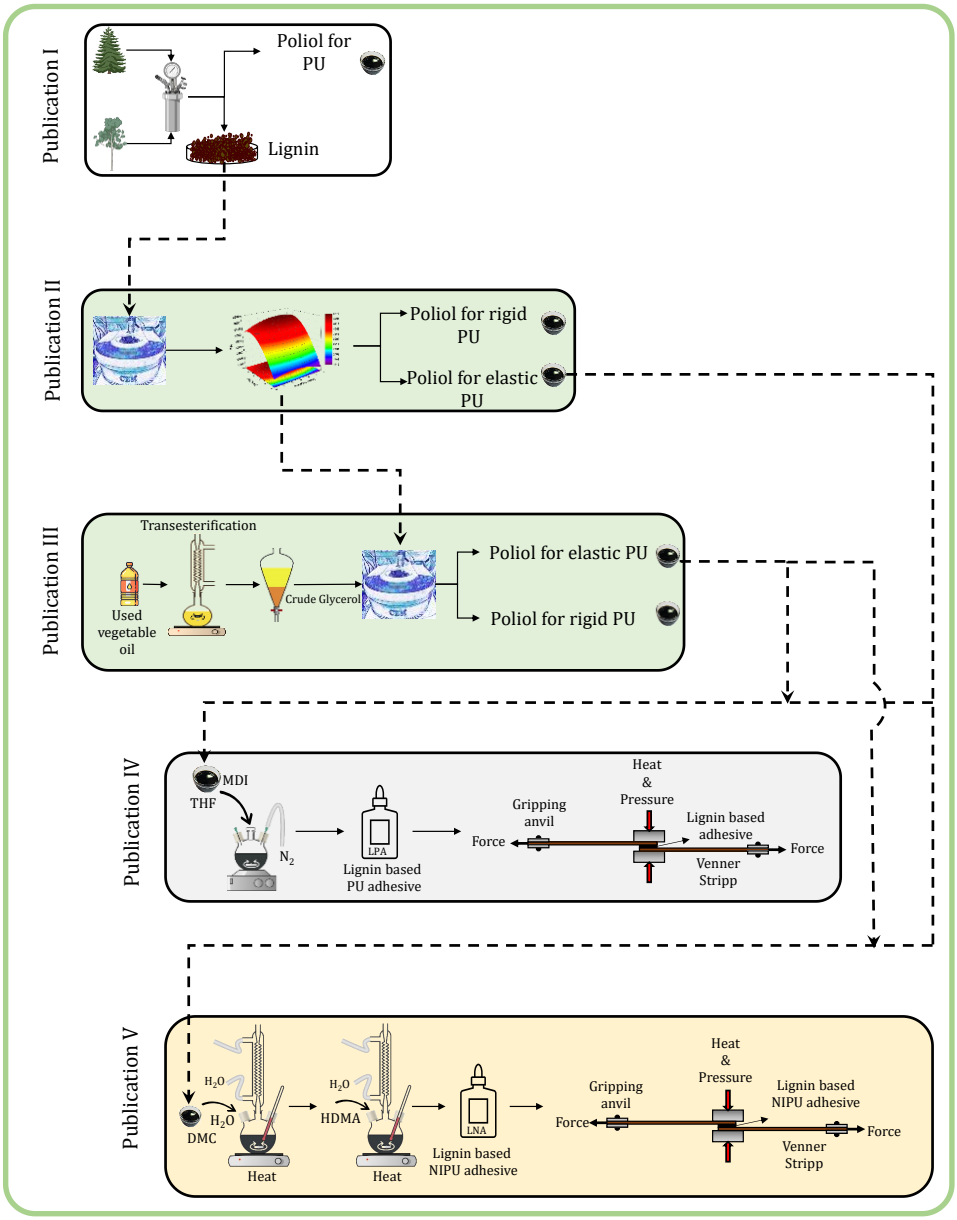

Figure I.15. Schematic explanation of the experimental procedure

1.9. References

[1] A. Bonanno, H. Schlattl, L. Paternò, Astron. Astrophys. 390(3) (2002) 1115–8. 10.1051/0004-6361:20020749.

[2] S.F. Portegies Zwart, Astrophys. J. 696(1 PART 2) (2009) 2007–10. 10.1088/0004-637X/696/1/L13.

[3] M.S. Dodd, D. Papineau, T. Grenne, J.F. Slack, M. Rittner, F. Pirajno, J. O'Neil, C.T.S. Little, Nature 543(7643) (2017) 60–4. 10.1038/nature21377.

[4] B.E. Schirrmeister, A. Antonelli, H.C. Bagheri, BMC Evol. Biol. 11(1) (2011). 10.1186/1471-2148-11-45.

[5] B.E. Schirrmeister, M. Gugger, P.C.J. Donoghue, Palaeontology 58(5) (2015) 769–85. 10.1111/pala.12178.

[6] P. Sánchez-Baracaldo, T. Cardona, New Phytol. 225(4) (2020) 1440–6. 10.1111/nph.16249.

[7] E.U. Hammarlund, E. Flashman, S. Mohlin, F. Licausi, Science (80-.). 370(6515) (2020). 10.1126/science.aba3512.

[8] P.A. Cohen, R.B. Kodner, Trends Ecol. Evol. 37(3) (2022) 246–56. 10.1016/j.tree.2021.11.005.

[9] J.K. Weng, C. Chapple, New Phytol. 187(2) (2010) 273–85. 10.1111/j.1469-8137.2010.03327.x.

[10] J.A. RAVEN, Bot. J. Linn. Soc. 88(1–2) (1984) 105–26. 10.1111/j.1095-8339.1984.tb01566.x.

[11] B. Lowry, D. Lee, C. Hébant, Taxon 29(2–3) (1980) 183–97.

10.2307/1220280.

[12] R.M. Bateman, P.R. Crane, W.A. Dimichele, P.R. Kenrick, N.P. Rowe, T. Speck, W.E. Stein, Annu. Rev. Ecol. Evol. Syst. 29 (1998) 263–92. 10.1146/annurev.ecolsys.29.1.263.

[13] A.R. Barceló, L.V.G. Ros, A.E. Carrasco, Trends Plant Sci. 12(11) (2007) 486–91. 10.1016/j.tplants.2007.09.002.

[14] P.J. Crutzen, Nature 415(January) (2002) 2002.

[15] Y. Chen, Engineering 3(5) (2017) 588–95. 10.1016/J.ENG.2017.04.009.

[16] L. Coleman, Energy Policy 40(1) (2012) 318–24. 10.1016/j.enpol.2011.10.012.

[17] C. MacFarling Meure, D. Etheridge, C. Trudinger, P. Steele, R. Langenfelds, T. Van Ommen, A. Smith, J. Elkins, Geophys. Res. Lett. 33(14) (2006) 2000–3. 10.1029/2006GL026152.

[18] R.B. Domínguez-Espíndola, D.M. Arias, C. Rodríguez-González, P.J. Sebastian, Appl. Therm. Eng. 216(June) (2022). 10.1016/j.applthermaleng.2022.119009.

[19] D. Lüthi, M. Le Floch, B. Bereiter, T. Blunier, J.M. Barnola, U. Siegenthaler, D. Raynaud, J. Jouzel, H. Fischer, K. Kawamura, T.F. Stocker, Nature 453(7193) (2008) 379–82. 10.1038/nature06949.

[20] Permissions and data sources | The Keeling Curve. Available at: https://keelingcurve.ucsd.edu/permissions-and-data-sources/. Accessed January 1, 2023.

[21] BP, [Online] London BP Stat. Rev. World Energy. (2022) 1–60.

[22] E. Parlamient, Taxonomy: MEPs do not object to inclusion of gas and nuclear activities | News | European Parliament. Available at: https://www.europarl.europa.eu/news/en/press-room/20220701IPR34365/taxonomy-meps-do-not-object-to-inclusion-of-gas-and-nuclear-activities. Accessed September 29, 2022.

[23] C.J. Rhodes, Sci. Prog. 102(3) (2019) 218–48. 10.1177/0036850419867204.

[24] R. Geyer, J.R. Jambeck, K.L. Law, Sci. Adv. 3(7) (2017) 25–9. 10.1126/sciadv.1700782.

[25] Plasticseurope, Plastics Europe. Available at: https://plasticseurope.org/resources/market-data/page/2/. Accessed October 1, 2022.

[26] Plastics Europe, Plast. - Facts 2021 (2021) 34.

[27] V.K. Ponnusamy, D.D. Nguyen, J. Dharmaraja, S. Shobana, J.R. Banu, R.G. Saratale, S.W. Chang, G. Kumar, Bioresour. Technol. (2019). 10.1016/j.biortech.2018.09.070.

[28] J.E.Q. Quinsaat, E. Feghali, D.J. Van De Pas, R. Vendamme, K.M. Torr, ACS Appl. Polym. Mater. (2021). 10.1021/acsapm.1c01081.

[29] H. Haridevan, D.A.C. Evans, A.J. Ragauskas, D.J. Martin, P.K. Annamalai, Green Chem. (2021). 10.1039/d1gc02744a.

[30] J. Peyrton, L. Avérous, Mater. Sci. Eng. R Reports (2021). 10.1016/j.mser.2021.100608.

[31] F.M. de Souza, P.K. Kahol, R.K. Gupta, Advances in Science, Technology

and Innovation, 2021, p. .

[32] N. Mahmood, Z. Yuan, J. Schmidt, C. Xu, Renew. Sustain. Energy Rev. (2016) 317–29. 10.1016/j.rser.2016.01.037.

[33] J.O. Akindoyo, M.D.H. Beg, S. Ghazali, M.R. Islam, N. Jeyaratnam, A.R. Yuvaraj, RSC Adv. (2016). 10.1039/c6ra14525f.

[34] M. Izadi, H. Mardani, H. Roghani-Mamaqani, M. Salami-Kalajahi, K. Khezri, ChemistrySelect 6(11) (2021) 2692–9. 10.1002/slct.202004307.

[35] S. Arévalo-Alquichire, M. Morales-Gonzalez, K. Navas-Gómez, L.E. Diaz, J.A. Gómez-Tejedor, M.A. Serrano, M.F. Valero, Polymers (Basel). 12(3) (2020). 10.3390/polym12030666.

[36] N. Karak, Biobased Smart Polyurethane Nanocomposites: From Synthesis to Applications, Royal Society of Chemistry, 2017, pp. 1–40.

[37] X. Sang, R. Wang, X. Chen, L. Zhang, M. An, Y. Shen, Adv. Mater. Res. 284–286 (2011) 1746–9. 10.4028/www.scientific.net/AMR.284-286.1746.

[38] C.S. Wong, K.H. Badri, Mater. Sci. Appl. 03(02) (2012) 78–86. 10.4236/msa.2012.32012.

[39] J. Perez-arce, A. Centeno-pedrazo, J. Labidi, J.R. Ochoa-gomez, E.J. Garcia-suarez, Polymers (Basel). 13(4) (2021) 1–12. 10.3390/polym13040651.

[40] P. Parcheta, J. Datta, Crit. Rev. Environ. Sci. Technol. 47(20) (2017) 1986–2016. 10.1080/10643389.2017.1400861.

[41] Y.Y. Li, X. Luo, S. Hu, Bio-based Polyols and Polyurethanes, 2015, pp.

1–79.

[42] M. Ionescu, [Set Polyols for Polyurethanes, Volume 1+2], 2019, pp. 27–46.

[43] P. Stachak, I. Łukaszewska, E. Hebda, K. Pielichowski, Materials (Basel). 14(13) (2021). 10.3390/ma14133497.

[44] S. Ebnesajjad, Handbook of Adhesives and Surface Preparation: Technology, Applications and Manufacturing, Elsevier Inc., 2010, pp. 3–13.

[45] L.F.M. da Silva, A. Öchsner, R.D. Adams, Handb. Adhes. Technol. Second Ed. 1–2 (2018) 1–1805. 10.1007/978-3-319-55411-2.

[46] B. Burchardt, Advances in polyurethane structural adhesives, Woodhead Publishing Limited, 2010.

[47] K.C. Frisch, Adhesion Science and Engineering, Elsevier B.V., 2002, pp. 759–812.

[48] R. V. Gadhave, P.A. Mahanwar, P.T. Gadekar, Open J. Polym. Chem. 07(04) (2017) 57–75. 10.4236/ojpchem.2017.74005.

[49] M. Alinejad, C. Henry, S. Nikafshar, A. Gondaliya, S. Bagheri, N. Chen, S.K. Singh, D.B. Hodge, M. Nejad, Polymers (Basel). 11(7) (2019). 10.3390/polym11071202.

[50] X. Xi, A. Pizzi, L. Delmotte, Polymers (Basel). 10(4) (2018) 1–21. 10.3390/polym10040402.

[51] R. Khiari, M.C. Brochier-Salon, M.F. Mhenni, E. Mauret, M.N. Belgacem, ChemSusChem 9(16) (2016) 2143–8. 10.1002/cssc.201600430.

[52] A. Fridrihsone, F. Romagnoli, V. Kirsanovs, U. Cabulis, J. Clean. Prod. 266 (2020) 121403. 10.1016/j.jclepro.2020.121403.

[53] P.M. Paraskar, R.D. Kulkarni, J. Polym. Environ. 29(1) (2020) 54–70. 10.1007/s10924-020-01849-x.

[54] X. Junming, J. Jianchun, L. Jing, J. Appl. Polym. Sci. 126(4) (2012) 1377–84. 10.1002/app.36740.

[55] S. Mohd Norhisham, T.I. Tuan Noor Maznee, H. Nurul Ain, P.P. Kosheela Devi, A. Srihanum, M.N. Norhayati, S.K. Yeong, A.H. Hazimah, C.M. Schiffman, A. Sendijarevic, V. Sendijarevic, I. Sendijarevic, Int. J. Adhes. Adhes. 73(October 2016) (2017) 38–44. 10.1016/j.ijadhadh.2016.10.012.

[56] T.N.M. Tuan Ismail, N.A. Ibrahim, M.A. Mohd Noor, S.S. Hoong, K.D. Poo Palam, S.K. Yeong, Z. Idris, C.M. Schiffman, I. Sendijarevic, E. Abd Malek, N. Zainuddin, V. Sendijarevic, JAOCS, J. Am. Oil Chem. Soc. 95(4) (2018) 509–23. 10.1002/aocs.12044.

[57] S. Cui, Z. Liu, Y. Li, Ind. Crops Prod. 108(July) (2017) 798–805. 10.1016/j.indcrop.2017.07.043.

[58] Y.Y. Li, X. Luo, S. Hu, Bio-based Polyols and Polyurethanes, 2015, pp. 1–79.

[59] B. Annevelink, L.G. Chavez, R. Van Ree, I.V. Gursel, Global biorefinery status report 2022, IEA Bioenergy, 2022.

[60] BioPlat, Suschem, I. y C. Ministerio de Economia, Minist. Econ. Ind. Y Compet. (2017) 1–92.

[61] E. de Jong, G. Jungmeier, Biorefinery Concepts in Comparison to

Petrochemical Refineries, Elsevier B.V., 2015.

[62] Y. Liu, Y. Lyu, J. Tian, J. Zhao, N. Ye, Y. Zhang, L. Chen, Renew. Sustain. Energy Rev. 139(January) (2021) 110716. 10.1016/j.rser.2021.110716.

[63] M. Zhou, O.A. Fakayode, A.E. Ahmed Yagoub, Q. Ji, C. Zhou, Renew. Sustain. Energy Rev. 156(December 2021) (2022) 111986. 10.1016/j.rser.2021.111986.

[64] H. Kawaguchi, K. Takada, T. Elkasaby, R. Pangestu, M. Toyoshima, P. Kahar, C. Ogino, T. Kaneko, A. Kondo, Bioresour. Technol. (2022). 10.1016/j.biortech.2021.126165.

[65] A. Saravanan, P. Senthil Kumar, S. Jeevanantham, S. Karishma, D.-V.N. Vo, Bioresour. Technol. (2022). 10.1016/j.biortech.2021.126203.

[66] P. Khemthong, C. Yimsukanan, T. Narkkun, A. Srifa, T. Witoon, S. Pongchaiphol, S. Kiatphuengporn, K. Faungnawakij, Biomass and Bioenergy (2021). 10.1016/j.biombioe.2021.106033.

[67] S. Malherbe, T.E. Cloete, Rev. Environ. Sci. Biotechnol. 1(2) (2002) 105–14. 10.1023/A:1020858910646.

[68] L. Sillero, R. Prado, M.A. Andrés, J. Labidi, Ind. Crops Prod. 137(May) (2019) 276–84. 10.1016/j.indcrop.2019.05.033.

[69] H.H. Cheng, L.M. Whang, Bioresour. Technol. (2022). 10.1016/j.biortech.2021.126097.

[70] A. Dadwal, S. Sharma, T. Satyanarayana, Int. J. Biol. Macromol. (2021). 10.1016/j.ijbiomac.2021.08.024.

[71] L. Bai, A. Ding, G. Li, H. Liang, Chemosphere 308(P3) (2022) 136426.

10.1016/j.chemosphere.2022.136426.

[72] S. Sugiarto, R.R. Pong, Y.C. Tan, Y. Leow, T. Sathasivam, Q. Zhu, X.J. Loh, D. Kai, Mater. Today Chem. 26 (2022) 101022. 10.1016/j.mtchem.2022.101022.

[73] J.Y. Kim, H.W. Lee, S.M. Lee, J. Jae, Y.K. Park, Bioresour. Technol. (2019). 10.1016/j.biortech.2019.01.055.

[74] S. Kassaye, K.K. Pant, S. Jain, Fuel Process. Technol. (2016). 10.1016/j.fuproc.2015.12.032.

[75] D. Kumari, R. Singh, Renew. Sustain. Energy Rev. (2018). 10.1016/j.rser.2018.03.111.

[76] J. Deng, S.F. Sun, E.Q. Zhu, J. Yang, H.Y. Yang, D.W. Wang, M.G. Ma, Z.J. Shi, Ind. Crops Prod. (2021). 10.1016/j.indcrop.2021.113412.

[77] C.G. Yoo, X. Meng, Y. Pu, A.J. Ragauskas, Bioresour. Technol. (2020). 10.1016/j.biortech.2020.122784.

[78] S. Gillet, M. Aguedo, L. Petitjean, A.R.C. Morais, A.M. Da Costa Lopes, R.M. Łukasik, P.T. Anastas, Green Chem. (2017). 10.1039/c7gc01479a.

[79] D.S. Bajwa, G. Pourhashem, A.H. Ullah, S.G. Bajwa, Ind. Crops Prod. 139(February) (2019) 111526. 10.1016/j.indcrop.2019.111526.

[80] P. Jędrzejczak, M.N. Collins, T. Jesionowski, Ł. Klapiszewski, Int. J. Biol. Macromol. (2021). 10.1016/j.ijbiomac.2021.07.125.

[81] A.W. Bhutto, K. Qureshi, K. Harijan, R. Abro, T. Abbas, A.A. Bazmi, S. Karim, G. Yu, Energy (2017). 10.1016/j.energy.2017.01.005.

[82] D. Sidiras, D. Politi, G. Giakoumakis, I. Salapa, Bioresour. Technol.

(2022). 10.1016/j.biortech.2021.126158.

[83] Y. Yu, J. Wu, X. Ren, A. Lau, H. Rezaei, M. Takada, X. Bi, S. Sokhansanj, Renew. Sustain. Energy Rev. (2022). 10.1016/j.rser.2021.111871.

[84] P. Das, R.B. Stoffel, M.C. Area, A.J. Ragauskas, Biomass and Bioenergy 120(November 2018) (2019) 350–8. 10.1016/j.biombioe.2018.11.029.

[85] Z. Usmani, M. Sharma, P. Gupta, Y. Karpichev, N. Gathergood, R. Bhat, V.K. Gupta, Bioresour. Technol. (2020). 10.1016/j.biortech.2020.123003.

[86] Z. Chen, A. Ragauskas, C. Wan, Ind. Crops Prod. (2020). 10.1016/j.indcrop.2020.112241.

[87] W. Graham Forsythe, M.D. Garrett, C. Hardacre, M. Nieuwenhuyzen, G.N. Sheldrake, Green Chem. 15(11) (2013) 3031–8. 10.1039/c3gc41110a.

[88] L. Zhang, T.U. Rao, J. Wang, D. Ren, S. Sirisommboonchai, C. Choi, H. Machida, Z. Huo, K. Norinaga, Fuel Process. Technol. (2022). 10.1016/j.fuproc.2021.107097.

[89] D. Kai, M.J. Tan, P.L. Chee, Y.K. Chua, Y.L. Yap, X.J. Loh, Green Chem. (2016). 10.1039/c5gc02616d.

[90] D. Huang, R. Li, P. Xu, T. Li, R. Deng, S. Chen, Q. Zhang, Chem. Eng. J. (2020). 10.1016/j.cej.2020.126237.

[91] C. Chio, M. Sain, W. Qin, Renew. Sustain. Energy Rev. 107(March) (2019) 232–49. 10.1016/j.rser.2019.03.008.

[92] E. Leng, Y. Guo, J. Chen, S. Liu, J. E, Y. Xue, Fuel (2022).

10.1016/j.fuel.2021.122102.

[93] X. Wu, N. Luo, S. Xie, H. Zhang, Q. Zhang, F. Wang, Y. Wang, Chem. Soc. Rev. (2020). 10.1039/d0cs00314j.

[94] X. Meng, C. Crestini, H. Ben, N. Hao, Y. Pu, A.J. Ragauskas, D.S. Argyropoulos, Nat. Protoc. 14(9) (2019) 2627–47. 10.1038/s41596-019-0191-1.

[95] W. Gao, P. Fatehi, Can. J. Chem. Eng. (2019). 10.1002/cjce.23620.

[96] Y. Meng, J. Lu, Y. Cheng, Q. Li, H. Wang, Int. J. Biol. Macromol. (2019). 10.1016/j.ijbiomac.2019.05.198.

[97] S. Magina, N. Gama, L. Carvalho, A. Barros-Timmons, D.V. Evtuguin, Materials (Basel). 14(22) (2021) 1–18. 10.3390/ma14227072.

[98] T.A.P. Hai, M. Tessman, N. Neelakantan, A.A. Samoylov, Y. Ito, B.S. Rajput, N. Pourahmady, M.D. Burkart, Biomacromolecules 22(5) (2021) 1770–94. 10.1021/acs.biomac.0c01610.

[99] M.A.C. Mhd. Haniffa, K. Munawar, Y.C. Ching, H.A. Illias, C.H. Chuah, Chem. - An Asian J. 16(11) (2021) 1281–97. 10.1002/asia.202100226.

[100] M. Ghasemlou, F. Daver, E.P. Ivanova, B. Adhikari, Eur. Polym. J. 118(May) (2019) 668–84. 10.1016/j.eurpolymj.2019.06.032.

[101] J. Sternberg, O. Sequerth, S. Pilla, Prog. Polym. Sci. (2021). 10.1016/j.progpolymsci.2020.101344.

[102] B.M. Upton, A.M. Kasko, Chem. Rev. 116(4) (2016) 2275–306. 10.1021/acs.chemrev.5b00345.

[103] S. Laurichesse, L. Avérous, Prog. Polym. Sci. 39(7) (2014) 1266–90.

10.1016/j.progpolymsci.2013.11.004.

[104] K. Gosz, P. Kosmela, A. Hejna, G. Gajowiec, Ł. Piszczyk, Wood Sci. Technol. 52(3) (2018) 599–617. 10.1007/s00226-018-0991-4.

[105] J. Zhang, N. Hori, A. Takemura, J. Clean. Prod. 277 (2020) 124015. 10.1016/j.jclepro.2020.124015.

[106] M.R. Haverly, T.C. Schulz, L.E. Whitmer, A.J. Friend, J.M. Funkhouser, R.G. Smith, M.K. Young, R.C. Brown, Fuel (2018). 10.1016/j.fuel.2017.09.072.

[107] M. Vale, M.M. Mateus, R. Galhano dos Santos, C. Nieto de Castro, A. de Schrijver, J.C. Bordado, A.C. Marques, J. Clean. Prod. 212 (2019) 1036–43. 10.1016/j.jclepro.2018.12.088.

[108] S.H.F. da Silva, I. Egüés, J. Labidi, Ind. Crops Prod. 137(March) (2019) 687–93. 10.1016/j.indcrop.2019.05.075.

[109] E. barbary M. Hassan, N. Shukry, Ind. Crops Prod. 27(1) (2008) 33–8. 10.1016/j.indcrop.2007.07.004.

[110] S. Hu, Y. Li, Ind. Crops Prod. 57 (2014) 188–94. 10.1016/j.indcrop.2014.03.032.

[111] S. Hu, X. Luo, Y. Li, ChemSusChem 7(1) (2014) 66–72. 10.1002/cssc.201300760.

[112] U.A. Amran, S. Zakaria, C.H. Chia, Z. Fang, M.Z. Masli, Energy and Fuels (2017). 10.1021/acs.energyfuels.7b02098.

[113] B.L. Xue, J.L. Wen, R.C. Sun, Materials (Basel). 8(2) (2015) 586–99. 10.3390/ma8020586.

[114] S.H.F. da Silva, P.S.B. dos Santos, D. Thomas da Silva, R. Briones, D.A. Gatto, J. Labidi, J. Wood Chem. Technol. 37(5) (2017) 343–58. 10.1080/02773813.2017.1303513.

[115] J.C. Thompson, B.B. He, Appl. Eng. Agric. 22(2) (2006) 261–5. 10.13031/2013.20272.

[116] Eurostat, Statistics | Eurostat. Available at: https://ec.europa.eu/eurostat/databrowser/view/NRG_INF_LBPC__custom_1487898/default/table. Accessed May 10, 2022.

[117] L.R. Kumar, R. Kaur, R.D. Tyagi, P. Drogui, Bioresour. Technol. 323(December 2020) (2021) 124565. 10.1016/j.biortech.2020.124565.

[118] L.C. Muller, S. Marx, H.C.M. Vosloo, J. Renew. Mater. 5(1) (2017) 67–80. 10.7569/JRM.2016.634130.

[119] L.C. Muller, S. Marx, H.C.M. Vosloo, E. Fosso-Kankeu, I. Chiyanzu, Polym. from Renew. Resour. 9(3–4) (2018) 111–32. 10.1177/2041247918803187.

[120] L.C. Muller, S. Marx, H.C.M. Vosloo, I. Chiyanzu, Polym. from Renew. Resour. 10(1–3) (2019) 3–18. 10.1177/2041247919830833.

[121] M.H. Tran, J.H. Yu, E.Y. Lee, Polymers (Basel). 13(9) (2021). 10.3390/polym13091491.

[122] J. Sternberg, S. Pilla, Green Chem. 22(20) (2020) 6922–35. 10.1039/d0gc01659d.

[123] A. Salanti, L. Zoia, M. Mauri, M. Orlandi, RSC Adv. 7(40) (2017) 25054–65. 10.1039/c7ra03416d.

[124] W. Zhao, Z. Liang, Z. Feng, B. Xue, C. Xiong, C. Duan, Y. Ni, ACS Appl. Mater. Interfaces 13(24) (2021) 28938–48. 10.1021/acsami.1c06822.

[125] V. Mimini, H. Amer, H. Hettegger, M. Bacher, I. Gebauer, R. Bischof, K. Fackler, A. Potthast, T. Rosenau, Holzforschung 74(2) (2020) 203–11. 10.1515/hf-2018-0298.

[126] R. Ménard, S. Caillol, F. Allais, ACS Sustain. Chem. Eng. 5(2) (2017) 1446–56. 10.1021/acssuschemeng.6b02022.

[127] M. Janvier, P.H. Ducrot, F. Allais, ACS Sustain. Chem. Eng. 5(10) (2017) 8648–56. 10.1021/acssuschemeng.7b01271.

[128] Q. Chen, K. Gao, C. Peng, H. Xie, Z.K. Zhao, M. Bao, Green Chem. 17(9) (2015) 4546–51. 10.1039/c5gc01340b.

[129] S. Sen, S. Patil, D.S. Argyropoulos, Green Chem. 17(11) (2015) 4862–87. 10.1039/c5gc01066g.

[130] M.A. Aristri, M.A.R. Lubis, S.M. Yadav, P. Antov, A.N. Papadopoulos, A. Pizzi, W. Fatriasari, M. Ismayati, A.H. Iswanto, Appl. Sci. 11(9) (2021) 1–29. 10.3390/app11094242.

[131] D.J. Dos Santos, L.B. Tavares, J.R. Gouveia, G.F. Batalha, Arch. Mater. Sci. Eng. 107(2) (2021) 56–63. 10.5604/01.3001.0015.0242.

[132] Y.C. Chen, S. Fu, H. Zhang, Colloids Surfaces A Physicochem. Eng. Asp. 585 (2020) 124164. 10.1016/J.COLSURFA.2019.124164.

[133] Y.Y. Wang, C.E. Wyman, C.M. Cai, A.J. Ragauskas, ACS Appl. Polym. Mater. 1(7) (2019) 1672–9. 10.1021/ACSAPM.9B00228.

[134] Y. Chen, H. Zhang, Z. Zhu, S. Fu, Int. J. Biol. Macromol. (2020). 10.1016/j.ijbiomac.2020.02.321.

[135] L.B. Tavares, C. V. Boas, G.R. Schleder, A.M. Nacas, D.S. Rosa, D.J. Santos, Express Polym. Lett. 10(11) (2016) 927–40. 10.3144/EXPRESSPOLYMLETT.2016.86.

[136] J.R. Gouveia, L.D. Antonino, G.E.S. Garcia, L.B. Tavares, A.N.B. Santos, D.J. do. Santos, Https://Doi.Org/10.1080/00218464.2020.1784148 97(15) (2020) 1423–39. 10.1080/00218464.2020.1784148.

[137] R. V. Gadhave, P. S. Kasbe, P.A. Mahanwar, P.T. Gadekar, Int. J. Adhes. Adhes. 95 (2019) 102427. 10.1016/J.IJADHADH.2019.102427.

[138] M.H. Hussin, N.H. Abd Latif, T.S. Hamidon, N.N. Idris, R. Hashim, J.N. Appaturi, N. Brosse, I. Ziegler-Devin, L. Chrusiel, W. Fatriasari, F.A. Syamani, A.H. Iswanto, L.S. Hua, S.S. Azry Osman Al Edrus, L.W. Chen, P. Antov, V. Savov, M.A. Rahandi Lubis, L. Kristak, R. Reh, J. Sedliačik, J. Mater. Res. Technol. (2022). 10.1016/j.jmrt.2022.10.156.

[139] A. Arias, E. Entrena-Barbero, G. Feijoo, M.T. Moreira, J. Environ. Chem. Eng. 10(1) (2022) 107053. 10.1016/j.jece.2021.107053.

[140] J. Saražin, A. Pizzi, S. Amirou, D. Schmiedl, M. Šernek, J. Renew. Mater. 9(5) (2021) 881–907. 10.32604/jrm.2021.015047.

[141] X. Xi, A. Pizzi, C. Gerardin, H. Lei, X. Chen, S. Amirou, Polymers (Basel). 11(11) (2019). 10.3390/polym11111802.

[142] X. Chen, A. Pizzi, H. Essawy, E. Fredon, C. Gerardin, N. Guigo, N. Sbirrazzuoli, Polymers (Basel). 13(3) (2021) 1–13. 10.3390/polym13030372.

[143] X. Chen, A. Pizzi, E. Fredon, C. Gerardin, X. Zhou, B. Zhang, G. Du, Int. J. Adhes. Adhes. 112(September 2021) (2022) 103001. 10.1016/j.ijadhadh.2021.103001.

[144] F.J. Santiago-Medina, M.C. Basso, A. Pizzi, L. Delmotte, J. Renew. Mater. 6(4) (2018) 413–25. 10.7569/JRM.2017.634172.

2nd PART

METHODOLOGY

“I never question anything…

Until after I’ve done it.”

Han Solo

2.1. Raw materials and chemicals

The raw materials, used for this thesis were wood residues from different industries from the Basque Country (Spain). On the one hand, *Eucalyptus globulus* chips were supplied by Papelera Guipuzcoana Zikuñaga S.A., while *Pinus radiata* sawdust was obtained from Ebaki XXI S.A. The used vegetable oil employed to obtain the crude glycerol for the liquefaction process in ***Publication III*** was collected at the restaurant of the Faculty of Engineering of Gipuzkoa in Eibar. The commercial chemical employed in this thesis are summarised in Table M.1.

Table M. 1. Commercial chemical compounds employed in the thesis

Chemical compound	Abbreviation	Purity	Supplier
Ethanol			Scharlab
Methanol			
Ethyl acetate		HPLC grade	
Sodium sulphate anhydrous		≥99%	
Dimethylformamide	DMF	HPLC ≥99.9%	
Lithium bromide			Fisher Scientific
1,4-dioxane		≥99.8%	
Pyridine		99.50%	
Tetrahydrofuran	THF	Analytical reagent grade	
Phthalic anhydride		98%	
Sulfuric acid		96%	
Polyethylene glycol -400	PEG-400	Technical	
Glycerol	Gly	99%	Panreac
Potassium Hydroxyde	KOH	85%	
Sodium Hydroxyde	NaOH		
4,4'-Methylene diphenyl diisocyanate	MDI		Merk
Dimethyl Carbonate	DMC	99%	Alfa Aesar
Hexamethylenediamine	HDMA	>98%	
Dibutyltin dilaurate	DBTDL	95%	Alfa Aesar
3(Aminopropyl)trimethoxysilane	APTMS		

2.2. Delignification of raw material and sonication process of black liquors

For obtaining the lignin employed in this work, both raw materials were subjected to the process described in Figure M.1 and summarized below. Firstly, an organosolv delignification process was carried out using the reaction conditions summarized in Table M.2. To do that, a 1.5 L stainless 5500 steel parr reactor with a 4848 Parr controller was employed. A triplicate of each organosolv treatment were carried out employing 50 grams of raw material.

Table M. 2. Reaction conditions of organosolv delignification processes

	Solvent (w/w)	Solid/liquid ratio	Temperature (°C)	Time (min)
Eucalyptus globulus	EtOH/H2O (50%)	1:6	200	75
Pinus radiata		1:8	210	

The black liquors (BL) were separated from the pulp through vacuum filtration employing paper filters with a retention capacity of 7-12 μm (Macherey-Nagel 640w). After the filtration process, the BL were sonicated using a Sonoplus ultrasonic homogenizer HD 3100 under the following reaction conditions: 35°C, 60 min and an output amplitude of 35%. To precipitate the lignin contained in the BL two volumes of acidified water (pH2) was added, and then the lignin was separated by filtration from the liquid phase employing a Stainless Steel holder with 2 L of capacity and a nylon filter with a pore diameter of 0.22 μm. The lignin was washed with distilled water until neutral pH.

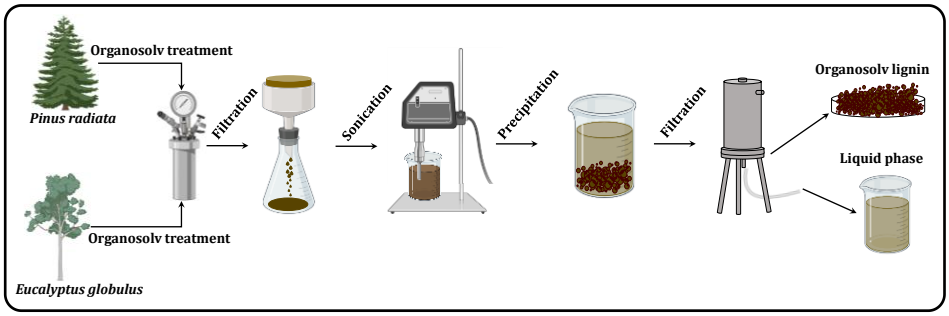

Figure M. 1. Scheme of the delignification process followed in this thesis

2.3. Synthesis procedure of bio-polyols

The bio-polyols produced in ***Publication I*** were obtained as described below (Figure M.2).

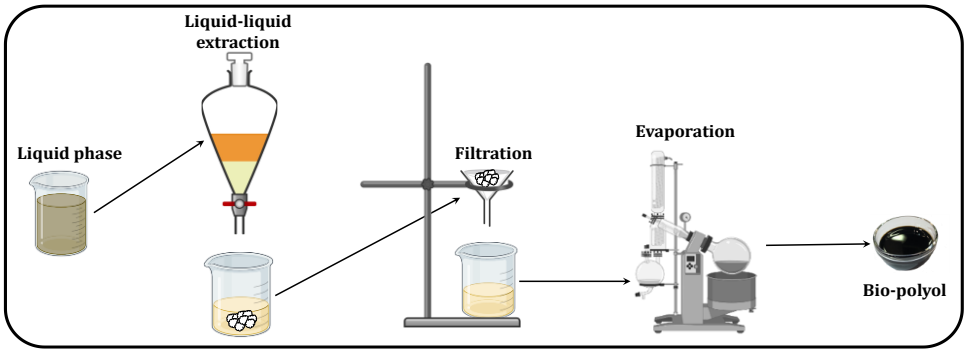

Figure M. 2. Diagram for obtaining the bio-polyols in ***Publication I***

After the delignification and lignin extraction processes described above, the resulting liquid phase was subjected to a liquid-liquid extraction with ethyl acetate. Four extractions were carried out employing a liquid phase/ethyl acetate ratio of 1:0.25 for each one, resulting in a final ratio of 1:1. Then, the organic phase was separated from the aqueous phase, filtered, and treated with anhydrous sodium sulphate to remove moisture. Finally, the ethyl acetate was evaporated under vacuum using a rotary evaporator to obtain the bio-polyol.

The synthesis of the bio-polyols of the ***Publications II and III*** were carried out by a liquefaction reaction employing microwave irradiation technology using a CEM Microwave Discover System Model with a temperature controller instrument and an internal temperature sensor. The reaction conditions to synthesise bio-polyols for rigid and elastic PUs were optimised using commercial PEG-400 and glycerol as solvents and sulphuric acid as catalyst. Then, employing the optimised reaction conditions the technical grade glycerol was substituted by a crude glycerol obtained from a used vegetable oil through transesterification reaction. The procedure followed to perform the reaction in both articles was the same (see Figure M.3) and is described below.

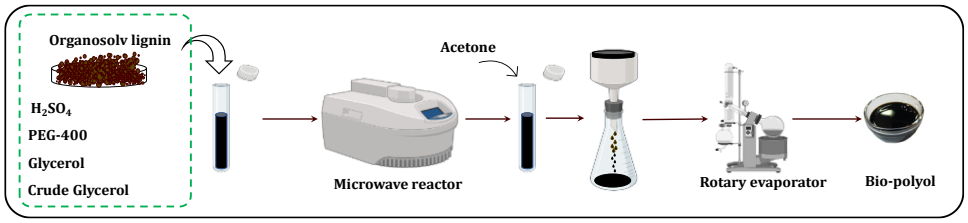

Figure M. 3. Synthesis of the bio-polyols formulated in ***Publication II and III***

Firstly, a predetermined amount of each component (lignin, PEG-400, glycerol and sulphuric acid) was weighed and mixed in the reactor vessel using a vortex. Once the sample (4g) was homogenised, the vessel was introduced into the microwave reactor and the reaction was carried out for 5 minutes under constant stirring. As soon as the reaction time finished, the reactor cooling system was activated to cool the vessel until 50°C. Then the vessel was introduced into a recipient with cold water to reach a safe handling temperature. Once finished, the obtained product was dissolved in acetone and filtered under vacuum to separate the solids. Finally, the liquid phase was evaporated using a rotary evaporator to obtain the final bio-polyol.

2.3.1. Scale-up of the liquefaction reaction

To synthesise the bio-polyols used in ***Publications IV and V***, a 10-fold scale-up of the reaction was performed using a CEM Microwave Discover 2.0 reactor with 100 ml capacity vessels. The reactions were carried out in the same way as in ***Publications II and III*** (see Figure M.3)

2.4. Transesterification of vegetable oil to obtain crude glycerol

The transesterification reaction of used vegetable oil to obtain the crude glycerol was carried out with methanol in a molar ratio of 6:1 (methanol:oil). The reaction was catalysed by KOH (1% wt. of oil). Oleic acid with a molecular weight of 884 g/mol was assumed as the predominant triglyceride for the calculations. The reaction was performed as follows: firstly, the oil was filtered to remove the impurities; then it was heated to 60 °C in a volumetric flask employing a heating plate with magnetic stirring (600 rpm).

Once the temperature of 60 °C was reached, a previously prepared methanol/KOH mixture was added. The reaction was kept for 120 min under reflux to maximise the conversion. The reaction was considered finished as soon as a good phase separation of the mixture was observed, and it was left for 24h in a separation funnel to separate the biodiesel and glycerol.

2.5. Synthesis procedure of lignin based polyurethane adhesive

A schematic diagram of the experimental procedure for the synthesis of lignin-based polyurethane adhesives (LPA) using commercial isocyanate is shown in Figure M.4.

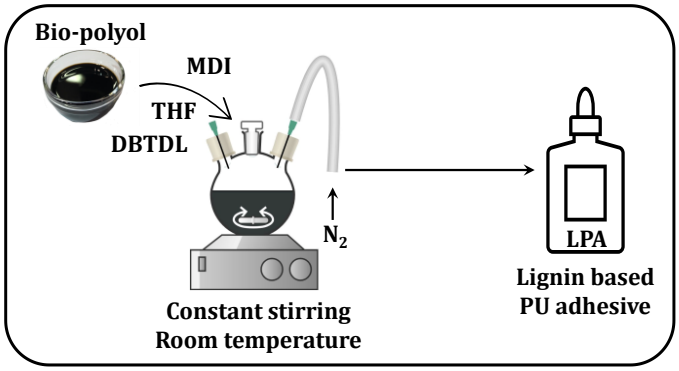

Figure M. 4. Schematic diagram of the synthesis of LPA adhesives

The synthesis was carried out using the one-shot method under inert atmosphere and room temperature. Firstly, the bio-polyol was poured together with the THF into the three necks round bottom flask and stirred vigorously, then the catalyst DBTDL and the MDI were added and stirred until the mixture could not flow, thus reaching the gel time. The different NCO/OH ratios used are listed in ***Publication IV***.

2.6. Synthesis procedure of lignin based non-isocyanate polyurethane adhesive

The synthesis of the lignin-based NIPU adhesive (LNA) was carried out through a polycondensation reaction using DMC and HDMA. The reaction process used was described by Saražin et al., (2021) [140] with some modifications.

A molar ratio between hydroxyl groups, DMC and HDMA (OH: DMC: HDMA) of (1:2:2) was employed. The reaction was performed under magnetic stirring and reflux. The bio-polyol was first reacted with the DMC and a predetermined amount of water (see ***Publication V***) for 60 minutes at 65°C temperature. After that, HDMA was added and kept for 120 minutes at 90°C.

Finally, a silane coupling agent, namely 3-Aminopropyltrimethoxysilane, was added to improve the adhesion properties of the NIPUs.

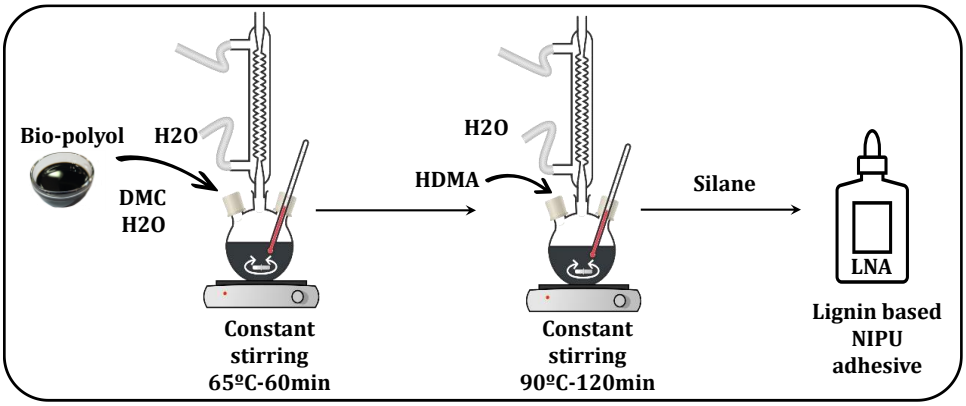

Figure M. 5. Procedure to synthesise LNA adhesives through polycondensation reaction between lignin-based bio-polyols with DMC and HDMA

2.7. Characterisation methods

A summary of the characterisation techniques used in the different publications included in this work is shown in Table M.3, which are described in detail in **Appendix II**.

Table M. 3. Characterisation techniques employed in the Publications

Characterisation	Publication						
	I	II		III		V	VI
	Bp	L	Bp	CG	Bp	LPA adhesive	LNA adhesive
Composition (GC-MS)	√	✗	✗	√	✗	✗	✗
Chemical structure (ATR-FTIR)	√	√	✗	√	✗	√	√
Molecular weight (GPC)	√	√	√	✗	√	✗	✗
IOH,An	√	✗	√	✗	√	✗	✗
Reological behaviour	√	✗	√	✗	√	✗	✗
Thermal degradation (TGA)	√	✗	✗	✗	√	√	√
Thermal Degradation kinetic & Lifetime estimation (TGA)	✗	✗	✗	✗	✗	√	√
Adhesion test (ABES)	✗	✗	✗	✗	✗	√	√

L: Lignin; Bp: Bio-polyol; CG:Crude glycerol

3rd PART

RESULTS AND DISCUSSION

OBTAINING AND SYNTHESIS OF BIO-POLYOLS

Remember, concentrate on the moment.

Feel, don't think. Use your instincts."

Qui-Gon Jinn

“Always two there are, no more, no less.

A master and an apprentice”

Master Yoda

Publication I

Renewable bio-polyols from residual aqueous phase resulting after lignin precipitation

ABSTRACT

The aim of this work was to obtain two bio-polyols from the liquid residue resulting from the precipitation of lignin contained in two different black liquors, *Eucalyptus globulus* organosolv black liquor (EOBL) and *Pinus radiata* organosolv black liquor (POBL), thus adding value to this residue. Eucalyptus Organosolv Polyol (EOP) and Pine Organosolv Polyol (POP) were characterised in order to know their viscosity, hydroxyl number (I_{OH}) and functionality according to the corresponding standard American Society for Testing Materials (ASTM). The molecular weight of bio-polyols was measured through Gel Permeation Chromatography (GPC), the chemical structure and composition were characterised by FTIR and GC-MS respectively and the thermal degradation (TGA) of two bio-polyols was determined. The bio-polyols showed suitable properties to be employed in the production of polyurethanes (PU).

1. MATERIALS AND METHODS

1.1. Materials

The raw materials, *Eucalyptus globulus* chips and *Pinus radiata* sawdust, as well as the reagents used in this publication are described in ***section 2.1*** of the **2nd PART**.

1.2. Delignification of raw materials and sonication treatments of the black liquors

The organosolv delignification processes of both raw materials, as well as the sonication treatments of the BLs are described in detail in ***section 2.2*** of the **2nd PART**.

1.3. Black liquor characterisation

BLs from *Eucalyptus globulus* (EOBL) and *Pinus radiata* (POBL) were characterised employing the corresponding TAPPI standards which are described in **Appendix I**.

1.4. Bio-polyol obtaining

The procedure for obtaining the bio-polyol from the residual aqueous phase resulting after lignin precipitation is described in ***section 2.3*** of the **2nd PART**

1.5. Bio-polyol characterisation

The two bio-polyols, EOP and POP obtained from EOBL and POBL respectively, were characterised employing the techniques listed in Table 2.3 of the **2nd PART**, **(*section 2.6*)**. These characterisation techniques are described in detail in Appendix II.

2. RESULTS AND DISCUSSION

2.1. Black liquors

Black liquors were characterised, and the results are outlined in Table P 1.1. As it was expected there were no significant differences in the pH and density values between both raw materials. Otherwise, although in the case of POBL a small amount of IM is observed, it can be concluded that in both cases the

TDS corresponded to the OM. However, in the case of POBL it was observed that lignin accounted for 61.62% of the organic matter while in the case of EOBL this percentage was 53.92%. The rest of the organic matter can be attributed to degradation products derived from the hemicellulosic fraction and to the extractives that were also solubilised in the liquor.

Table P1. 1 Characterisation of the black liquors

	Black liquor	
	Eucalyptus globulus	***Pinus radiata***
pH	3.600 ± 0.035	3.787 ± 0.031
Density (g/mL)	0.926 ± 0.003	0.911 ± 0.001
TDS	5.527 ± 0.373	2.313 ± 0.021
IM	0.027 ± 0.003	-
OM	5.509 ± 0.367	2.313 ± 0.021
Lignin (%)	2.970 ± 0.103	1.425 ± 0.076

2.2. Bio-polyol

As mentioned above, a triplicate of the organosolv treatments was performed for each raw material. The average yield of bio-polyols obtained was 5.45 ± 0.533% (EOP) and 5.24 ± 0.285% (POP) with respect the initial raw material.

The chemical structures of EOP and POP were analysed by FTIR. The chromatograms obtained by this technique are shown in Figure P1.1a and 1b. As can be seen in Figure P1.1a, both bio-polyols showed a broad band at 3400 cm^{-1} which corresponds to O-H stretchings of phenolic or alcoholic units. The characteristic vibration of aliphatic C-H bonds (3000-2840 cm^{-1}) was also visible [1]. On the other hand, in the fingerprint region (1800cm^{-1} – 800cm^{-1}) showed in Figure P1.1b, carbohydrates and lignin had their characteristic absorption peaks. Regarding the characteristic peaks of lignin, some small differences were observed that could be attributed to the different nature of the feedstock which was employed, since softwood is mostly composed by G

units while hardwood is usually formed by an equal amount of S and G units. In this sense, the signals from 1330 cm^{-1} to 815 cm^{-1} are referred to the bands that correspond to G units (1270 cm^{-1}, 815 cm^{-1}), S units (1330 cm^{-1}, 1114 cm^{-1}) and both G and S units (1026 cm^{-1}) [2–4].

It was also remarkable, that signals at wavenumbers of 1270 cm^{-1}, which corresponds to G ring plus C=O stretching in G units, was much more intense in the case of POP than in EOP where it appeared like a shoulder. Furthermore, the signal corresponding to C-H group in G units (815 cm^{-1}), was only visible in the sample coming from pine, while in the case of eucalyptus disappeared. These confirm that the bio-polyol from pine was richer in G units as it was expected for a softwood while bio-polyol from eucalyptus had more S units. The signal that corresponds to C=O in S units (1330 cm^{-1}) was only present in EOP while the aromatic deformation of C-H in S units (1114 cm^{-1}) gave a small signal also in the case of POP. It was also visible that the band at 1026 cm^{-1} associated with the aromatic ring in G units was more intense in the case of POP than in EOP as it was expected.

Finally, a variation in the intensity of the bands corresponding to the C=O stretching in conjugated arylketones (1674 cm^{-1}) and C-H deformation (1460 cm^{-1}) could also be observed [2]. In the case of POP, the signal assigned to C=O stretching increased while CH deformation band decreased. In the case of EOP the opposite occurred. As mentioned above, carbohydrate-related peaks also appeared in the fingertip region. Thus, peaks at 1603 cm^{-1}, 1424 cm^{-1}, 1114 cm^{-1} and 1026 cm^{-1} were indicative of the existence of carbohydrate-derived compounds [5].

The chemical composition of bio-polyols was determined through GC-MS whose chromatograms are shown in Figure P1.2. For a better understanding, the chromatograms were delimited in three zones named ***a***, ***b*** and ***c***. The first zone ***a***, corresponded to carbohydrate degradation compounds, which

confirmed the presence of these compounds in both samples, as mentioned in the previous section. It was possible to observe some differences between both samples due to the origin of the raw materials.

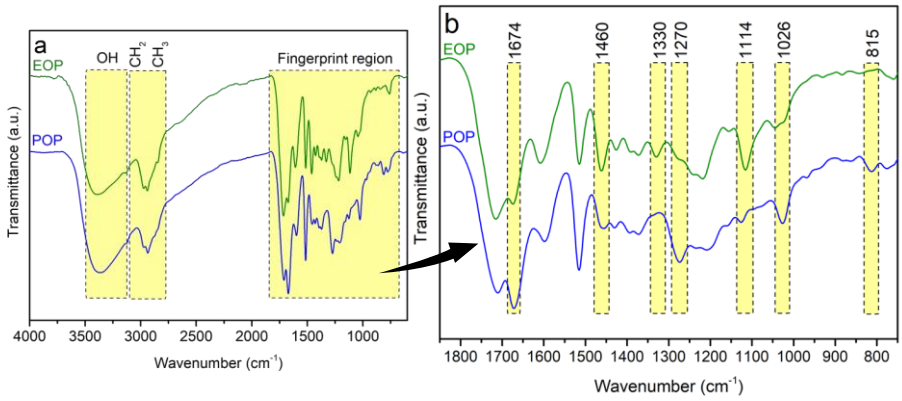

Figure P1.1 ATR-FTIR spectra (a) and Fingerprint region of FTIR spectra (b) of EOP and POP

Thus, in the case of EOP the most abundant peak corresponded to furfural and no HMF was observed. Since hardwood hemicelluloses are mainly constituted by pentoses, they are mostly decomposed in furfural. On the other hand, in the case of POP, which comes from softwood, the main peak corresponded to HMF, that is the principal degradation compound of hexoses [6]. Other degradation compounds such as ethyl glycolate and ethyl lactate from esterification of glycolic and lactic acid were observed.

In contrast, regions identified as ***b*** and ***c***, represented the compounds generated by the depolymerisation of lignin during organosolv delignification process in which the α and β ether bonds of lignin are hydrolytically broken [7].

Firstly, the zone noted as ***b*** is the region where the monomeric compounds of lignin were visible. As it was previously mentioned, there were differences between EOP and POP due to the origin of the feedstocks. Hence, EOP was

richer in S derived compounds, such as syringaldehyde among others, which was the most abundant. However, as it was expected, G derived compounds were also appreciable though in lesser proportion. On the other hand, G derived compounds were majority in POP as it is summarised in Table P1.2.

Finally, in the last section titled as ***c***, the presence of dimers and trimers could be observed, although with low abundance due to the low volatility of these compounds. Nevertheless, this could indicate that bio-polyols may contain bigger compounds derived from lignin depolymerisation, which were not visible in GC-MS.

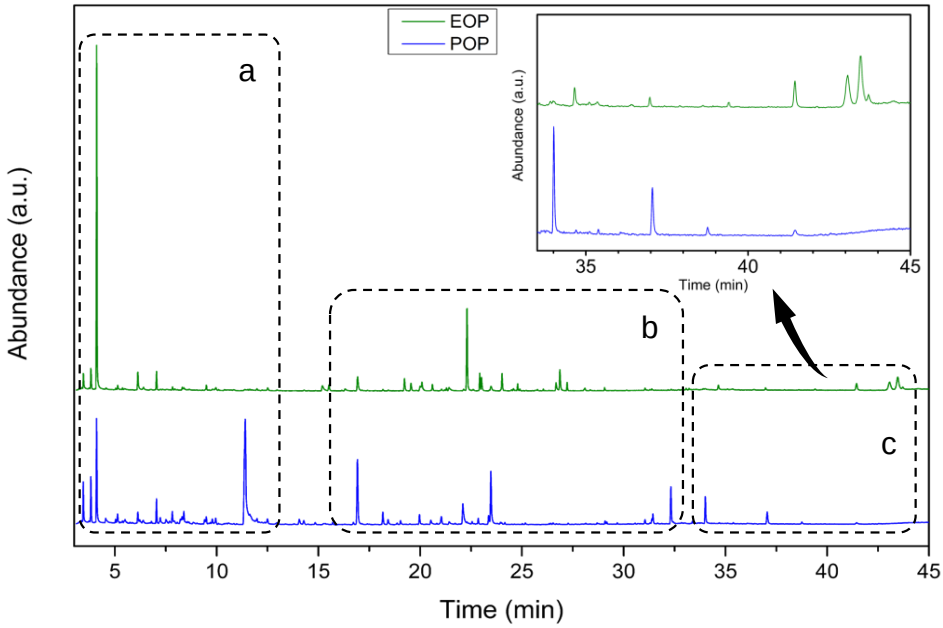

Figure P1.2 GC-MS chromatograms of EOP and POP

Table P1.2. Identification of the compounds from EOP and POP observed in CG-MS chromatograms

RT (min)	COMPOUND	EOP	POP	Origin
3.451	Ethyl glycolate	✓	✓	C
3.823	Ethyl lactate	✓	✓	C
4.107	Furfural	✓	✓	C
6.129	5-Methylfurfural	✓	✓	C
7.042	Ethyl 2-acetoxy-2-methylacetoacetate	✓	✓	C
11.045	Hydroxymethylfurfural (HMF)	✗	✓	C
16.992	Vanillin	✓	✓	G
22.101	Dihydroconiferyl alcohol	✗	✓	G
22.305	Syringaldehyde	✓	✗	S
22.934	4-propenyl syringol	✓	✗	S
23.014	Homosyringaldehyde	✓	✗	S
23.475	Coniferyl aldehyde	✗	✓	G
24.025	Syringylacetone	✓	✗	S
26.863	Sinapyl aldehyde	✓	✗	S
34.011	4,4'-stilbenediol,3,3'-dimethoxy-(E)	✗	✓	G#
37.053	3,4-Divanillyltetrahydrofuran	✗	✓	G#
38.755	Secoisolariciresinol	✗	✓	G#
41.443	4,4'-stilbenediol,3,3',5,5'-tetramethoxy-	✓	✗	S#
41.451	Dibenzylbutyrolactone	✗	✓	G#
43.265	Syringaresinol	✓	✗	S#

C (Carbohydrate), G (Cuaiacol), S (Syringol), # Two phenolic rings

EOP and POP were thermogravimetrically analysed in order to study the relationship between chemical structure and degradation. The TGA thermograms for each bio-polyol and its corresponding DTG are shown in Figure P1.3.

The DTG curves revealed clear differences between both bio-polyols. Firstly, the EOP showed three peaks that corresponded to two degradation zones. The first degradation zone, which represents a total mass loss of 37.64%, was located in the range from 120 °C to 260 °C and it can be associated with the degradation of monomeric compounds from lignin [8] and the degradation

of carbohydrates [9]. This region had two maximum degradation peaks, one at 130 °C which is associated with the most volatile compounds accounting for 10.33% of the mass loss, and the second at 236 °C that is related to the monomeric compounds with higher boiling points [8] and represented a mass loss of 27.31%. The last degradation zone (300 °C-500 °C) had a maximum degradation peak at 331 °C and the largest mass loss with 29.76% of the total mass. This zone is usually attributed with the degradation of lignin, hence it could be attributed to dimers, trimers and oligomers which are expected to be in the bio-polyol [10].

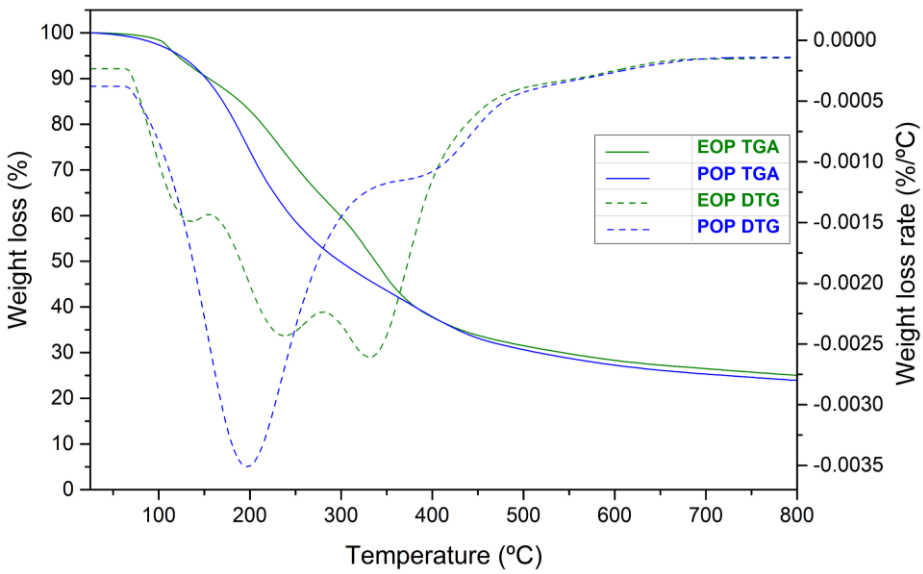

Figure P1.3. TGA and DTG thermograms of EOP and POP

POP, for its part, even though had the same two degradation areas, did not show the same peaks. Thus, in the first degradation zone, which accounted for 52.14% of mass loss, it showed a single maximum degradation peak at 200 °C. Whereas the zone identified as the degradation zone of larger lignin molecules, the maximum degradation peak at about 380 °C is shoulder-shaped and represented only the 16.2% of the total mass loss. In both cases,

as the temperature was increased over 500 °C, a loss of mass of about 75% took place, and a total residue of 25.07% and 23.96% was left, respectively.

The molecular weight distribution of each bio-polyol was analysed in order to determine M_w, M_n and PI. As expected, due to the origin of bio-polyols, both showed low molecular weights compounds ranging from 848 g/mol to 235 g/mol. Since the detection limit of the equipment is around 230 g/mol, hemicellulose degradation compounds, such as furfural and HMF among others, and lignin derived small monomers are outside the detection range. However, it can be concluded that bio-polyols were also composed by dimers and oligomers from the depolymerisation of lignin during the delignification process. Furthermore, the average molecular weights and polydispersity index (PI) of both bio-polyols were very similar as summarised in Table P1.3.

As regards the PI, which is an important factor to consider, since it has a direct effect on the applicability of the bio-polyol [11], EOP and POP showed low values, 1.493 and 1.579 respectively. This indicated a homogeneous molecular weight distribution for both bio-polyols. Furthermore, these values were very similar to those of industrial polyethers and polyesters, 1.05 and 1.3 respectively [11].

Table P1.3. M_w (g/mol), M_n (g/mol) and PI of EOP and POP

Bio-polyol	M_w (g/mol)	M_n (g/mol)	PI
EOP	648	437	1.493
POP	563	357	1.579

As can be seen in Figure P1.4, there were three clear signals in both chromatograms with virtually equal retention times in both cases (24.8 min, 25.8 min and 26.7 min). Nevertheless, there were differences in the intensities of these signals, indicating that the distribution of molecular weights was different in each case. Thus, the first peak (24.8 min) was more

intense in the case of EOP, which indicated a higher concentration of trimers and oligomers (M_w ≈815 g/mol) than in the POP, which was in accordance with the results from TGA analysis.

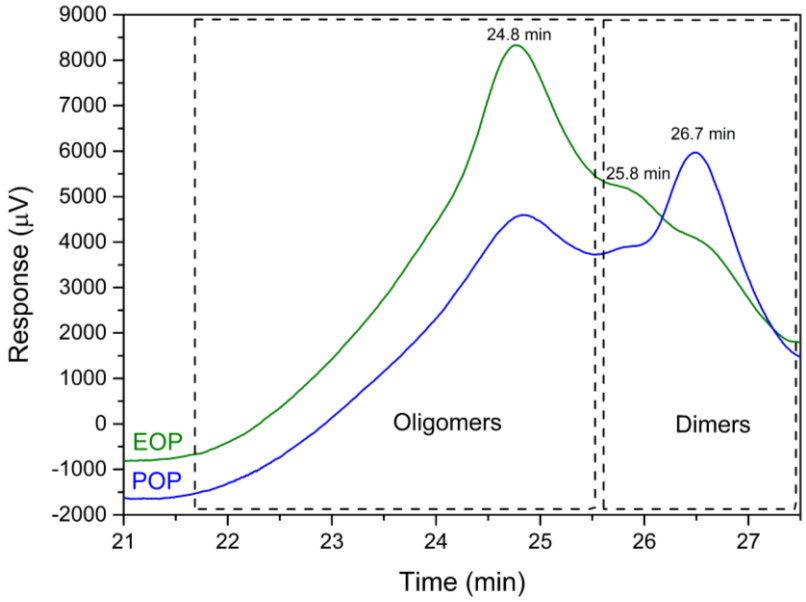

Figure P1.4. Molecular weight distribution of EOP and POP

Signals displayed at 25.8 min and 26.7 min retention times corresponded to areas with molecular weights of around 274 g/mol and 235 g/mol respectively, indicating the presence of dimers in bio-polyols. This last signal showed an intense peak in POP whereas in EOP chromatogram it was only a shoulder. This would indicate a higher number of dimmers in POP than in EOP. However, taking into account the obtained results, it can be concluded that the molecular weights of both bio-polyols are in the required range (200-8000 g/mol) for PU production [12].

Acidic number (A_n), hydroxyl number (I_{OH}) and functionality (*f*) of bio-polyols are summarised in Table P1.4.

Table P1.4. A_n, I_{OH} and f of EOP and POP

Bio-polyol	A_n (mg KOH/g)	I_{OH} (mg KOH/g)	*f*
EOP	85.06 ± 2.51	618.07 ± 9.79	4.81
POP	64.34 ± 1.69	587.63 ± 0.63	3.74

As can be seen, two bio-polyols presented an elevated A_n, 85.06 and 64.31 mg KOH/g for the EOP and POP respectively. These high A_n values were due to the generation of organic acids such as formic, levulinic, acetic, glycolic and lactic acid during the organosolv delignification process. A low A_n value is preferable, since acid groups can react with the amine groups of the catalyst decreasing the efficiency of the reaction [13]. However, polyols from lignocellulosic biomass usually presented high A_n values, which can be greater than 40 mg KOH/g [12].To solve this problem, bio-polyols could be neutralised using bases such as NaOH or MgOH before their employment to produce PU [14].

The EOP and POP I_{OH} values were 618.07 mg KOH/g and 587 mg KOH/g respectively. Similar values of I_{OH} were obtained by other authors through liquefaction of lignin [15–18]. Gosz et al., (2018) [15] used Kraft pine lignin to produce bio-polyols through liquefaction obtaining 610-670 mg KOH/g of I_{OH} value. Similarly, Da Silva et al., (2019) [17] employed Kraft lignin to obtain bio-polyols with 660 mg KOH/g when employing lactic acid as catalyst. In another case, I_{OH} values of 538 mg KOH/g were achieved through liquefaction of commercial lignin by Mohammadpour et al., (2020) [18]. These relatively high values can be explained by the presence of compounds with abundant OH-reactive groups, such as dimers and oligomers from lignin, among others. These lignin derived compounds were formed during the delignification process in which lignin molecules were broken into smaller fragments that were solubilised in the medium [19]. On the other hand, the presence of these lignin derived compounds, explains the functionality values that were obtained. The I_{OH} and functionality values indicate that the bio-polyols could

be used for the manufacture of PU, such as rigid foams, rigid coatings and elastoplastics which required polyols with a I_{OH} values from 250-1000 mg KOH/g and functionalities of 3-8 [20].

Finally, the rheological behaviour of bio-polyols was analysed. Firstly, an oscillatory test was carried out to determine the viscoelastic properties of the two bio-polyols. For this purpose, a comparison was made between the loss module or viscous module (G'') and the storage or elastic module (G') used to measure the degree of liquid and solid of the bio-polyol respectively [21]. Figures P1.5a and b show that the two polyols had a liquid behaviour since G" presented higher values than G' over the entire frequency range. In addition, as it was expected taking into account the molecular weights of the two bio-polyols (Table P1.3), the values of EOP modules were higher than those obtained from POP since they decrease as the M_w is reduced [22].

Additionally, a rotational test was performed to analyse the fluid behaviour through the study of the relation between viscosity (η), shear stress (τ) and shear rate ($\dot{\gamma}$). The parameters were fitted to the Power-Law equation as indicated in ***section V*** of **Appendix II**. A summary of the data obtained by the software is shown in Table P1.5 and the corresponding flow curves are presented in Figure P1.6a.

Table P1.5. Power-Law linear functions base don the rheological data from EOP and POP

Bio-polyol	κ(Pa·sⁿ)	n	R^2
EOP	0.016710	0.9650	0.9983
POP	0.005897	0.9226	0.9418

As can be seen from the study of the data summarised in Table P1.5, both rheograms showed a good fit as indicated by the R^2 values. In addition, the n values were very close to unity, indicating that both bio-polyols behaved as Newtonian fluids. This behaviour can be observed in Figure P1.6a, where the

viscosity had a constant value regardless of the applied strain rate. Thus, it can be said that consistency index is simply the constant viscosity, η [23].

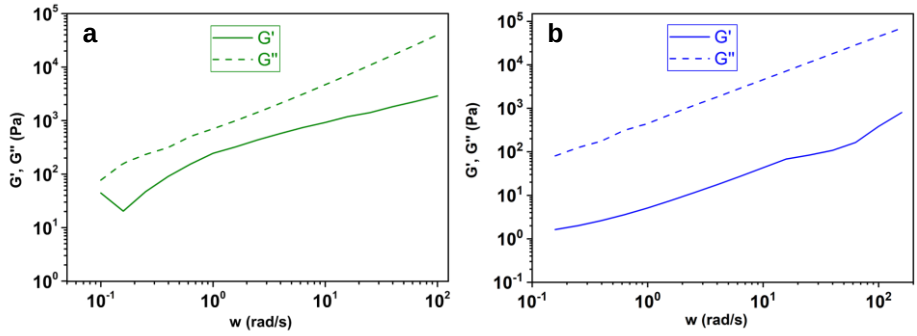

Figure P1.5. Storage (G') and loss (G") modulus (Pa) as a function of ω(rad/s) of EOP (a) and POP (b)

Nevertheless, in order to confirm the Newtonian behaviour of the bio-polyols, the relation between shear stress (τ) and shear rate ($\dot{\gamma}$) was studied and they were represented in Figure P1.6b.

It was possible to confirm that both had a linear relation as it is expected from a Newtonian fluid where the slope of the line must correspond to the viscosity. This was confirmed since the slopes of the lines in Figure 6b were exactly the same of the κ values reported in table 5. Thus, EOP had a viscosity of 0.0168 $Pa \cdot s$ while the viscosity of POP was 0.0059 $Pa \cdot s$.

These values are very low but they are in accordance with the obtained by other authors [16,17] and are below 300 Pa·s which resulted suitable values for PU production [24]. The higher in viscosity values in EOP could be explained by its higher molecular weight comparing to POP since viscosity is intrinsically related to the molecular weight [25].

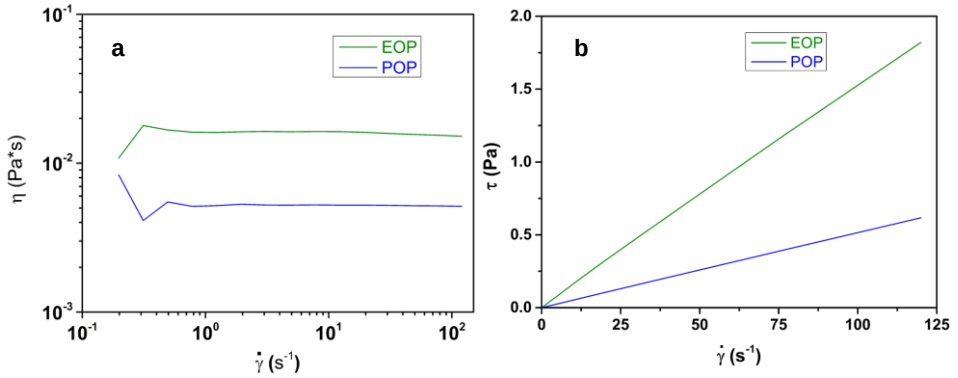

Figure P1.6. (a) Viscosity (η) VS shear rate ($\dot{\gamma}$) and (b) Shear stress (τ) VS shear rate ($\dot{\gamma}$) of EOP and POP

3. CONCLUSIONS

In summary, two bio-polyols were obtained from the aqueous residue resulting from the precipitation of the lignin contained in the organosolv liquors. Yields of 5.43% and 5.24% were obtained with respect to the initial raw material for EOP and POP respectively. The average molecular weights of these bio-polyols were 648 g/mol for EOP and 563 g/mol for POP and polydispersity indexes of 1.493 and 1.579 respectively, which were very similar to those for industrial polyether and polyester polyols (1.05 and 1.3 respectively). On the other hand, I_{OH} and functionalities values were 618mg KOH/g and 4.81 in the case of EOP and 587 mg KOH/g and 3.74 in the case of POP. However, due to the origin of the bio-polyols, the acidic numbers of both bio-polyols were elevated. Finally, the study of the rheological behaviour of the bio-polyols revealed that both bio-polyolss behaved as Newtonians fluids with viscosity values of 0.0168 $Pa \cdot s$ and 0.0059 $Pa \cdot s$ for EOP and POP respectively. All these characteristics indicated that both bio-polyols were suitable for the manufacture of polyurethanes. Therefore, the aqueous residue from organosolv black liquors was successfully valorised.

REFERENCES

[1] Z. Chi, Z. Wang, Y. Liu, G. Yang, Chem. Eng. J. 331(August 2017) (2018) 317–25. 10.1016/j.cej.2017.08.121.

[2] L. Chen, X. Wang, H. Yang, Q. Lu, D. Li, Q. Yang, H. Chen, J. Anal. Appl. Pyrolysis 113 (2015) 499–507.

[3] J. Fernández-Rodríguez, X. Erdocia, C. Sánchez, M. González Alriols, J. Labidi, J. Energy Chem. 26(4) (2017) 622–31. 10.1016/j.jechem.2017.02.007.

[4] X. Jiang, (5) (2012) 827–33. 10.1002/ceat.201000400.

[5] A. Morales, F. Hernández-ramos, L. Sillero, R. Fernández-marín, 315(May) (2020). 10.1016/j.biortech.2020.123896.

[6] F. Hernández-Ramos, J. Fernández-Rodríguez, M.G. Alriols, J. Labidi, X. Erdocia, Fuel 280(February) (2020) 118524. 10.1016/j.fuel.2020.118524.

[7] Z. Zhang, M.D. Harrison, D.W. Rackemann, W.O.S. Doherty, I.M. O'Hara, Green Chem. 18(2) (2016) 360–81. 10.1039/c5gc02034d.

[8] M.M. Jensen, D.T. Djajadi, C. Torri, H.B. Rasmussen, R.B. Madsen, E. Venturini, I. Vassura, J. Becker, B.B. Iversen, A.S. Meyer, H. Jørgensen, D. Fabbri, M. Glasius, ACS Sustain. Chem. Eng. 6(5) (2018) 5940–9. 10.1021/acssuschemeng.7b04338.

[9] C. Girometta, D. Dondi, R.M. Baiguera, F. Bracco, D.S. Branciforti, S. Buratti, S. Lazzaroni, E. Savino, Cellulose 27(11) (2020) 6133–48. 10.1007/s10570-020-03208-4.

[10] A. Morales, B. Gullón, I. Dávila, G. Eibes, J. Labidi, P. Gullón, Ind. Crops Prod. 124(May) (2018) 582–92. 10.1016/j.indcrop.2018.08.032.

[11] J. D'Souza, R. Camargo, N. Yan, Polym. Rev. 57(4) (2017) 668–94. 10.1080/15583724.2017.1283328.

[12] S. Hu, X. Luo, Y. Li, ChemSusChem 7(1) (2014) 66–72. 10.1002/cssc.201300760.

[13] S. Hu, Y. Li, Ind. Crops Prod. 57 (2014) 188–94. 10.1016/j.indcrop.2014.03.032.

[14] W. Jiang, A. Kumar, S. Adamopoulos, Ind. Crops Prod. 124(March) (2018) 325–42. 10.1016/j.indcrop.2018.07.053.

[15] K. Gosz, P. Kosmela, A. Hejna, G. Gajowiec, Ł. Piszczyk, Wood Sci. Technol. 52(3) (2018) 599–617. 10.1007/s00226-018-0991-4.

[16] R. Briones, L. Serrano, J. Labidi, J. Chem. Technol. Biotechnol. 87(2) (2012) 244–9. 10.1002/jctb.2706.

[17] S.H.F. da Silva, I. Egüés, J. Labidi, Ind. Crops Prod. 137(March) (2019) 687–93. 10.1016/j.indcrop.2019.05.075.

[18] R. Mohammadpour, G. Mir Mohamad Sadeghi, J. Polym. Environ. 28(3) (2020) 892–905. 10.1007/s10924-019-01650-5.

[19] R. El Hage, N. Brosse, P. Sannigrahi, A. Ragauskas, Polym. Degrad. Stab. 95(6) (2010) 997–1003. 10.1016/j.polymdegradstab.2010.03.012.

[20] Y. LI, X. LUO, S. HU, Bio-based Polyols and Polyurethanes, Springer, 2015.

[21] Y.C. Tseng, Y.C. Hsieh, N.Y. Chin, W.Y. Huang, S.S. Hou, J.S. Jan, Polymer

(Guildf). 196(1) (2020) 122426. 10.1016/j.polymer.2020.122426.

[22] K. Behera, Y.H. Chang, F.C. Chiu, J.C. Yang, Polym. Test. 60 (2017) 132–9. 10.1016/j.polymertesting.2017.03.015.

[23] P. Parcheta, J. Datta, Polym. Test. 67(January) (2018) 110–21. 10.1016/j.polymertesting.2018.02.022.

[24] C.A. Cateto, M.F. Barreiro, A.E. Rodrigues, M.N. Belgacem, Ind. Eng. Chem. Res. 48(5) (2009) 2583–9. 10.1021/ie801251r.

[25] S.H.F. da Silva, P.S.B. dos Santos, D. Thomas da Silva, R. Briones, D.A. Gatto, J. Labidi, J. Wood Chem. Technol. 37(5) (2017) 343–58. 10.1080/02773813.2017.1303513.

“Patience you must have my young Padawan”

Master Yoda

Publication II

Organosolv lignin-based bio-polyols for polyurethane production: Process optimisation through response surface methodology

ABSTRACT

The polyurethane industry relies on polyols of petrochemical origin. However, although the polyol industry is a growing business, the environmental consequences associated with the excessive petroleum consumption can be serious. Therefore, the use of renewable raw materials, such as lignin, to manufacture bio-polyols is being studied to replace partially or totally the use of petrochemical polyols. Lignin is the most abundant renewable phenolic polymer available on Earth and can be employed for different industrial applications, such as polyurethane manufacture, thus diminishing the dependence on oil. In this work, hardwood (*Eucalyptus globulus*) and softwood (*Pinus Radiata*) organosolv lignins were employed for producing bio-polyols, through microwave assisted liquefaction, with specific properties to be used in the synthesis of rigid and elastic polyurethanes. The reaction parameter values were optimised by response surface methodology to establish the most suitable conditions to produce bio-polyols from both type of lignins for rigid and elastic polyurethane formulation.

The effect of the independent variables catalyst concentration (%wt.), temperature (°C) and Polyethylene glycol/Glycerol weight ratio on the molecular weight and hydroxyl number index of bio-polyols was evaluated. The optimum reaction conditions of bio-polyols for rigid polyurethanes were virtually equal for the two lignins, 159-161°C, Polyethylene glycol/Glycerol

ratio of 3 and no catalyst. Conversely, the bio-polyols for elastic polyurethanes required different reaction parameters depending on the lignin used, 180 °C, 7.57 (Polyethylene glycol/Glycerol ratio) and 5% wt. of catalyst for hardwood lignin and 160 °C, 7.34 (Polyethylene glycol/Glycerol ratio) and 3.85% wt. of catalyst for softwood lignin. In addition, the bio-polyols obtained at optimised conditions were fully characterised and acid number, polydispersity index, functionality and the rheological behaviour of them was studied.

1. MATERIALS AND METHODS

1.1. Materials

The raw materials and chemicals used for this work were obtained as described in s***ection 2.1*** of the **2nd PART.**

1.2. Lignin obtaining procedure

Lignin used in this work were obtained after the organosolv delignification process and the subsequent ultrasound treatment of the black liquor described in ***section 2.2*** of the **2nd PART**.

1.3. Lignin characterisation

Eucalyptus globulus and *Pinus radiata* organosolv lignins obtained before (EOL and POL) and after ultrasound treatment (EOUL and POUL) were analysed using the techniques listed in Table 2.3 of the **2nd PART**, **(*section 2.6*)** and described in **Appendix II**.

1.4. Experimental design of microwave assisted lignin liquefaction

1.4.1. Microwave assisted lignin liquefaction procedure

Liquefaction reaction of lignins obtained after ultrasound treatment was carried out through the methodology described in ***section 2.3*** of the **2nd PART**.

1.4.2. Experimental design

A response surface methodology (RSM) was used to determine the effect of the independent variables: Catalyst concentration (%wt.) (Cat), Temperature (°C) (Temp) and Polyethylene glycol/Glycerol weight ratio (%wt.) (PEG/Gly) on the molecular weight (M_w) and hydroxyl number index (I_{OH}) of bio-polyols. A three block Box-Benkhen Design (BBD), which consisted in 15 experiment, with three central point was selected for the experimental design and optimisation.

A second-order polynomial equation (Equation P2.1) was used to fit the experimental data:

$$y = b_0 + \sum_{i=1}^{3} b_i x_i + \sum \sum_{i<j=2}^{3} b_{ij} x_i x_j + \sum_{i=1}^{3} b_{ii} x_i^2 + \varepsilon \qquad \text{Equation P2.1}$$

where y_j represent the dependent variables (M_w and I_{OH}), b_0, b_i, b_{ii}, b_{ij} correspond to the regression coefficients estimated from the experimental results employing the least-squares method and x_i and x_j are the dimensionless normalised independent variables Cat, Temp and PEG/Gly, with a variation range from -1 to 1.

Through the evaluation of the lack of fit, the R^2 determination coefficient, the significance of the regression coefficients and the F-test value obtained from the analysis of variance, the suitability of the model was validated. The

experimental design, statistical analysis and regression model were generated employing the Statgraphics Centurion version XVI (Statpoint Technolgies Inc., Warrenton, VA, USA). Optimal conditions to produce polyols for rigid and elastic PU, predicted by the desirability function of the abovementioned software, were obtained by adjusting the dependent variables M_w and I_{OH}. Microsoft Excel´s Data Analysis Add-In version 2016 (Microsoft, USA), was employed to fit the experimental data. Model validation was carried out by performing a triplicate of each experiment under optimal conditions and comparing them with the values predicted by the model.

Table P2.1. Experimental design involved in the study

Variable	Definition	Units	Nomenclature	Value
Fixed	Time	min		5
	SLR*	(w/w)		1/6
Independent	Catalyst	(% wt.)	Cat	0-5
	Temperature	°C	Temp	140-180
	PEG/Gly ratio	(w/w)	PEG/Gly	3-9
Dependents	Molecular weight	g/mol	M_w	
	Hydroxyl number	mg KOH/g	I_{OH}	

*Solid to liquid ratio (SLR)

The experimental variables considered in this study (Table P2.1), include the fixed variables, the independent variables, as well as the dependent ones, including the corresponding variation ranges of each variable.

1.4.3. Characterisation of the obtained bio-polyols

Bio-polyols synthesised to perform the experimental design were analysed to determine the molecular weight distribution (M_w, M_n and M_w/M_n) as well

as the I_{OH}. For the determination of the molecular weight distribution, GPC was employed following the procedure described in **Appendix II**.

1.4.4. Characterisation of bio-polyols at the optimised reaction conditions

To validate the model, experiments were triplicated under the optimal conditions and the results (M_w and I_{OH} values) were compared with the theoretical ones. Once the model was validated, the bio-polyols obtained under the optimal conditions were further characterised employing the techniques listed in Table 2.3 of the **2nd PART**, **(*section 2.6*)**. These characterisation techniques are described in detail in **Appendix II.**

2. RESULTS AND DISCUSSION

2.1. Lignin characterisation

Since lignins with low molecular weight are desired to produce polyols [1], the obtained EOL and POL were ultrasonicated. These ultrasonicated lignins, called EOUL and POUL from the ultrasonication of EOL and POL respectively, showed lower molecular weight than the originals as summarised in Table P2.2.

Table P2.2. Mw (g/mol), Mn (g/mol) and PDI of organosolv lignins and ultrasonicated organosolv lignins

Sample	M_w (g/mol)	M_n (g/mol)	PDI
EOL	3632	952	3.81
EOUL	2837	888	3.20
POL	3529	1035	3.41
POUL	2924	911	3.21

In both cases, similar molecular weight reduction was achieved with respect to the original lignins. Concretely, a 21.8% reduction in the case of EOUL and 17.1% for POUL. The molecular weight reduction, although considerable, was far from that obtained by Wells et al. (2013) [2], who obtained a reduction of 85.9% under the studied conditions.

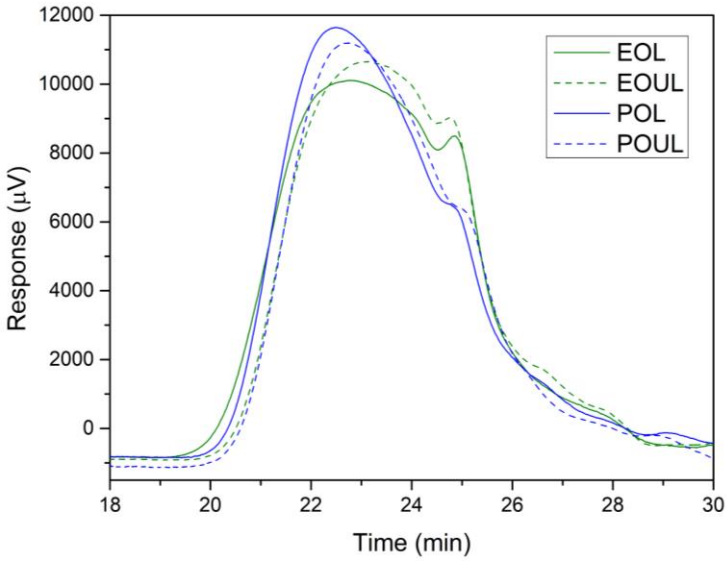

Figure P2.1. Molecular weight distribution of organosolv lignins

This difference could be due to a lower effect of cavitation because of the employed equipment. This decrease in the molecular weights can be observed in Figure P2.1 since the chromatograms corresponding to the ultrasonicated lignins (EOUL and POUL) exhibited lower retention times than the original ones.

ATR-FTIR spectroscopy was employed to characterise lignins to confirm that their chemical structure was not altered during the ultrasound fractionation process. As can be seen in Figure P2.2, no differences were observed between lignin samples from the same raw material before and after being subjected

to the ultrasonication process. Thus, it can be concluded that the ultrasound process did not produce any changes in the chemical structure of the lignins.

As can be observed, the fingerprint region of the ATR-FTIR spectra (Figure P2.2) showed the characteristic bands of lignin. In all samples a broad peak (3415 cm^{-1}) corresponding to OH stretching of phenolic units is observed. The vibration of aliphatic CH bonds was also visible at between 2970 cm^{-1} and 2840 cm^{-1}. The band of carbonyl group, the vibration of the aromatic skeleton plus CO stretching and the stretching of CC plus C-O plus C=O at 1705 cm^{-1}, 1595 cm^{-1} and 1213 cm^{-1} respectively appeared in all samples. Nevertheless, since hardwood lignins are generally composed by an equal proportion of S and G units, whereas softwood lignin is predominantly constituted by G units several differences could be observed between lignin from hardwood and softwood. Thus, the spectra of lignin from *Eucalyptus globulus* showed more intense signal in the peaks at 1326 cm^{-1}, 1110 cm^{-1} and 833 cm^{-1}. These bands correspond to the condensed S and G rings, the aromatic CH deformation of S units and to CH group out of plane in positions 2 and 6 in S units. On the other hand, in the case of lignin from *Pinus radiata*, the signals were more intense in the bands corresponding to the G units, i.e: vibration of the aromatic ring in G units (1510 cm^{-1}), G ring plus CO (1265 cm^{-1}), aromatic CH in plane deformation of G units (1029 cm^{-1}) and CH out of plane in position 2, 5 and 6 in G units (860 cm^{-1} and 811 cm^{-1}) [3].

2.2. Optimisation of the conditions for obtaining suitable bio-polyols for PU applications

In the present study, microwave-assisted irradiation method was employed. A response surface methodology in combination with a Box-Behnken design was employed to accomplish the optimisation of the bio-polyols obtaining reaction conditions. Statgraphic software was used to establish the experiments set, which is summarised in Table P2.3, as well as the

experimental values that corresponded to the dependent variables (Y_{IOH} and Y_{Mw}).

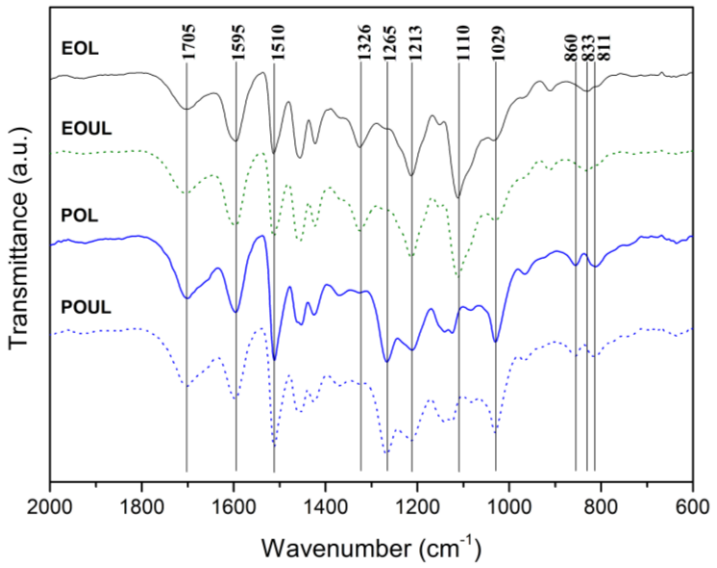

Figure P2.2. Fingerprint region of ATR-FTIR spectra of non-ultrasonicated and ultrasonicated organosolv lignins

Regarding Table P2.3, the I_{OH} values ranged from 221.5 mgKOH/g (exp. 3) to 688.2 mgKOH/g (exp. 10) for *Eucalyptus globulus* bio-polyol, and from 211.3 mgKOH/g (exp. 1) to 592.6 mgKOH/g (exp. 4) for *Pinus radiata* bio-polyol. On the other hand, M_w ranged between 1637 g/mol (exp. 13) and 5692 g/mol (exp. 6) and between 1372 g/mol (exp. 14) and 5469 g/mol (exp. 2) for the bio-polyols obtained from the liquefaction of lignin from *Eucalyptus globulus* and *Pinus radiata,* respectively.

In Table P2.4 the regression coefficients and their corresponding confidence levels according to Student's t-test (above 90%), as well as the R^2 determination coefficient, the adjusted R^2 and the statistical significance (Fisher's F-test) are summarised. $F_{\alpha=0.05}$, which is the value of the distribution that leaves an area behind the density function equal to 0.05 on its right (95% of confidence level), was calculated employing the free software R (version

4.1.1) were the degrees of freedom are expressed through Equation P2.2. On the other hand, the experimental *F* (*F*-exp) was determined using Equation P2.3.

$$\text{Degrees of freedom} = K; n-(K+1) \qquad \text{Equation P2.2}$$

$$F = \frac{R^2/K}{(1-R^2)/[n-(K+1)]} \qquad \text{Equation P2.3}$$

where *K* is the number of model parameters, *n* is the number of data points and R^2 is the determination coefficient.

Table P2.3. Independent normalised (Norm.) and not normalised (Not norm.) variables, Cat (%wt.) (X_1); Temperature (°C) (X_2) and PEG/Gly (w/w) (X_3), together with the dependent variables, average molecular weight (Y_{Mw}) (g/mol) and hydroxyl number (Y_{IOH}) (mgKOH/g), of the Box-Behnken experimental design

Exp	Independent variables						Dependent variables			
	Not norm. variables			Norm. Variables			*Eucalyptus globulus*		*Pinus radiata*	
	Cat	T (°C)	PEG/Gly (w/w)	X_1	X_2	X_3	Y_{Mw}	Y_{IOH}	Y_{Mw}	Y_{IOH}
1	2.5	180	9	0	1	1	3532	236	3576	211
2	2.5	160	6	0	0	0	2904	312	5469	294
3	0	180	6	-1	1	0	1752	222	1710	331
4	2.5	180	3	0	1	-1	3753	563	4896	593
5	2.5	140	9	0	-1	1	2169	243	4012	321
6	5	180	6	1	1	0	5926	290	4594	383
7	0	140	6	-1	-1	0	1662	261	1461	330
8	5	160	3	1	0	-1	3854	688	5136	552
9	2.5	160	6	0	0	0	3005	263	4469	232
10	2.5	140	3	0	-1	-1	2269	485	2922	457
11	5	160	9	1	0	1	3623	224	4116	194
12	2.5	160	6	0	0	0	2700	290	4077	247
13	0	160	9	-1	0	1	1637	326	1497	354
14	0	160	3	-1	0	-1	1771	645	1372	458
15	5	140	6	1	-1	0	3472	248	3991	262

Table P2.4. Regression coefficient plus their statistical parameters

Coefficients	*Eucalyptus globulus*		*Pinus radiata*	
	Y_{Mw}	Y_{IOH}	Y_{Mw}	Y_{IOH}
b_0	2869.67[a]	288.02[a]	4671.67[a]	257.78[a]
b_1	1256.63[a]	-0.43	1474.63[a]	-10.04
b_2	673.88[a]	13.85	298.75	18.42
b_3	-85.75	-164.38[a]	-140.63	-122.31[a]
b_{12}	591.00[b]	20.40	88.50	29.96[c]
b_{13}	-24.25	-36.49	-286.25	-63.49[a]
b_{23}	-30.25	-11.99	-602.50[c]	-61.37[a]
b_{11}	61.92	23.42	-1276.96[a]	31.27[c]
b_{22}	271.42	-56.36[c]	-455.71	37.30[c]
b_{33}	-210.33	159.27[a]	-364.46	100.30[a]
R^2	0.97	0.97	0.96	0.98
R^2-adjusted	0.92	0.90	0.87	0.95
$F_{\alpha=0.05}$	4.773			
F-exp	19.516	15.463	11.795	28.588
Area under *F*-exp	0.002	0.004	0.007	0.001
Significance level	99.779	99.618	99.287	99.911

[a]Significant coefficients at the 99% of confidence level.
[b]Significant coefficients at the 95% of confidence level.
[c]Significant coefficients at the 90% of confidence level.

According to Table P2.4, the obtained R^2 determination coefficients were above 0.95 in all cases. Regarding the bio-polyol obtained from the liquefaction of *Eucalyptus globulus* lignin, R^2 of 0.97 was obtained for both M_w and I_{OH}, while for the polyol obtained from the liquefaction of *Pinus radiata* lignin these values were 0.96 for M_w and 0.98 for I_{OH}. This indicated that only a small number of total variations remained unexplained using the selected model, concretely 3% for the former and 4% and 2% for the latter. According with the obtained R^2 determination coefficients, it could be concluded that the model was appropriate to describe the interactions between the selected variables, since the R^2 determination coefficient indicate the validity of the design via the explanation of the total variations of the model [4].

Furthermore, the predictivity of the model obtained through Fisher's F-test confirmed that the selected model was statistically relevant since the *F*-experimental values were higher than the F_α values in all cases, which indicates that the models were statistically relevant above 95%. [5].

Regression coefficients presented in Table P2.4 showed a different behaviour depending on the used raw material. Thus, X_1, X_2 and the interaction X_{12} were the most relevant independent variables for the molecular weight in the case of the bio-polyol obtained from *Eucalyptus globulus*, while in the case of the bio-polyol from *Pinus radiata* it was the independent variable catalyst concentration X_1, the interaction X_{23} and the quadratic effect of X_{11}. On the other hand, the independent variables that demonstrated a significant relevance for the I_{OH} were the effect of the PEG/Gly (X_3) and the quadratic effects X_{22} and X_{33} for the bio-polyol obtained from *Eucalyptus globulus*, whereas for the bio-polyol from *Pinus radiata* only the independent variables catalyst concentration (X_1) and temperature (X_2) did not show a significant effect, while the remaining variables were significantly relevant.

2.2.1. Average molecular weight (M_w)

Figure P2.3 shows the influence of the independent variables as well as their interactions on the molecular weight of bio-polyols obtained through the liquefaction of *Eucalyptus globulus* (2.3a, 2.3b and 2.3c) and *Pinus radiata* (2.3d, 2.3e and 2.3f).

Figures 2.3a and 2.3d represent the response surfaces in which the interaction effect between the independent variables X_1 and X_3 is shown. As is evident in both figures, the independent variable X_3 had almost no influence on the response (M_w). On the other hand, in both cases, an increment in the concentration of the catalyst increased the molecular weight of the obtained bio-polyols. It should be noted in Figure P2.3d that, for the bio-polyols that were obtained from the

liquefaction of lignin from *Pinus radiata*, the maximum value of M_w was obtained for a catalyst concentration between 4% and 4.5%, after which the molecular weight decreased as the concentration increased. This behaviour could be explained by the influence of the quadratic term of the catalyst (X_{11}) on the molecular weight equation.

The influence of the independent variables X_1 and X_2 and their interaction on the molecular weight for a fixed value of the independent variable X_3 (X_3=0) is shown in Figure P2.3b and 2.3e. In both cases, an increase of the catalyst concentration (X_1) and the temperature (X_2) resulted in an increase of the molecular weight of the bio-polyols. As can be seen, the bio-polyol from the liquefaction of *Eucalyptus globulus* lignin reached the maximum molecular weight at one of the extremes of the design (Temperature of 80 ºC and Catalyst concentration of 5%). On the other hand, the bio-polyol from *Pinus radiata* lignin reached its maximum value of M_w for a catalyst concentration around 4% and decreased from this point as the concentration increased due to the quadratic effect of the independent variable (X_1) on the molecular weight equation. As for temperature, the highest M_w was obtained for a temperature of 175ºC and decreased as the temperature increased above this point, although the quadratic term X_{22} was not significantly relevant (Table P2.4).

Figures P2.3c and 2.3f show the response surface of M_w in function of temperature and PEG/Gly for a fixed value of concentration (X_1=0). According to the regression coefficients summarised in Table P2.4, the molecular weight of the bio-polyol from *Eucalyptus globulus* was not affected by the independent variable PEG/Gly whilst the influence of the temperature was significantly relevant. This is evident from Figure P2.3c, where it can be observed that a variation on the temperature had a significant impact on the molecular weight of the bio-polyol, whereas the PEG/Gly had little influence on the molecular weight regardless of the reaction temperature. On the other hand, in the case of bio-polyol from the liquefaction of lignin from *Pinus radiata* (Figure P2.3f), neither the independent

variable temperature nor PEG/Gly had a relevant significance in the molecular weight equation, although the interaction between both (X_{23}) proved to be significantly relevant. In Figure P2.3f, it can be noticed that the molecular weight of the bio-polyols is favoured by a high temperature and low PEG/Gly, obtaining the maximum when the temperature was at its highest (180 ºC) and the PEG/Gly was at its lowest, that is, at one of the extremes of the design.

One explanation for the high influence of the independent variables X_1 and X_2 on the M_w, could be that lignin during the microwave liquefaction process first degrades into small fragments that react with polyhydric alcohols (polyethylene glycol and glycerol) via ether bonds. Nevertheless, in the presence of catalyst and elevated temperatures, these lignin fragments can repolymerise, resulting in larger molecules and thus increasing the molecular weight [6,7].

2.2.2. Hydroxyl number (I_{OH})

The influence of the independent variables and their interactions upon I_{OH} of the liquefied bio-polyols are shown in Figures P2.4a, 2.4b and 2.4c (*Eucalyputs globulus*) and 2.4d, 2.4e and 2.4f (*Pinus radiata*). For a fixed value of the temperature (X_2=0), the influence of the independent variables X_1 and X_3 as well as the interactions between them are shown in Figures P2.4a and 2.4d. As mentioned above, the independent variable X_1 did not show significant influence on the I_{OH} of the bio-polyols regardless the used raw material. On the other hand, the independent variable X_3 exhibited a significant influence in both cases, as indicated in Table P2.4. This behaviour is illustrated in the response surfaces curves. In both cases, an increase in the ratio resulted in a reduction of the hydroxyl number, whereas increasing the amount of glycerol in the mixture, i.e., reducing the PEG/Gly, drastically increased the hydroxyl number. It should be noted that, although the catalyst was not significantly influential, both the maximum and minimum hydroxyl value of the bio-polyols were obtained by using high concentrations of catalyst.

The response surfaces 2.4b and 2.4e were obtained by fixing the independent variable X_3 to 0. Figure 4b present a saddle point as a critical point, which means that the equilibrium is an inflection point between a relative maximum and a relative minimum. Therefore, this point does not serve as an optimal value. However, it is possible to identify the optimal region by visual observation of the surface [8]. Thus, to maximise the I_{OH}, a high temperature (180 ºC) and a catalyst concentration around 3.5% is preferable, while the minimum I_{OH} value was obtained employing a reaction temperature around 170 ºC without catalyst. On the other hand, a clear minimum I_{OH} value at 170 ºC and a catalyst concentration of 1.5% was observed in the case of the bio-polyol obtained from the liquefaction of *Pinus radiata* lignin (Figure P2.4e).

Finally, the response surfaces corresponding to the interaction of the independent variables temperature (X_2) and PEG/Gly (X_3), as well as their interactions, for a fixed value of X_1=0 are plotted in Figures P2.4c and 2.4f. Similarly, to Figures P2.4a and 2.4d, it is possible to appreciate the great influence of the independent variable X_3 on the I_{OH}. Thus, a lower PEG/Gly implied an increase in the I_{OH}, while a higher ratio resulted in a decrease of the hydroxyl number of the bio-polyols. Therefore, a minimum of hydroxyls was obtained for a PEG/Gly of almost 9 at a temperature of 170 ºC in the case of bio-polyol from the liquefaction of *Pinus radiata* lignin (Figure P2.4f). On the other hand, the response surface corresponding to the liquefaction of *Eucalyputs globulus* lignin (Figure P2.4c) exhibited a saddle point. In this case, the maximum I_{OH} was obtained for a temperature of 165 ºC and a maximum PEG/Gly (3), whereas the minimum I_{OH} corresponded to the maximum temperature (180 °C) and a PEG/Gly close to 8.

From the regression data summarised in Table P2.4 and the response surfaces, it can be noticed that the independent variable X_3 had the largest influence on the I_{OH}. This is due to the fact that polyethylene glycol has a lower number of free hydroxyls than glycerol, and therefore, as the amount of PEG increases with respect to glycerol, the hydroxyl number of the polyol decreases [9].

2.2.3. Optimisation and model validation

The aim of the optimisation was to determine the optimal reaction conditions for the synthesis of bio-polyols suitable for the manufacture of rigid and elastic polyurethanes. To do that, the desirability function of the Statgraphic Centurion XVI software was employed. In the optimisation of the bio-polyol conditions for the synthesis for rigid polyurethanes, the objective was to minimise the molecular weight while increasing the hydroxyl groups, whereas the opposite was sought for the optimisation of reaction conditions in the case of elastic polyurethane bio-polyols, i.e., an increase in the molecular weight of the bio-polyols while reducing the hydroxyl groups [10]. The optimised reaction settings for the above-mentioned bio-polyols are summarised in Table P2.5, where the not-normalised and the normalised values of the independent variables are included as well.

Table P2.5. Not-normalised and normalised values of the optimal points

Origin	Independent variables	Rigid bio-polyol		Elastic bio-polyol	
		Not-norm.	Norm.	Not-norm.	Norm.
Eucalyptus globulus	X_1	-1	0.00	1	5.00
	X_2	0.0479	160.96	1	180.00
	X_3	-1	3.00	0.5246	7.57
Pinus radiata	X_1	-1	0.00	0.5430	3.86
	X_2	-0.0456	159.09	0.0066	160.13
	X_3	-1	3.00	0.4466	7.34

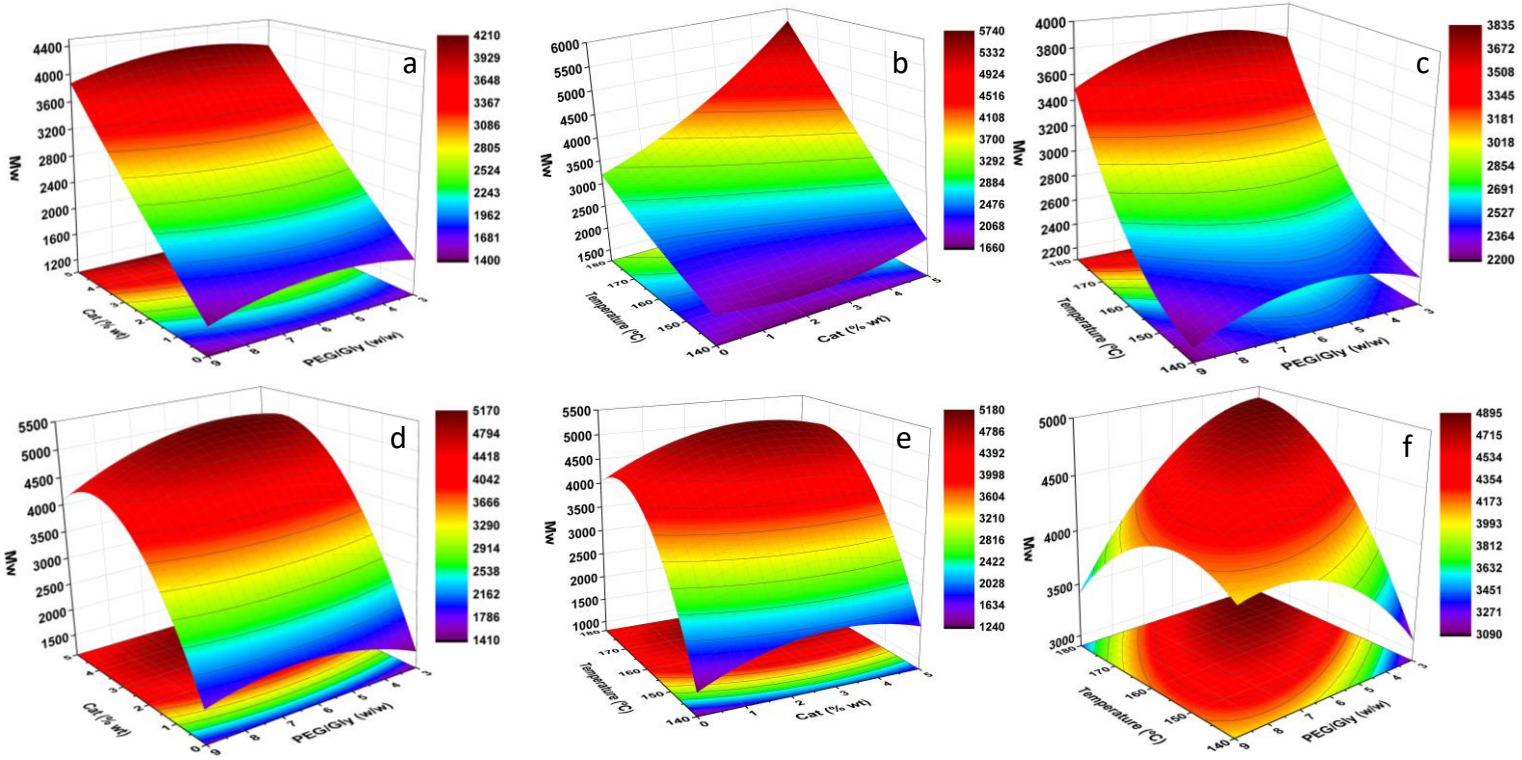

Figure P2.3. Response Surface for M_W: *Eucalyptus globulus* (a, b, c); *Pinus radiata* (d, e, f)

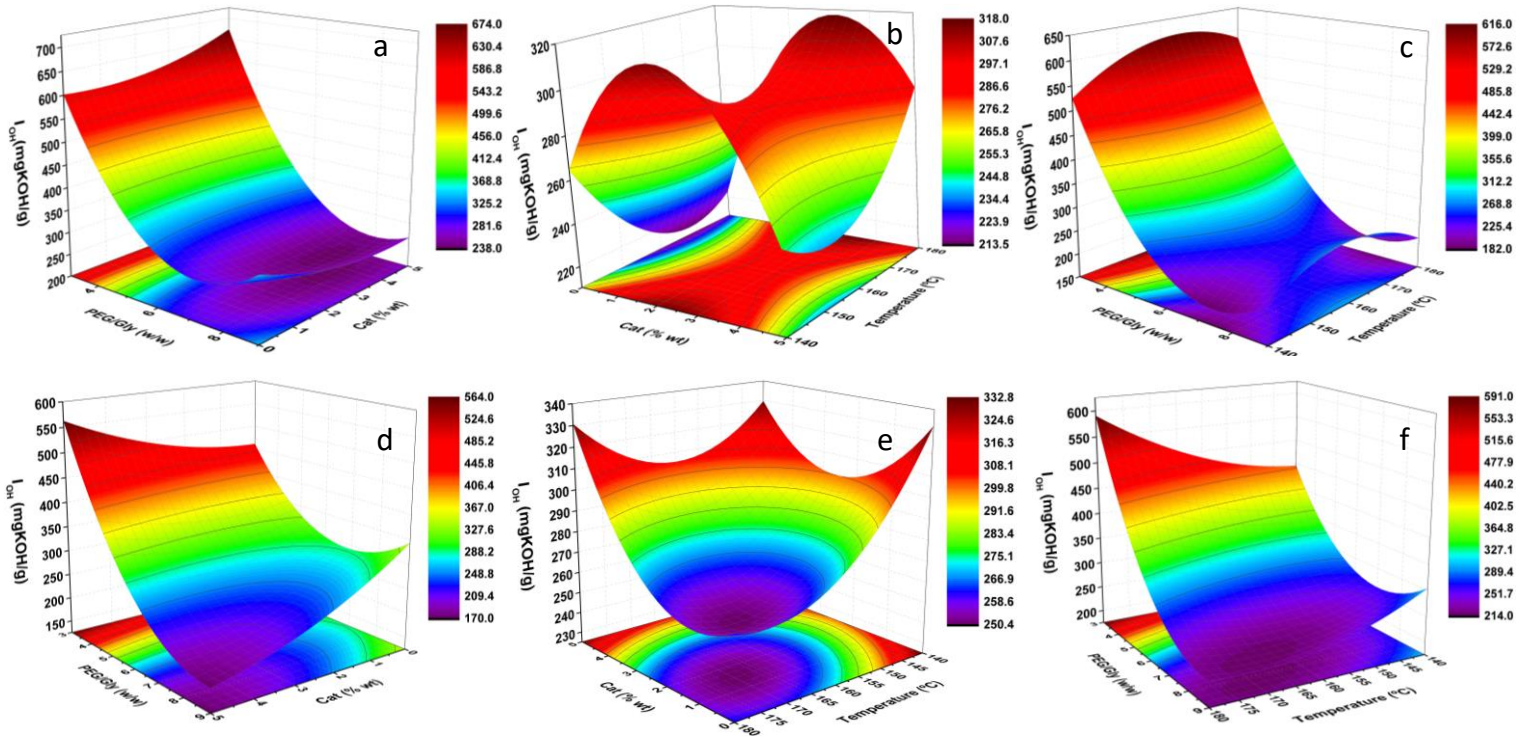

Figure P2.4. Response Surface for I_{OH}: *Eucalyptus globulus* (a, b, c); *Pinus radiata* (d, e, f)

To verify the model, a triplicate of each experiment was performed under the optimal reaction conditions and the experimental results were compared with the theoretical results presented in Table P2.6. As a result of this comparison, it was established that the experimental results were in good concordance with the data predicted by the software, and therefore, the Box-Behnken design was validated.

Table P2.6. Theoretical values of M_w and corrected I_{OH} predicted by the software and experimental values at optimum conditions

Parameter	Sample	Theoretical value	Experimental value
M_w (g/mol)	EOPR[a]	1532	1394 ± 12
	EOPE[b]	5593	4895 ± 325
	POPR[c]	1372	1383 ± 43
	POPE[d]	4891	5408 ± 765
I_{OH} (mg KOH/g)	EOPR	599.2	595.2 ± 33.9
	EOPE	221.1	253.8± 60.6
	POPR	456.0	514.3± 42.7
	POPE	211.6	209.7 ± 3.7

[a]EOPR (*Eucalyptus globulus* Organosolv Polyols for Rigid PU)
[b]POPR (*Pinus radiata* Organosolv Polyol for Rigid PU)
[c]EOPE (*Eucalyptus globulus* Organosolv Polyol for Elastic PU)
[d]POPE (*Pinus radiata* Organosolv Polyol for Elastic PU)

2.2.4. Characterisation of the optimised bio-polyols

In reference to the molecular weight (Table P2.6), it should be noted that, as indicated in the previous section (2.2.1), an increase in the catalyst concentration resulted in an increase in the molecular weight of the bio-polyols. Hence, EOPE and POPE bio-polyols presented higher M_w than EOPR and POPR bio-polyols in which no catalyst was used. In addition, the molecular weights of EOPE and POPE bio-polyols were higher than the ones of the employed lignins, EOUL and POUL respectively, in contrast to the reports of other authors. Thus, in the study by da Silva et al., (2017) [11] for the optimal liquefaction conditions of Kraft lignin, authors reported smaller molecular weights than the employed Kraft lignin for all points of the

experimental design. In another study, da Silva et al., (2019) [12] proved that the molecular weights of the bio-polyols obtained by liquefaction employing organic acids as catalyst were lower than the molecular weights of the Kraft lignin used. Similarly, Xue et al., (2015) [6] also obtained bio-polyols through liquefaction reactions with lower molecular weights than the ones of the employed original lignin using a catalyst concentration of 1.5%. The increase in molecular weight can be explained as the repolymerisation reactions of lignin are favoured by the presence of acid catalyst [13]. On the other hand, a concentration of sulphuric acid over 3% could enhance the repolymerisation reactions of lignin [7]. According to the literature, the molecular weight of polyols for rigid and elastic PU should be between 300-1000 (g/mol) and 2000-10000 (g/mol), respectively [10]. Considering the obtained results, though the molecular weights of EOPR and POPR bio-polyols were slightly above the stipulated range, it could be considered that the obtained bio-polyols are suitable for PU fabrication.

Regarding the I_{OH} of the studied bio-polyols, EOPR and POPR showed higher values than EOPE and POPE. This increment could be explained by two main reasons: firstly, an increase in catalyst concentration could decrease the hydroxyl number of the bio-polyol [9] and secondly, an increase in glycerol content, with a higher number of free hydroxyl than PEG, could enhance the hydroxyl number of the final bio-polyol [14]. According to the literature, bio-polyols for rigid PUs, EOPR and POPR, are in the range of I_{OH} required for the manufacture of rigid PUs (200-1000 mg KOH/g). However, the bio-polyols EOPE and POPE were slightly above the range of 28-160 mg KOH/g, which is the one required for the manufacture of elastic PU [15].

In the literature, most of the existing works are focused on two parameters: hydroxyl number and yield. Nevertheless, parameters such as the number average molecular weight (M_n), polydispesrity index (PDI), acid number (A_n) and functionality (*f*) should be considered in the synthesis of polyols [16].

Thus, although these parameters were not considered in the experimental design, they are summarised in Table P2.7 together with the obtained yield. Bio-polyols *f* and the liquefaction yield (η) were calculated using the Equations P2.4 and 2.5:

$$f = \frac{M_n \cdot I_{OH}}{1000 \cdot 56.1} \qquad \text{Equation P2.4}$$

$$\eta = \frac{M}{M_0} \cdot 100 \qquad \text{Equation P2.5}$$

Where, M is the final bio-polyol mass and M_0 is the mass of the initial mixture of the liquefaction procedure.

Table P2.7. Mn (g/mol), PDI (Mw/Mn), An (mg KOH/g), f and yield (%) of bio-polyols at optimum conditions

Sample	$M_{n\,(g/mol)}$	PDI (M_w/M_n)	A_n (mg KOH/g)	*f*	Yield (%)
EOPR	380 ± 7	3.69 ± 0.08	2.74 ± 0.00	4.03 ± 0.15	98.63 ± 0.71
EOPE	524 ± 28	9.37 ± 1.12	33.01 ± 0.00	2.36 ± 0.44	71.98 ± 1.41
POPR	387 ± 4	3.58 ± 0.08	5.36 ± 0.23	3.55 ± 0.26	98.93 ± 0.10
POPE	778 ± 7	6.95 ± 0.91	30.56 ± 0.15	2.91 ± 0.08	87.56 ± 3.30

The polydispersity index indicated that the EOPE and POPE bio-polyols had wider molecular weight distribution than EOPR and POPR bio-polyols. The reason for this could be due to a higher number of repolymerisation reactions in the synthesis of EOPE and POPE bio-polyols, as discussed previously. Wider molecular weight distributions of EOPE and POPE indicates that the chain length variability of these bio-polyols is higher than in EOPR and POPR. This variability has a direct impact on the properties of the polyurethane, hence a bio-polyol with lower PDI is preferable for the manufacture of polyurethane foams, as a wide variability of the bio-polyol chain lengths could result in softening of the foam or in a mechanical collapse due to stresses that occur in the weaker regions of the foam [17].

In the synthesis of polyurethanes, the A_n value of bio-polyols is an important parameter to be considered, since acid groups could decrease the efficiency of the reaction [18]. According to the literature, the bio-polyols studied in this work showed an A_n index within the range reported by other authors, usually ranging from 0 to 40 mg KOH/g [7]. As it can be seen in Table P2.7, those bio-polyols in which no catalyst was used (EOPR and POPR) showed a lower A_n index than in the bio-polyols with higher acid concentration (EOPE and POPE). This is because the number of acid substances generated during the liquefaction tended to increase, as the catalyst concentration increased [12]. Furthermore, as expected, the bio-polyols with the lowest acid number (EOPR and POPR) showed the highest hydroxyl number, since there is a direct correlation between the increase of acid number and the decrease hydroxyl number values [19].

Regarding functionality, to the best of our knowledge, no work has been reported indicating the functionality of polyols obtained by liquefaction of lignin with PEG and glycerol. A summary of the functionalities obtained in this study is presented in Table P2.7. Obtained values for EOPR and POPR bio-polyols (4.03 ± 0.15 and 3.55 ± 0.26), as well as for EOPE and POPE bio-polyols (2.36 ± 0.44 and 2.91 ± 0.08) are suitable for the synthesis of rigid and elastic PUs, whose functionalities should be between 3-8 and 2-3 [10].

Finally, as summarised in Table P2.7, significant differences were found in the obtained yields between the bio-polyols for rigid PUs and those for elastic PUs. Thus, the EOPR and POPR bio-polyols showed quite similar yields between them, 98.63 ± 0.71% and 98.93 ± 0.10% respectively. These results are very similar to those published by other authors who used the same microwave liquefaction reaction time that was employed in this work. For instance, da Silva et al., (2017) [11] documented a yield of 95.27% for the liquefaction of Kraft lignin using 3% catalyst, while Sequeiros et al., (2013) [20] obtained yields over 94% for all points of their experimental design

employing organosolv lignin from olive tree pruning. Xue et al., (2015) [6] liquefied alkaline lignin from corncob waste applying a catalyst concentration of 1.5% to obtain a yield of 94.47%. On the other hand, Gosz et al., (2018) [21] obtained a yield of 93% by liquefying pine Kraft lignin with 1,4-butanediol and crude glycerol without catalyst. In contrast, EOPE and POPE bio-polyols exhibited significantly lower yields, 71.98 ± 1.41% and 87.56 ± 3.30%. Two reasons could explain the large difference between the yields of bio-polyols for rigid PU (EOPR and POPR) and bio-polyols for elastic PU (EOPE and POPE). On the one hand, as mentioned above, an increase in the concentration of the acid catalyst enhances the lignin repolymerisation reactions, which increases the solid residue, leading to a reduction in the final yield. On the other hand, an excess of glycerol in the mixture promotes the reaction yield. This is because during the reaction the glycerol can be condensed into polyglycerol forming water as a by-product. Such water fragments the lignin into smaller and more reactive molecules through hydrolysis, enhancing the reaction yield [21].

To analyse the relationship between chemical structure and degradation, the bio-polyols were subjected to a thermogravimetric analysis. The TGA thermograms and their corresponding DTG derivative thermogravimetric curves are presented in Figure P2.5. Through the study of the DTG curves, three degradation stages were observed which are summarised in Table P2.8.

Table P2.8. Main degradation stages on TGA-DTG analysis

Sample	1st degradation stage		2nd degradation stage		3rd degradation stage	
	T interval(°C)	T_{max} (°C)	T interval(°C)	T_{max} (°C)	T interval (°C)	T_{max} (°C)
EOPR	40-120	70	130-246	208	246-417	356
POPR	40-120	68	132-260	218	260-430	371
EOPE	40-120	78	135-293	225	293-452	380
POPE	40-120	80	139-298	230	298-452	399

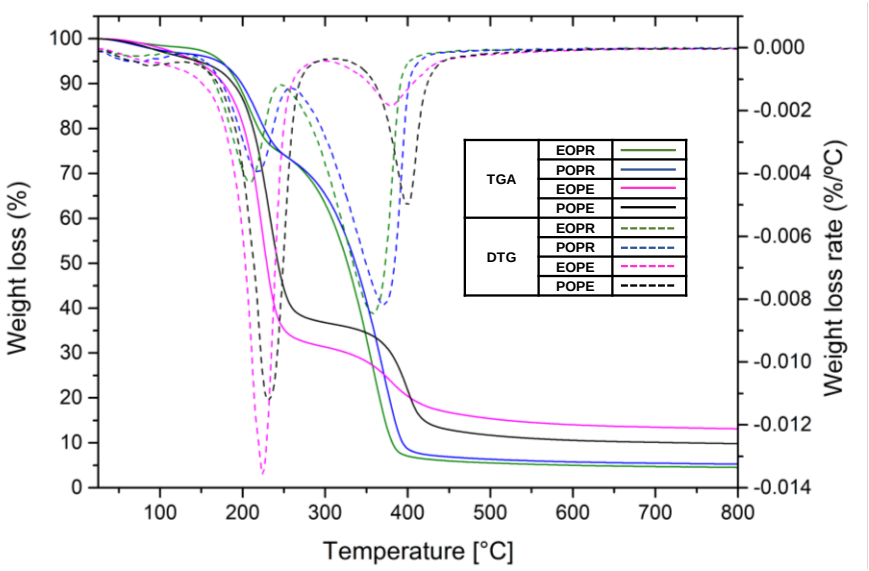

Figure P2.5. TGA thermograms and DTG curves of bio-polyols

The first degradation stage corresponds to the weight loss of the humidity of the samples. The second degradation stage correspond to the degradation of glycerol (153-267 °C) and the third degradation stage corresponded to the degradation of PEG (267-392°C) and lignin [22]. Since lignin degradation takes place between 300-500 °C, this third degradation region of bio-polyols reaches higher temperatures than if only PEG were present. It can be observed that, as the M_w of bio-polyols increases, the degradation temperature is delayed; moreover, the lower the reaction yield, the lower the weight loss. An explanation for this, is that the lower the yield, the higher the lignin repolymerisation reactions, which results in a greater solid residue and, therefore, a lower final amount of lignin in the bio-polyol. These results confirmed that the combination of the liquefying solvents and lignin was successful.

Finally, to determine the rheological behaviour of the bio-polyols, a rotational test was performed. Through this test, the relationship between viscosity (η), shear stress (τ) and shear rate ($\dot{\gamma}$), which were fitted to the

Ostwald-de Waele (power-law) equation (Equation P2.6), was studied to determine the bio-polyols' fluid behaviour as well as their viscosity.

$$\tau = k \cdot \dot{\gamma}^{n} \qquad \text{Equation P2.6}$$

where n and k are adjustment parameters dependent on both the measurement conditions and the nature of the fluid. Depending on the value of the flow index parameter (n) the fluid could be Newtonian when n=1, pseudoplastic if n<1 and dilatant for n>1. The parameter k, also called consistency index, which is associated to the apparent viscosity of the fluid at a shear rate of 1 s^{-1}, exhibits higher values as the viscosity increases. In Table P2.9 and Figures P2.6a and 2.6b, a summary of the data, obtained by the software and the flow curves, are presented.

Table P2.9. Power-Law Linear functions based on the rheological data from bio-polyol samples

Sample	Function	k (Pa*s^n)	n	R^2
EOPR	$\tau = 0.2623 \cdot \dot{\gamma}^{0.9709}$	0.2623	0.9709	0.9995
POPR	$\tau = 0.4394 \cdot \dot{\gamma}^{1.0043}$	0.4394	1.0043	0.9998
EOPE	$\tau = 0.8137 \cdot \dot{\gamma}^{0.9541}$	0.8137	0.9541	0.9995
POPE	$\tau = 1.1885 \cdot \dot{\gamma}^{0.9525}$	1.1885	0.9525	0.9998

The high values of R^2 reported in Table P2.9 indicated that all the rheograms are well fitted. Therefore, it could be concluded that the selected model was adequate to evaluate the rheological behaviour of the bio-polyols. Considering that the flow index parameter (n) of all bio-polyols is very close to unity, it could be concluded that all bio-polyols behave as Newtonian fluids. However, analysing the Figure 6a, the rheograms corresponding to EOPE and POPE showed a pseudoplastic behaviour, i.e., the viscosity (η) decreased as the shear rate ($\dot{\gamma}$) increased, while EOPR and POPR bio-polyols exhibit a clearly Newtonian behaviour, where the viscosity remained constant regardless the applied shear rate.

Figure P2.6b, where the relationship between the shear stress (τ) and shear rate ($\dot{\gamma}$) is represented, confirms that EOPR and POPR bio-polyols behaved as Newtonian fluids since their graphical representation is a line passing through the origin, while the representation of EOPE and POPE bio-polyols subtly exhibited the characteristic curve of pseudoplastics fluids, where τ decreases as $\dot{\gamma}$ increases.

It is well known that the power-law becomes Newton's Law when a fluid behaves in a Newtonian way and therefor the viscosity of the fluid corresponds to any point along the *plateau* in the Figure P2.6a, i.e., the consistency index *k* is equal to the viscosity. Therefore, the viscosities for EOPR and POPR are 0.2626 Pa·s and 0.4394 Pa·s respectively. On the other hand, the viscosities of EOPE and POPE are in the range of 0.7286-0.6676 Pa·s and 1-0.9310 Pa·s respectively at the studied shear rate. As it was expected, since viscosity and molecular weight are closely related [11], the bio-polyols with the highest viscosities were those with the highest molecular weight. According to literature, these viscosities values are suitable for PU production since they are below 300 Pa·s [23] and are similar to the viscosities obtained by other authors by liquefying lignin [6,12,22].

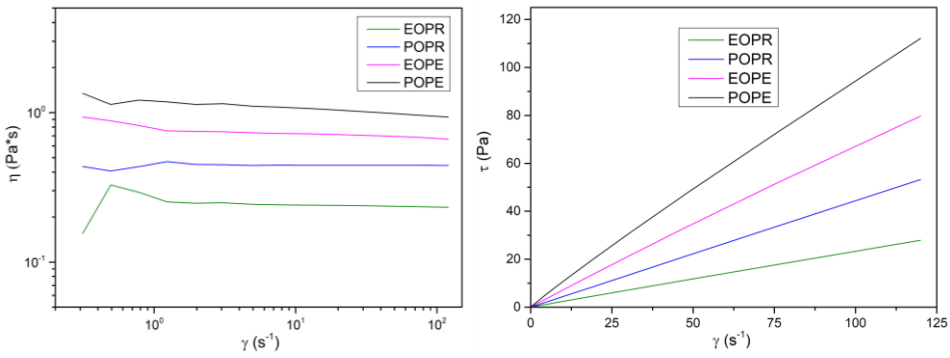

Figure P2.6. Viscosity (η) VS shear rate ($\dot{\gamma}$) and (b) shear stress (τ) VS shear rate ($\dot{\gamma}$) of bio-polyols at optimum point

3. CONCLUSIONS

Through Box Behnken experimental design and employing response surface methodology, the optimal lignin liquefaction reaction conditions using microwave irradiation technology for obtaining bio-polyols to formulate rigid and elastic polyurethanes were obtained. Two different organosolv lignins were employed: *Eucalyptus globulus* lignin and *Pinus radiata* lignin. Four optimum points were obtained, of which two for bio-polyols for rigid polyurethanes (EOPR and POPR), and two for bio-polyols for elastic polyurethanes (EOPE and POPE). The R^2 determination coefficients obtained for the studied parameters (M_w and I_{OH}) were 0.97 and 0.97 for *Eucalyptus globulus* lignin, while for *Pinus radiata* lignin the coefficients were 0.96 and 0.98. The elevated R^2 coefficients together with Fisher's F-test confirmed that the selected models were appropriate and that the models were well adjusted. The optimum reaction conditions for EOPR and POPR bio-polyols were virtually equals, around 160°C and PEG/Gly ratio of 3, noteworthy is the absence of catalyst in both cases. On the other hand, the optimum reaction conditions were 180°C and polyethylene glycol/glycerol ratio of 7.57 for EOPE and 160.13°C and polyethylene glycol/glycerol ratio of 7.34 for POPE. The high concentration of catalyst, 5% and 3.85% respectively, is remarkable in both cases. The molecular weight of EOPR and POPR bio-polyols at the optimum points was slightly higher than that required for the manufacture of rigid polyurethanes. Similarly, the hydroxyl number of EOPE and POPE bio-polyols was slightly higher than the required for the manufacture of elastic PUs. However, considering the rest of the studied parameters: A_n, PDI, *f* and the rheological behaviour, it could be concluded that the bio-polyols were suitable for the synthesis of polyurethanes. Nevertheless, before their use, the bio-polyols should be neutralised due to the high acid number value and for polyurethane foams preparation the high polydispersity should be taken into account.

REFERENCES

[1] Y.Y. Li, X. Luo, S. Hu, Bio-based Polyols and Polyurethanes, 2015, pp. 1–79.

[2] T. Wells, M. Kosa, A.J. Ragauskas, Ultrason. - Sonochemistry 20(6) (2013) 1463–9. 10.1016/j.ultsonch.2013.05.001.

[3] L. Chen, X. Wang, H. Yang, Q. Lu, D. Li, Q. Yang, H. Chen, J. Anal. Appl. Pyrolysis 113 (2015) 499–507. 10.1016/j.jaap.2015.03.018.

[4] A. Morales, B. Gullón, I. Dávila, G. Eibes, J. Labidi, P. Gullón, Ind. Crops Prod. 124(July) (2018) 582–92. 10.1016/j.indcrop.2018.08.032.

[5] R. Fernández-Marín, F. Hernández-Ramos, A.M. Salaberria, M.Á. Andrés, J. Labidi, S.C.M. Fernandes, Int. J. Biol. Macromol. 186(January) (2021) 218–26. 10.1016/j.ijbiomac.2021.07.048.

[6] B.L. Xue, J.L. Wen, R.C. Sun, Materials (Basel). 8(2) (2015) 586–99. 10.3390/ma8020586.

[7] S. Hu, X. Luo, Y. Li, ChemSusChem 7(1) (2014) 66–72. 10.1002/cssc.201300760.

[8] M.A. Bezerra, R.E. Santelli, E.P. Oliveira, L.S. Villar, L.A. Escaleira, Talanta 76(5) (2008) 965–77. 10.1016/j.talanta.2008.05.019.

[9] Y. Jin, X. Ruan, X. Cheng, Q. Lü, Bioresour. Technol. 102(3) (2011) 3581–3. 10.1016/j.biortech.2010.10.050.

[10] M. Ionescu, in: De Gruyter (Ed.), Polyols for Polyrethanes, Boston, Berlin, 2019, pp. 1–10.

[11] S.H.F. da Silva, P.S.B. dos Santos, D. Thomas da Silva, R. Briones, D.A.

Gatto, J. Labidi, J. Wood Chem. Technol. 37(5) (2017) 343–58. 10.1080/02773813.2017.1303513.

[12] S.H.F. da Silva, I. Egüés, J. Labidi, Ind. Crops Prod. 137(March) (2019) 687–93. 10.1016/j.indcrop.2019.05.075.

[13] Y. Lee, E.Y. Lee, J. Wood Chem. Technol. 36(5) (2016) 353–64. 10.1080/02773813.2016.1156132.

[14] F. Chen, Z. Lu, J. Appl. Polym. Sci. 111 (2009) 508–16. 10.1002/app.29107.

[15] Y.Y. Li, X. Luo, S. Hu, Bio-based Polyols and Polyurethanes, 2015, pp. 1–79.

[16] F. Hernández-Ramos, M.G. Alriols, T. Calvo-Correas, J. Labidi, X. Erdocia, ACS Sustain. Chem. Eng. (2021). 10.1021/acssuschemeng.0c09357.

[17] J. D'Souza, R. Camargo, N. Yan, Polym. Rev. 57(4) (2017) 668–94. 10.1080/15583724.2017.1283328.

[18] S. Hu, Y. Li, Ind. Crops Prod. 57 (2014) 188–94. 10.1016/j.indcrop.2014.03.032.

[19] S.H. Lee, M. Yoshioka, N. Shiraishi, J. Appl. Polym. Sci. 78(2) (2000) 319–25. 10.1002/1097-4628(20001010)78:2<319::AID-APP120>3.0.CO;2-Z.

[20] A. Sequeiros, L. Serrano, R. Briones, J. Labidi, J. Appl. Polym. Sci. 130(5) (2013) 3292–8. 10.1002/app.39577.

[21] K. Gosz, P. Kosmela, A. Hejna, G. Gajowiec, Ł. Piszczyk, Wood Sci. Technol. 52(3) (2018) 599–617. 10.1007/s00226-018-0991-4.

[22] R. Briones, L. Serrano, J. Labidi, J. Chem. Technol. Biotechnol. 87(2) (2012) 244–9. 10.1002/jctb.2706.

[23] C.A. Cateto, M.F. Barreiro, A.E. Rodrigues, M.N. Belgacem, Ind. Eng. Chem. Res. 48(5) (2009) 2583–9. 10.1021/ie801251r.

“All mentors have a way of seeing more of our faults

than we would like. It’s the only way we grow”

Senator Padmé Amidala

Publication III

Valorisation of crude glycerol in the production of liquefied lignin bio-polyols for polyurethane formulation

ABSTRACT

Bio-polyols with suitable properties to be used as precursors of rigid and elastic polyurethanes were synthesised under reaction parameters optimised in ***Publication II*** and employing crude glycerol generated as by-product in the transesterification reaction for biodiesel obtaining from used vegetable oil. Bio-polyols were prepared employing organosolv lignins from *Eucalyptus globulus* and *Pinus radiata* through a microwave assisted liquefaction reaction. Polyethylene glycol and the previously mentioned CG were employed as liquefaction solvents and the reaction was catalysed with sulphuric acid. Different parameters of bio-polyols were determined, such as hydroxyl number, acid number, molecular weight, functionality, and the liquefaction yield. Bio-polyols, formulated with CG, for rigid polyurethanes from *Eucalyptus globulus* ($EOPR_{CG}$) and *Pinus radiata* ($POPR_{CG}$) showed an I_{OH} of 534 ± 4 (mg KOH/g) and 383 ± 8 (mg KOH/g), while for elastic PUs, the I_{OH} of bio-polyols $EOPE_{CG}$ (from Eucalyptus) and $POPE_{CG}$ (from Pine), were 228 ± 36 (mg KOH/g) and 173 ± 16 (mg KOH/g). The A_n of the liquefied bio-polyols ranged between 1.91 and 25.09 (mg KOH/g) and the functionalities of bio-polyols were 4.16 and 3.14 for $EOPR_{CG}$ and $POPR_{CG}$, while for $EOPE_{CG}$ and $POPE_{CG}$ the functionalities were 3.51 and 2.08. Different yields were obtained depending on the used catalyst concentration, varying from over 90% for $EOPR_{CG}$ and $POPR_{CG}$ to 70-80% for $EOPE_{CG}$ and $POPE_{CG}$.

1. MATERIALS AND METHODS

1.1. Materials

The raw materials, *Eucalyptus globulus* chips and *Pinus radiata*, as well as the used vegetable oil and chemicals employed in this work were obtained as described in s***ection 2.1*** of the **2nd PART.**

1.2. Lignin obtaining procedure

Lignins used in this work were obtained after the organosolv delignification process and the subsequent ultrasound treatment of the black liquor described in ***section 2.2*** of the **2nd PART**. These lignins called EOUL and POUL were characterised in ***Publication II***.

1.3. Transesterification of vegetable oil to obtain crude glycerol

Crude glycerol (CG) was obtained by the transesterification reaction outlined in **section 2.4** of the **2nd PART**.

1.4. Synthesis of bio-polyols through microwave assisted liquefaction

The liquefaction of organosolv lignins (EOUL and POUL) were performed following the methodology detailed in the ***section 2.3*** of the **2nd PART**.

The catalyst concentration, as well as the reaction temperature and the PEG/CG ratio involved in the reaction, were obtained in the process optimisation carried out in ***Publication II*** and are summarised below (Table P3.1).

Table P3.1. Liquefaction reaction conditions optimised in ***Publication II***

Bio-polyol	Rigid bio-polyol		Elastic bio-polyol	
	$EOPR_{CG}$	$POPR_{CG}$	$EOPE_{CG}$	$POPE_{CG}$
Cat (% wt.)	0	0	5	3.86
Temperature (°C)	161	159	180	160
PEG/CG (% wt.)	3/1	3/1	7.57/1	7.34/1

1.5. Characterisation of crude glycerol

The CG was characterised in accordance with the techniques indicated in Table 2.3 of the **2nd PART (*section 6*)**, which are described in **Appendix II.** In addition, physical properties, such as density, pH and viscosity were measured. The density was calculated by measuring the weight of a known volume of CG at room temperature. The pH of the CG was determined at room temperature employing a pH meter Crison basic 20 by dissolving 1.00 ± 0.1 g of CG in 50 mL of deionized water. Ash content was analysed following the ISO 2098-1972 Standard method, which consist in burning at 750 °C for 3 h 1 g of CG in a muffle furnace.

1.6. Characterisation of the obtained bio-polyols

Bio-polyols obtained through the liquefaction reaction of EOUL and POUL employing PEG400 and CG from used vegetable oil were characterised to determine important parameters, such as M_w, number average molecular weight (M_n) and polydispersity index (PDI), I_{OH}, A_n and *f*. Furthermore, the thermal degradation of bio-polyols was studied through a thermogravimetric analysis (TGA) and their rheological behaviour was assessed, as outlined in Table 2.3 of **2nd PART**, ***section 2.6*** This characterisation was conducted according to the methodologies explained in **Appendix II**.

2. RESULTS AND DISCUSSION

2.1. Crude glycerol characterisation

This section contains the physical properties and composition of CG. The pH of the obtained crude glycerol was 10.55 ± 0.02, which indicates the presence of residual KOH catalyst and potassium salts formed during the transesterification reaction. This value is in agreement with those obtained by other authors who characterised CG from the transesterification reaction of vegetable oils with NaOH or KOH as catalyst [1–3]. As it was expected, the density of CG (1.03 ± 0.07 g/cm^3) resulted lower than that of pure glycerol (1.259 g/cm^3) due to the presence of lighter impurities such as fatty acids, fatty acids methyl esters (FAMEs) , water and methanol traces [2]. The water content in CG significantly varies depending on the manufacturing industry, from a 3.6% in the case of the soap industry to a 55.3% in CG from Stearin production. CG obtained from transesterification reaction presents water contents from 8.16% to 43.2% [4], although a maximum of 12% is recommended to reduce purification costs [5]. Therefore, the water content of the CG obtained in this work (11.64 ± 1.61%) is within the specifications of a CG obtained through transesterification reaction. Such water can hydrolyse the triglycerides to form free fatty acids (FFA) which results in soaps decreasing the reaction yield [4].

The elemental analysis of CG showed that the 46.00 ± 1.29% of the organic matter corresponded to Carbon (C). This high value can be explained by the high presence of impurities, such as, soaps, FAMEs and glycerides, which have higher C content than glycerol. Hu et al., (2012) [2] reported similar C values for CG obtained from different soy and vegetable oil wastes. In addition, the obtained nitrogen (0.15 ± 0.01%), hydrogen (8.17 ± 0.33%) and oxygen (35.6 ± 1.58%) percentages were in accordance with the values reported for different CG obtained from diverse vegetable oils [2,6,7].

Nevertheless, the measured sulphur concentration (1.33 ± 0.04) was higher than the values obtained in the mentioned studies, ranging from ppms to a maximum of 0.078%. The chemical composition of CG was determined through GC-MS. In addition to glycerol (41.84 ± 0.17 %), CG was found to be rich in other compounds which include fatty acids (11.46 ± 6.01%) and FAMEs (26.31 ± 7.68%), among others (Figure P3.1).

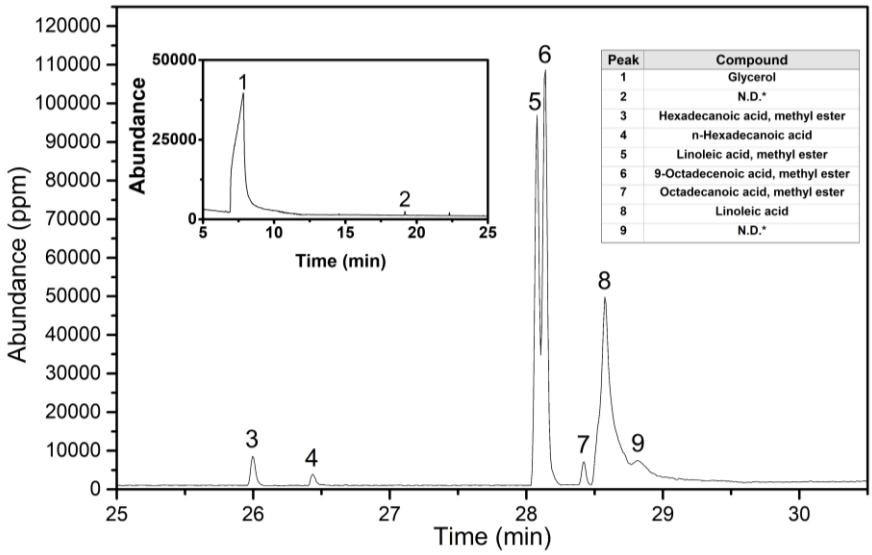

Figure P3.1. GC-MS chromatogram of CG

The chemical structure of the CG was determined through ATR-FTIR analysis, and it was compared with a commercial glycerol sample (Figure P3.2). CG showed the main functional groups of commercial grade glycerol: O-H stretching and bending (3300 cm^{-1} and 920 cm^{-1} respectively), C-H asymmetric and symmetric stretching (2920 cm^{-1} and 2851 cm^{-1} respectively), C-O stretching of primary alcohol (1456 cm^{-1}) and secondary alcohol (1110 cm^{-1}) as well as H_2O bending (1650 cm^{-1}) [1,8]. Moreover, characteristic peaks of CG were also observed. The first one, a small peak associated to C=C stretching (3015 cm^{-1}) related to unsaturated compounds [1]; the second one, associated with the presence of carbonyl groups (C=O)

of esters or carboxylic acids of fatty acids (1745 cm^{-1}) [9]. Finally, a signal related to the presence of carboxylate ions COO^- was observed (1560 cm^{-1}), indicating the presence of soap in the CG sample [1,9].

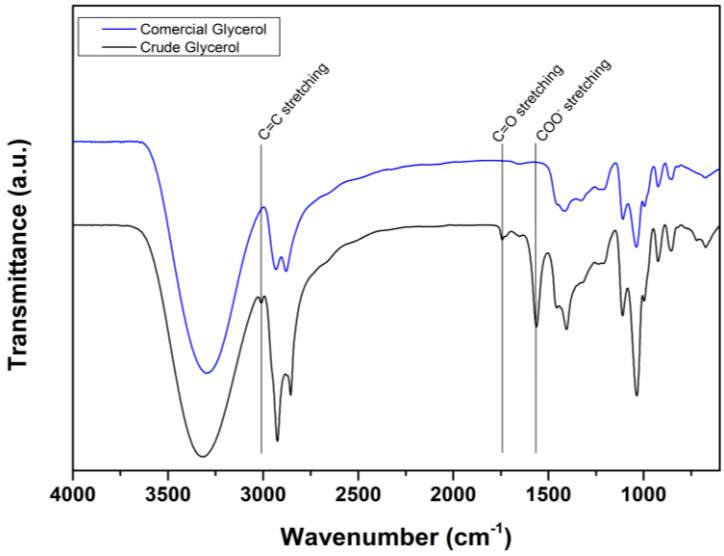

Figure P3.2. ATR-FTIR spectra of commercial glycerol and crude glycerol

2.2. Characterisation of the bio-polyols

Table P3.2 summarises the data obtained from the characterisation of the bio-polyols. An adequate M_w of polyols is essential to obtain PUs with the desired soft segment properties. Depending on the final application, the PUs' molecular weight should be between 300-1000 (g/mol) for rigid PU, and between 2000-10000 (g/mol) for elastic PU [10].

As expected, the higher the acid concentration, the higher the M_w. Thus, bio-polyols for rigid PU ($EOPR_{CG,}$ $POPR_{CG}$) where no catalyst was used, showed lower M_w than the bio-polyols for elastic PU ($EOPE_{CG,}$ $POPE_{CG}$) as can be observed in the Figure P3.3. This increase in the M_w is a consequence of the repolymerisation reactions which are favoured in the presence of an acid

catalyst [11]. In addition, $EOPE_{CG}$ bio-polyol showed a significantly higher M_w than $POPE_{CG}$ since, as the catalyst concentration increases above 3%, the repolymerisation reactions also increase [12].

Table P3.2. M_W, I_{OH}, A_n, f, Equivalent Weight of polyol (EW) and yield of bio-polyols

	$EOPR_{CG}$	$EOPE_{CG}$	$POPR_{CG}$	$POPE_{CG}$
M_n(g/mol)	442 ± 34	941 ± 30	453 ± 24	780 ± 20
M_w (g/mol)	1742 ± 275	8818 ± 127	1431 ± 362	5530 ± 131
PI	4.25± 0.55	9.38 ± 0.16	3.14 ± 0.63	7.10 ± 0.31
I_{OH} (mgKOH/g)	554 ± 4	228 ± 36	383 ± 8	173 ± 16
A_n (mgKOH/g)	1.91 ± 0.06	20.94 ± 2.75	4.21 ± 0.90	25.09 ± 2.59
f	4.16 ± 0.10	3.51 ± 0.68	3.14 ± 0.16	2.08 ± 0.27
EW	101.20 ± 0.66	248.98 ± 38.77	146.68 ± 3.23	325.36 ± 30.16
Yield (%)	93.55 ± 3.00	70.75 ± 0.47	90.60 ± 0.56	79.35 ± 0.83

On the other hand, the polymerisation reactions between glycerol, FFA and FAMEs of CG can also increase the M_w of bio-polyols [13]. However, it could be concluded that these reactions were of lesser importance than the repolymerisation reactions caused by the acid catalyst, since the bio-polyols with higher CG content but without catalyst showed the lowest M_w. The PDI is also crucial for the final application of the PU, as it is related to the chain length variation and, depending on the chain length of the polymer, the PU could show an undesired behaviour [14]. It was observed that the PDI was also affected by repolymerisation reactions caused by an increase in catalyst concentration. Thus, the bio-polyol with the highest catalyst concentration ($EOPE_{CG}$) exhibited the highest M_w and PDI, followed by $POPE_{CG}$. $EOPE_{CG}$ and $POPE_{CG}$ bio-polyols' M_w values fitted in the range for the manufacture of elastic PUs. On the other hand, although the molecular weights of $EOPR_{CG}$ and $POPR_{CG}$ bio-polyols were slightly higher than the required for the

manufacture of rigid PUs, they could be considered suitable for the manufacture of this kind of PUs.

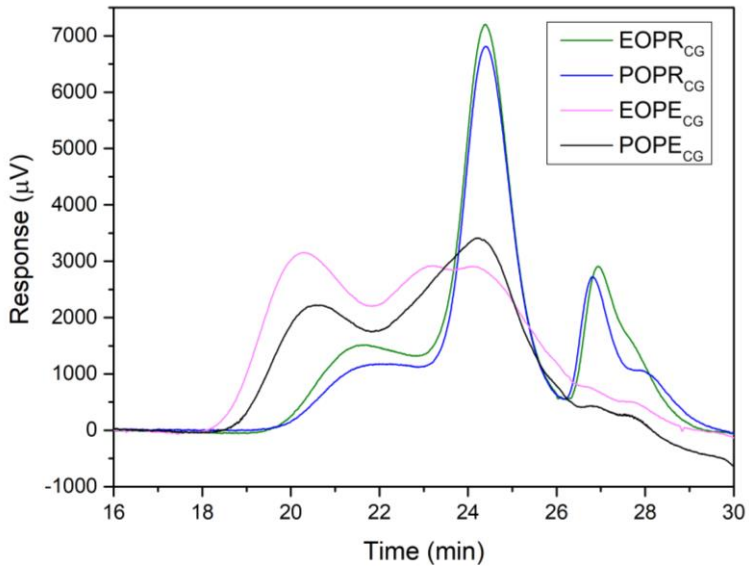

Figure P3.3. Molecular weight distribution of the liquefied bio-polyols

The I_{OH} required for the synthesis of rigid PUs ranges between 200-1000 mg KOH/g, while for elastic PUs it is between 28-160 mg KOH/g [15]. It is also well known that an elevated A_n can decrease the efficiency of the reaction, so a low A_n value is desired [16]. These two parameters are closely related, since an increase of the A_n decreases the hydroxyl number of the polyol [17]. This correlation is observed for the obtained bio-polyols, where those with the highest I_{OH} index ($EOPR_{CG}$ and $POPR_{CG}$) presented the lowest A_n value. The higher A_n index observed in $EOPE_{CG}$ and $POPE_{CG}$ compared to $EOPR_{CG}$ and $POPR_{CG}$ resulted from the use of sulphuric acid as reaction catalyst. The higher I_{OH} values of $EOPR_{CG}$ and $POPR_{CG}$ compared to $EOPE_{CG}$ and $POPE_{CG}$ can be explained, firstly, by the absence of catalyst in the reaction, which decreased the I_{OH} index [18]. On the other hand, the higher amount of glycerol used in the formulation of $EOPR_{CG}$ and $POPR_{CG}$ bio-polyols contributed to the increase of the I_{OH} index [19].

The synthesis of PUs requires different functionalities depending on the final application. Thus, for the synthesis of rigid PUs, high functionalities between 3-8 are preferred to produce crosslinks that reinforce the structure, while for elastic PUs, such as flexible foams, elastomers, or adhesives, among others, the desired functionalities are between 2 and 3. Such low functionalities result in materials with low crosslink density that allow the mobility of the polymer chains [10]. Therefore, the bio-polyols synthesised for rigid PU applications showed appropriate functionalities of 4.16 in the case of $EOPR_{CG}$ and 3.14 for $POPR_{CG}$. In the case of the bio-polyols for elastic PU applications, while $POPE_{CG}$ had an adequate functionality of 2.08, $EOPE_{CG}$ was slightly above 3. However, considering the I_{OH} and M_w, it could be suitable for the manufacture of elastic PUs. The chain derived from a hydroxyl group, or the equivalent weight (EW) of the polyol is also a relevant parameter to be considered (Equation P3.1). A short chain implies a higher density of urethane bonds and therefore more cohesion between them, mainly through secondary hydrogen bonds. This, together with the high functionality, results in a rigid structure. On the other hand, a long chain decreases the concentration of urethane bonds, decreasing the cohesion between them, and together with a low functionality and high mobility of the main polyol chain, resulting is an elastic PU [20].

$$EW = \frac{56.1 \cdot 100}{\text{Corrected } I_{OH}} \qquad \text{Equation P3.1}$$

As expected, according to the data summarised in Table P3.2, the bio-polyols $EOPR_{CG}$ and $POPR_{CG,}$ showed a low EW, which is adequate for the synthesis of rigid PUs, while bio-polyols with lower I_{OH} value, $EOPE_{CG}$ and $POPE_{CG}$, presented a higher EW more suitable for polyurethanes with a more flexible structure.

While all the studied properties are relevant to obtain bio-polyols with the appropriate characteristics for PU production, the yield constitutes another key factor and is equally important to make the process industrially feasible. In the lignin liquefaction process, the catalyst has a significant impact on the reaction yield, since in the presence of an acid catalyst the lignin repolymerisation reactions are increased, generating a higher amount of solid residue, and therefore reducing the yield [12]. The presence of water in the reaction can promote the fragmentation of lignin into smaller and more reactive molecules through hydrolysis increasing the reaction yield [21]. This water can be formed as a by-product of the condensation of glycerol into polyglycerol during the liquefaction reaction, therefore, the more glycerol in the medium, the more water and the higher the yield [22]. According to the results obtained and summarised in Table P3.2, $EOPR_{CG}$ and $POPR_{CG}$ bio-polyols with a higher amount of crude glycerol and without catalyst showed higher yield than $EOPE_{CG}$ and $POPE_{CG}$ bio-polyols where catalyst and lower concentration of glycerol were used. The use of CG in liquefaction reactions can reduce the yield of such reactions. This is due to the presence of impurities such as FA and FAMEs and a lower amount of glycerol in the reaction medium [16]. However, the presence of acid catalyst in the medium showed more influence on the reduction of the liquefaction yield. Thus, $EOPE_{CG}$ and $POPE_{CG}$ with a lesser CG content showed a substantially lower yield than $EOPR_{CG}$ and $POPR_{CG}$, which can only be explained by the greater influence of the acid catalyst. Furthermore, it was also observed that with a very similar PEG/CG ratio, but with a higher catalyst concentration, $EOPE_{CG}$ showed lower yield than $POPE_{CG}$.

A thermogravimetric analysis of bio-polyols was performed to determine the relation between chemical structure and degradation. The TGA thermograms and their corresponding derivative thermogravimetric (DTG) curves are shown in Figure P3.4. Based on the DTG curves, it was concluded that $EOPE_{CG}$

and $POPE_{CG}$ bio-polyols showed four degradation zones, while only three degradation zones were observed in $EOPR_{CG}$ and $POPR_{CG}$ bio-polyols. In addition, $EOPE_{CG}$, $POPE_{CG}$ and $POPR_{CG}$ showed an unidentified degradation zone which was not observed in $EOPR_{CG}$ sample. This degradation stages are summarised in Table P3.3.

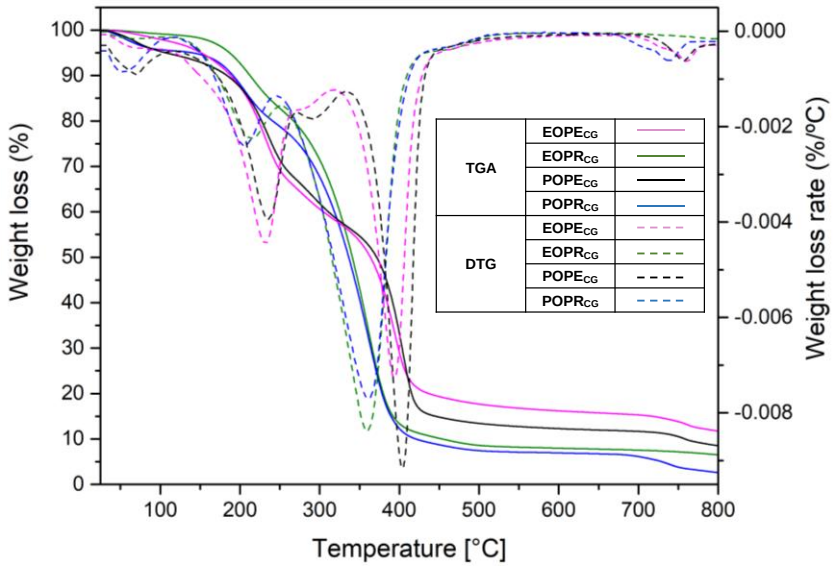

Figure P3.4. TGA thermograms and DTG curves of liquefied bio-polyols

The first one, between 30-110 °C, is associated with moisture or the presence of solvent in the sample. It could be observed a weight loss in all cases in this degradation zone. However, it was clearly visible a higher weight loss in $POPR_{CG}$ and $POPE_{CG}$ samples, which could be due to the presence of the acetone employed in the process.

The second degradation region (115-270 °C) corresponds to the degradation of glycerol [23]. The third degradation region takes place between 275-335 °C for $EOPE_{CG}$ and $POPE_{CG}$ and it is related to the degradation of PEG [23]. It should be noted that the degradation of the β-O-4 and C-C bonds of lignin occurs between 250-400 °C. Nevertheless, depending on the M_w and the

repolymerisation degree of the lignin molecule, this degradation could happen at different temperatures [24].

Thus, in the case of $EOPE_{CG}$ and $POPE_{CG}$, with higher M_w, lignin degradation (4^{th} degradation area) was observed between 315-450 °C, whereas in bio-polyols with lower M_w ($EOPR_{CG}$ and $POPR_{CG}$), this degradation takes place at lower temperatures. This is because, in the latter, the degradation zone of PEG and lignin overlap showing a single degradation zone, i.e. the third degradation region for these bio-polyols.

Finally, between 690 and 775 °C, a small weight loss was observed, possibly due to the presence of inorganic impurities in the samples. However, the origin of this peak could not be clearly determined.

Table P3.3. Interval temperature (T_{int}) and maximum degradation temperature (T_m) in °C of degradation stages of the TGA-DTG curves for the analysed bio-polyols

		$EOPE_{CG}$	$EOPR_{CG}$	$POPE_{CG}$	$POPR_{CG}$
1^{st}	Tinter (°C)	30-100	30-110	30-110	30-110
stage	Tmax (°C)	72	70	70	56
2^{nd}	Tinter (°C)	115-267	125-255	120-267	120-250
stage	Tmax (°C)	233	214	235	205
3^{rd}	Tinter (C)	267-315	214-430	267-335	250-430
stage	Tmax (°C)	283	360	291	361
4^{th}	Tinter (°C)	315-440	-	335-450	-
stage	Tmax (°C)	391	-	403	-
5^{th}	Tinter (°C)	705-775	-	705-775	690-770
stage	Tmax (°C)	758		758	740

Finally, to determine the viscoelastic properties and the fluid behaviour of the bio-polyols, a rheological study of the samples was performed employing the methodology outlined in **Appendix II.** To study the viscoelastic behaviour, an oscillatory test was carried out comparing the storage module (G') with the loss module (G'') (Figure P3.5).

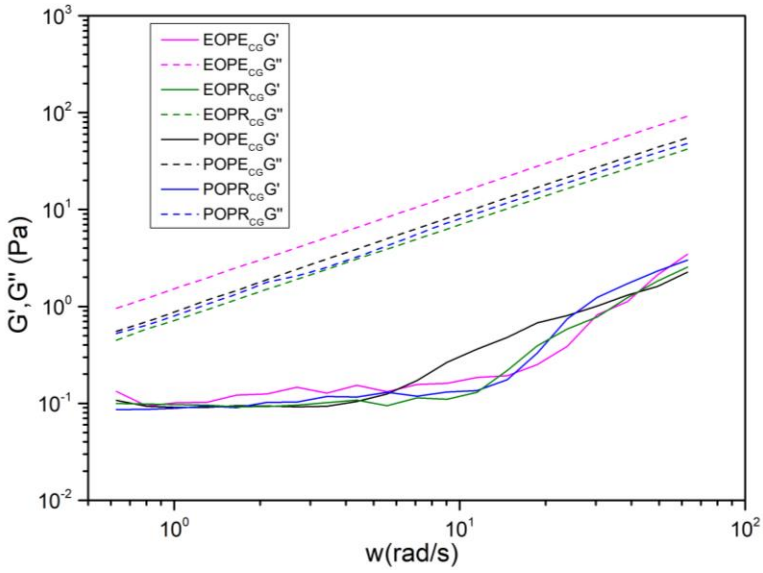

Figure P3.5. Storage module (G') and loss module (G'') (Pa) as function of ω (rad/s) of bio-polyols

Based on the analysis of this test, it was concluded that the bio-polyols exhibited a liquid behaviour, since in all cases the G'' was higher than the G' over the whole frequency range. Furthermore, as expected, since the modules increase with increasing molecular weights, $EOPE_{CG}$ and $POPE_{CG}$ showed higher modules than $EOPR_{CG}$ and $POPR_{CG}$ [25].

The fluid behaviour of bio-polyols as well as their viscosity was studied through a rotational test analysing the relation between the viscosity (η), shear stress (τ) and shear rate ($\dot{\gamma}$). These parameters were fitted to the Ostwald-de Waele power-law equation (**Appendix II**). In Table P3.4 a summary of the data provided by the software is presented, and the obtained flow curves are shown in Figures P3.6a and 6b.

Table P3.4. Power-Law linear functions based on the rheological data obtained from the studied bio-polyols

Sample	Function	k (Pa·s^n)	n	R^2
$EOPE_{CG}$	$\tau = 1.4299 \cdot \dot{\gamma}^{1.0176}$	1.4299	1.0176	0.9985
$EOPR_{CG}$	$\tau = 0.7290 \cdot \dot{\gamma}^{0.9911}$	0.7290	0.9911	0.9995
$POPE_{CG}$	$\tau = 0.9352 \cdot \dot{\gamma}^{0.9978}$	0.9352	0.9978	0.9988
$POPR_{CG}$	$\tau = 0.7927 \cdot \dot{\gamma}^{1.0011}$	0.7927	1.0011	0.9939

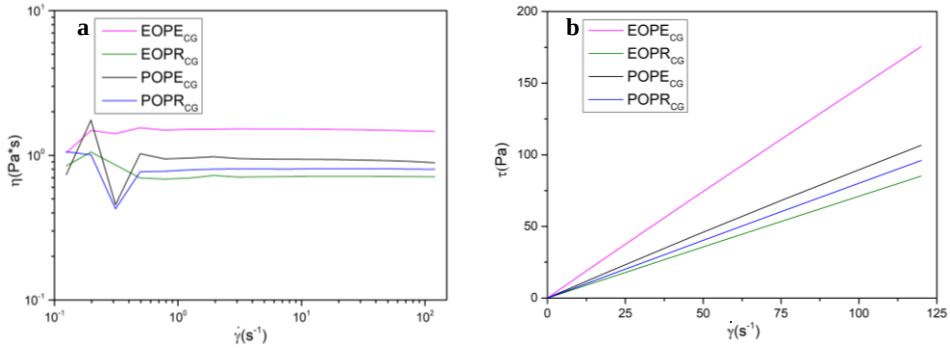

Figure P3.6. (a) Viscosity (η) as a function of shear rate ($\dot{\gamma}$); (b) shear stress (τ) as a function of shear rate ($\dot{\gamma}$)

R^2 values greater than 0.99 were obtained in all cases, indicating that the rheograms were well adjusted, and, therefore, the selected model to evaluate the rheological behaviour was adequate. In all cases, since the flow index (n) values were equal or very close to unity, it was concluded that the bio-polyols were Newtonian-type ones. This behaviour was observed in Figure P3.6a, where the viscosity remained constant regardless the applied shear rate ($\dot{\gamma}$) and was confirmed by studying the behaviour between the shear stress (τ) and shear rate ($\dot{\gamma}$) (Figure P3.6b). It was observed that, in all cases, the graphical representation of these parameters resulted in a straight line through the origin and whose slopes were equal to the k value of each bio-polyol. Furthermore, as expected, the viscosity of the bio-polyols with higher M_w were higher than those with lower molecular weights [26]. Thus, the viscosity of each bio-polyol was in concordance to its consistency index (k)

value [27], being 1.4299 Pa·s for $EOPE_{CG}$, 0.7290 Pa·s for $EOPR_{CG}$, and 0.9352 Pa·s and 0.7927 Pa·s for $POPE_{CG}$ and $POPR_{CG}$. Therefore, as these values were lower than 300 Pa·s, the bio-polyols were suitable for PU production.

2.3. Effect of crude glycerol in bio-polyols parameters

The results obtained by other authors by liquefying lignocellulosic biomass employing, among others, glycerol and CG as solvent are summarised in Table P3.5. Nonetheless, since the reaction conditions employed in this study were the optimal conditions stablished in ***Publication II***, results obtained in both studies were first compared.

The reaction yields employing CG and technical grade glycerol were very similar, however a decrease was observed when CG was used due to the presence of impurities and lower glycerol content, which decreased the reaction efficiency [16]. In addition, the lower amount of glycerol molecules in CG and the consumption of hydroxyl groups due to competitive reactions caused by impurities are the responsible of the decrease of the I_{OH} index in bio-polyols comparing to those obtained when commercial glycerol was employed [28]. The A_n exhibited the same behaviour as that observed in our previous study, i.e, the higher the catalyst concentration, the higher the A_n. Nonetheless, using CG as solvent, the A_n values were slightly lower since organic impurities in the CG could lead to the consumption of acidic compounds [28]. Comparing the M_w obtained in this work with those obtained in our previous work, where a technical grade glycerol was used for the liquefaction process, it is worth noting that in all cases the M_w increased, particularly in $EOPE_{CG}$ bio-polyol. This can be explained by the polymerisation reactions between glycerol, FFA and FAMEs [29]. Consequently, the PDI of the CG synthesised bio-polyols were higher than those obtained with technical grade glycerol. This increase in the M_w and PDI was in agreement with that reported by Hu et al., (2014b) [16]. It could also

be concluded that the functionalities were also similar in all cases and appropriate to the class of PUs for which they were synthesised. However, in the case of $EOPE_{CG}$, the functionality was slightly above the limit value for the synthesis of elastic PU. As for the viscosities, it should be noted that, as expected with the increase in the M_w of the samples obtained with CG, the viscosities also increased or remained practically equal, as in the case of $POPE_{CG}$.

$EOPR_{CG}$ and $POPR_{CG}$ bio-polyols yields were within the typical values obtained for the liquefaction of lignocellulosic biomass or lignin, despite using CG instead of technical grade glycerol (Table P3.5). Furthermore, the yields obtained by Tran et al., (2021) [35] liquefying soluble acetone lignin using CG and 1,4-BDO in the presence of sulphuric acid were very similar to those obtained for $EOPE_{CG}$ and $POPE_{CG}$. It is noteworthy that, in most of the studies that are summarised in Table P3.5, polyols were used for the manufacture of foams. In such studies, the I_{OH} varied between 100 mg KOH/g and 811.8 mg KOH/g. Therefore, the I_{OH} values obtained for $EOPR_{CG}$ and $POPR_{CG}$ bio-polyols, which are intended for rigid PUs, were found to be in good concordance with the values of the literature. Few of the studies summarised in Table P3.5 indicated the PDI of polyols, and those that did so, referred to polyols for the synthesis of PU foams. The PDI obtained for $EOPR_{CG}$ and $POPR_{CG}$ in this work were in line with those reported by other authors in such studies.

Lee and Lin, (2008) liquefied Taiwan acacia and China fir employing PEG and glycerol with sulphuric acid as catalyst to produce polyols. Such polyols, which showed a I_{OH} of 310 and 287 (mg KOH/g), were used to synthesise PU adhesives. $EOPE_{CG}$ and $POPE_{CG}$ bio-polyols, synthesised to be used in the elaboration of elastic PUs, showed a very similar I_{OH} to those obtained in that study. Similarly, Jiang et al., [37] (2021) synthesised PU adhesives employing

polyols from liquefied lignocellulosic biomass (Norway spruce). However, in that case the I_{OH} was significantly higher (825 and 623 mg KOH/g). As for PDI, unfortunately, to the best of our knowledge, no studies were found indicating the PDI value for polyols obtained through the liquefaction of lignin for PU adhesive synthesis. Likewise, no research works were found where the functionality of polyols obtained through this process was indicated. Finally, the A_n was, in all cases, within the usual value (0-40 mg KOH/g) for this type of process.

Table P3.5. Different studies of lignocellulosic biomass and lignin liquefaction employing commercial or crude glycerol

Raw material	Solvent	Yield (%)	I_{OH}	A_n	Mw	PDI	*f*	Catalyst H_2SO_4	USE	Ref.
Eucalyptus globulus organosolv lignin	PEG + G	98.63	595.15	2.74	1394	3.69	4.03	-	Rigid PU	Pending publication
		71.98	253.84	33.01	4895	9.37	2.36	5%	Elastic PU	
Pinus radiata organosolv lignin		98.93	514.28	5.63	1383	3.58	3.55	-	Rigid PU	
		87.56	209.67	30.56	5408	6.95	2.91	3.86%	Elastic PU	
Eucalyptus globulus Kraft lignin	PEG + G	95.27	537.95	-	1775	3.51	-	3%	-	[26]
Olive tree pruning organosolv lignin	PEG + G	99.07	811.8	-	-	-	-	1%	-	[30]
Eucalyptus globulus kraft lignin	PEG + G	>86	100-660.08	0.8-10.70	1459-1990	-	-	3, 6, 9% (organic acids)	-	[31]
Enzymatic hydrolysis lignin of cornstalk	PEG + G	>90	191-409	-	-	-	-	15%	-	[18]
Alkaline corncob lignin	PEG + G	97.47	484.03	-	525	1.13	-	1.5%	PU foam	[32]
Sugarcane bagasse Organosolv lignin	CG	-	435	-	-	-	-	-	PU foam	[33]
Softwood Kraft lignin		-	515	-	-	-	-			
Hardwood Lignosulphonate		-	529	-	-	-	-			
Kraft lignin (softwood)	CG	>0.61 (g/g CG)	412		5088	2.2	-	-	PU foam	[34]
Organosolv lignin (sugarcane bagasse)			224		7867	4.9	-			
Lignosulphonate (hardwood)			592		7384	3.3	-			

Raw material	Solvent	Yield (%)	I_{OH}	A_n	Mw	PDI	*f*	Catalyst H_2SO_4	USE	Ref.
Acetone soluble lignin	CG + 1,4-BDO	72.64	≈1100	≈4	-	-	-	1%	PU foam	[35]
Kraft pine lignin	CG + 1,4-BDO	93	670	-	-	-	-	-	PU foam	[21]
Repeseed cake	PEG + G	84	586	-	-	-	-	80:20:3 (PEG: G : H_2SO_4)	-	[23]
Data seeds		96	395	-	-	-	-			
Olive stone		92	496	-	-	-	-			
Corncob		91	504	-	-	-	-			
Apple pomace		97	428	-	-	-	-			
Wheat straw		-	350	28	1270	1.22		-	PU foam	[19]
Taiwan acacia	PEG + G	95.2	310	25.6	-	-	-	3:1:0.09 (solvent: biomass: H_2SO_4)	Adhesives	[36]
China fir		98.4	287	38.0	-	-	-			
Norway spruce	EG	99.7	825-623	48.2-47.8	-	-	-	4.5 g	Adhesives	[37]

3. CONCLUSIONS

Bio-polyols suitable for the manufacture of rigid and elastic PUs were successfully prepared through the liquefaction of organosolv lignins from *Eucalyptus globulus* and *Pinus radiata*. The liquefaction reaction was carried out employing a microwave reactor using the optimal reaction conditions established in a previous study. PEG and CG, which was obtained from used vegetable oil, were utilised as solvents for this process. The effect of crude glycerol is obvious when comparing the results obtained with those obtained in our previous work. The liquefaction yields decreased in all cases due to the lower amount of glycerol in the mixture. Thus, the yields obtained for bio-polyols produced for rigid PUs where no catalyst was employed the yield was higher than 90%, whereas for bio-polyols intended for elastic PUs, where sulphuric acid was used as catalyst, the yields were significantly lower, between 70 and 80%. The I_{OH} of bio-polyols were also affected by the lower glycerol content when CG was used. The I_{OH} values obtained in this study were 554 and 383 (mg KOH/g) for $EOPR_{CG}$ and $POPR_{CG}$ bio-polyols respectively and 228 and 173 (mg KOH/g) for $EOPE_{CG}$ and $POPE_{CG.}$ The A_n values of the samples were in the expected range for this type of polyols. Regarding the functionalities, though in the case of $EOPE_{CG}$ the obtained value was slightly above the desired one, it could be said that the functionalities were adequate for the manufacture of the type of PU for which they were intended. This was confirmed by analysing the results of the rest of the parameters that were studied. Overall, even though the results of some parameters have worsened, it is concluded that CG recovered from used oil can be employed for the manufacture of bio-polyols to produce elastic and rigid PUs.

REFERENCES

[1] S. Kongjao, S. Damronglerd, M. Hunsom, Korean J. Chem. Eng. 27(3) (2010) 944–9. 10.1007/s11814-010-0148-0.

[2] S. Hu, X. Luo, C. Wan, Y. Li, J. Agric. Food Chem. 60(23) (2012) 5915–21. 10.1021/jf3008629.

[3] C.V. Rodrigues, K.O. Santana, M.G. Nespeca, J. Eduardo de Oliveira, S.I. Maintinguer, Int. J. Hydrogen Energy 41(33) (2016) 14641–51. 10.1016/j.ijhydene.2016.06.209.

[4] L.R. Kumar, S.K. Yellapu, R.D. Tyagi, X. Zhang, Bioresour. Technol. 293(August) (2019) 122155. 10.1016/j.biortech.2019.122155.

[5] C.A.G. Quispe, C.J.R. Coronado, J.A. Carvalho, Renew. Sustain. Energy Rev. 27 (2013) 475–93. 10.1016/j.rser.2013.06.017.

[6] J.C. Thompson, B.B. He, Appl. Eng. Agric. 22(2) (2006) 261–5. 10.13031/2013.20272.

[7] M.D. Bohon, B.A. Metzger, W.P. Linak, C.J. King, W.L. Roberts, Proc. Combust. Inst. 33(2) (2011) 2717–24. 10.1016/j.proci.2010.06.154.

[8] A. Hejna, P. Kosmela, M. Klein, K. Formela, M. Kopczyńska, J. Haponiuk, Ł. Piszczyk, J. Polym. Environ. 26(8) (2018) 3334–44. 10.1007/s10924-018-1217-4.

[9] M. Nanda, Z. Yuan, W. Qin, Austin J. Chem. Eng. 1(1) (2014) 1–7.

[10] M. Ionescu, in: De Gruyter (Ed.), Polyols for Polyrethanes, Boston, Berlin, 2019, pp. 1–10.

[11] Y. Lee, E.Y. Lee, J. Wood Chem. Technol. 36(5) (2016) 353–64.

10.1080/02773813.2016.1156132.

[12] S. Hu, X. Luo, Y. Li, ChemSusChem 7(1) (2014a) 66–72. 10.1002/cssc.201300760.

[13] X. Luo, S. Hu, X. Zhang, Y. Li, Bioresour. Technol. 139 (2013) 323–9. 10.1016/j.biortech.2013.04.011.

[14] J. D'Souza, R. Camargo, N. Yan, Polym. Rev. 57(4) (2017) 668–94. 10.1080/15583724.2017.1283328.

[15] Y.Y. Li, X. Luo, S. Hu, Bio-based Polyols and Polyurethanes, 2015, pp. 1–79.

[16] S. Hu, Y. Li, Ind. Crops Prod. 57 (2014b) 188–94. 10.1016/j.indcrop.2014.03.032.

[17] S.H. Lee, M. Yoshioka, N. Shiraishi, J. Appl. Polym. Sci. 78(2) (2000) 319–25. 10.1002/1097-4628(20001010)78:2<319::AID-APP120>3.0.CO;2-Z.

[18] Y. Jin, X. Ruan, X. Cheng, Q. Lü, Bioresour. Technol. 102(3) (2011) 3581–3. 10.1016/j.biortech.2010.10.050.

[19] F. Chen, Z. Lu, J. Appl. Polym. Sci. 111 (2009) 508–16. 10.1002/app.29107.

[20] M. Ionescu, in: De Gruyter (Ed.), Polyols for Polyurethanes, Boston, Berlin, 2019, pp. 307–20.

[21] K. Gosz, P. Kosmela, A. Hejna, G. Gajowiec, Ł. Piszczyk, Wood Sci. Technol. 52(3) (2018) 599–617. 10.1007/s00226-018-0991-4.

[22] M. Ionescu, Z.S. Petrović, Eur. J. Lipid Sci. Technol. 120(6) (2018) 1–9.

10.1002/ejlt.201800004.

[23] R. Briones, L. Serrano, J. Labidi, J. Chem. Technol. Biotechnol. 87(2) (2012) 244–9. 10.1002/jctb.2706.

[24] A. Morales, B. Gullón, I. Dávila, G. Eibes, J. Labidi, P. Gullón, Ind. Crops Prod. 124(May) (2018) 582–92. 10.1016/j.indcrop.2018.08.032.

[25] K. Behera, Y.H. Chang, F.C. Chiu, J.C. Yang, Polym. Test. 60 (2017) 132–9. 10.1016/j.polymertesting.2017.03.015.

[26] S.H.F. da Silva, P.S.B. dos Santos, D. Thomas da Silva, R. Briones, D.A. Gatto, J. Labidi, J. Wood Chem. Technol. 37(5) (2017) 343–58. 10.1080/02773813.2017.1303513.

[27] P. Parcheta, J. Datta, Polym. Test. 67(January) (2018) 110–21. 10.1016/j.polymertesting.2018.02.022.

[28] S. Hu, C. Wan, Y. Li, Bioresour. Technol. 103(1) (2012) 227–33. 10.1016/j.biortech.2011.09.125.

[29] X. Luo, S. Hu, X. Zhang, Y. Li, Bioresour. Technol. 139 (2013) 323–9. 10.1016/j.biortech.2013.04.011.

[30] A. Sequeiros, L. Serrano, R. Briones, J. Labidi, J. Appl. Polym. Sci. 130(5) (2013) 3292–8. 10.1002/app.39577.

[31] S.H.F. da Silva, I. Egüés, J. Labidi, Ind. Crops Prod. 137(March) (2019) 687–93. 10.1016/j.indcrop.2019.05.075.

[32] B.L. Xue, J.L. Wen, R.C. Sun, Materials (Basel). 8(2) (2015) 586–99. 10.3390/ma8020586.

[33] L.C. Muller, S. Marx, H.C.M. Vosloo, J. Renew. Mater. 5(1) (2017) 67–

80. 10.7569/JRM.2016.634130.

[34] L.C. Muller, S. Marx, H.C.M. Vosloo, I. Chiyanzu, Polym. from Renew. Resour. 10(1–3) (2019) 3–18. 10.1177/2041247919830833.

[35] M.H. Tran, J.H. Yu, E.Y. Lee, Polymers (Basel). 13(9) (2021). 10.3390/polym13091491.

[36] W.-J. Lee, M.-S. Lin, J. Appl. Polym. Sci. 109(1) (2008) 23–31. 10.1002/app.28007.

[37] W. Jiang, R. Hosseinpourpia, V. Biziks, S.A. Ahmed, H. Militz, S. Adamopoulos, Polymers (Basel). 13(19) (2021) 1–18. 10.3390/polym13193267.

SYNTHESIS OF POLYURETHANE AND NON-ISOCYANATE POLYURETHANE WOOD ADHESIVES

“In my experience, when you think you understand The Force,

you realize just how little you know”

Ashoka Tano

Publication IV

Synthesis, characterisation, and thermal degradation kinetic of lignin-based polyurethane wood adhesives

ABSTRACT

In this work, different PU wood adhesives were synthesised using different ligno-based bio-polyols obtained in ***Publication II***. The synthesis of PUs was carried out by one-shot method using THF as solvent and MDI as diisocyanate employing different NCO:OH ratios (2.0:1, 2.5:1, and 3.0:1). The chemical structure of the formulated wood adhesive PUs was determined through ATR-FTIR and the shear strength was analysed using Automated Bonding Evaluation System (ABES). Through this technique it was concluded that an NCO:OH ratio of 2.5:1 was the formulation that showed the best shear strength for a pressing time of 120 s. Employing this ratio and the same synthesis procedure, two new PUs were synthesised using the bio-polyols obtained in ***Publication III***.

Finally, a study of thermal degradation kinetics employing the OFW and KAS isoconversional methods of the PUs synthesised with an NCO:OH ratio of 2.5:1 was carried out. On the one hand, the E_a of each system were estimated for the different α ratios, obtaining values of 226 (KJ/mol) (LPA_{EOPE}), 180.8 (KJ/mol) (LPA_{EOPECG}), 146.9 (KJ/mol) (LPA_{POPE}) and 143.4 (KJ/mol) ($LPA_{POPECG)}$. In addition, the pre-exponential factor was determined with which an estimation of the lifetime of the polymers was performed.

1. MATERIALS AND METHODS

1.1. Materials

The raw materials, *Eucalyptus globulus* chips and *Pinus radiata*, as well as the used vegetable oil and chemicals employed in this work were obtained as described in ***section 2.1*** of the **2nd PART.**

1.2. Lignin obtaining procedure

Lignins used in this work were obtained after the organosolv delignification process and the subsequent ultrasound treatment of the black liquor described in ***section 2.2*** of the **2nd PART**. These lignins called EOUL (*Eucalyptus globulus* organosolv lignin) and POUL (*Pinus radiata* organosolv lignin) were characterised in ***Publication II***.

1.3. Crude glycerol obtaining procedure

CG was obtained by the transesterification reaction outlined in **section 2.4** of the **2nd PART**.

1.4. Synthesis of bio-polyols through microwave assisted liquefaction

The liquefaction of organosolv lignins (EOUL and POUL) were performed following the methodology detailed in the ***section 2.3.1*** of the **2nd PART**.

The catalyst concentration, as well as the reaction temperature and the PEG/CG ratio involved in the reaction, were obtained from the optimisation carried out in ***Publication II*** and are summarised below (Table P4.1).

Table P4.1. Liquefaction reaction conditions optimised in ***Publication II***

Bio-polyol	EOPE & $EOPE_{CG}$	POPE & $POPE_{CG}$
Cat (% wt.)	5	3.86
Temperature (°C)	180	160
PEG/CG (% wt.)	7.57/1	7.34/1

1.5. Synthesis of lignin-based polyurethane adhesives

The synthesis of the different lignin-based polyurethane adhesives (LPA) using the above-mentioned bio-polyols, i.e., EOPE, $EOPE_{CG}$, POPE and $POPEC_{CG}$ was carried out following the procedure described in the ***section 2.5*** of the **2nd PART**. Three different NCO:OH ratios were employed in the synthesis of PUs using EOPE and POPE bio-polyols, viz. 2.0:1, 2.5:1 and 3.0:1. For the synthesis of PUs with $EOPE_{CG}$ and $POPEC_{CG}$, the ratio giving the best shear strength value was employed. Table P4.2 shows the recipe used for each of the synthesised LPA.

Table P4.2. Recipe used for the synthesis of LPAs

		LPA_{EOPE}	LPA_{POPE}	LPA_{EOPECG}	LPA_{POPECG}
Bio-polyol (g)		2.5	2.5	2.5	2.5
THF (g)		1.5	1.5	1.5	1.5
DBTDL (wt%)*		0.2	0.2	0.2	0.2
NCO:OH	2.0:1	3.68	2.03	-	-
	2.5:1	4.6	2.53	3.96	3.40
	3.0:1	5.52	3.04	-	-

1.6. Characterisation of the obtained bio-polyols

Important parameters, such as such as molecular weight distribution (M_w, M_n and PDI), hydroxyl number (I_{OH}), acid number (A_n) and functionality (*f*) of the bio-polyols obtained in the reaction scale-up were determined.

Furthermore, the thermal degradation of bio-polyols was studied through a thermogravimetric analysis (TGA) and their rheological behaviour was assessed. This characterisation was conducted according to the methodologies explained in **Appendix II**.

1.7. Characterisation of lignin-based polyurethane adhesives

The LPAs were characterised through ATR-FTIR to determine both their chemical structure and their degree of microphase separation and miscibility. In addition, thermogravimetric analysis was employed to study the thermal degradation, the thermal degradation kinetic by OFW and KAS methods and the lifetime estimation of the PUs by OFW method. In addition, the shear strength of the LPAs was assessed by adhesion test employing an automated bonding evaluation system (ABES). For these characterisations, the procedures described in **Appendix II** were used. The curing process of the PUs was carried out at room temperature for 7 days.

2. RESULTS AND DISCUSSION

2.1. Bio-polyols characterisation

The bio-polyols were characterised to establish their suitability for the synthesis of polyurethane adhesives. Therefore, the molecular weight distribution (M_w, M_n, PDI), hydroxyl number (I_{OH}), acid number (A_n), functionality (*f*), and the chain derived from a hydroxyl group (EW) of the different samples were analysed, and a summary of the results is presented in Table P4.3.

Table P4.3. Characterisation of bio-polyols employed to synthesise PUs

Sample	M_n	M_w	PDI	I_{OH}	A_n	*f*	EW
EOPE	739±43	3934 ± 98	5.33±0.18	330 ± 3	35 ± 0.36	4.16	153.7
POPE	707±32	4079 ± 50	6.29±0.92	182 ± 51	25 ± 0.00	2.29	271
$EOPE_{CG}$	852±8	6644 ± 89	7.79±0.18	284 ± 1	17 ± 0.24	4.29	186.4
$POPE_{CG}$	933±85	11035 ± 1059	12.63±0.00	182 ± 30	20 ± 0.64	2.83	277.7

M_n and M_W (g/mol), I_{OH} and A_n (mgKOH/g)

As expected, the obtained results were like those obtained in our previous works (data not published), although, expectedly, due to the scale-up of the

reaction, they differed slightly. Thus, the M_w was within the range required for this type of PU (2000-10000 g/mol) except for $POPE_{CG}$ which has a M_w of 11035 g/mol [1]. As with this type of bio-polyols synthesised through liquefaction reactions, the A_n in all cases was high, but within the usual values [2]. However, the I_{OH} values resulted to be higher than 28-160 mg KOH/g, which are the values suggested for the synthesis of these PUs [3]. This is especially pronounced for EOPE and $EOPE_{CG}$, while POPE and $POPE_{CG}$ were practically in the required range. In addition, *f* of POPE and $POPE_{CG}$ bio-polyols was between 2 and 3 in both cases, whereas that of the EOPE and $EOPE_{CG}$ bio-polyols was 4.16 and 4.29 respectively. The EW of POPE and $POPE_{CG}$ resulted to be higher than the EOPE and $EOPE_{CG}$, i.e., the chains derived from the hydroxyl groups of POPE and $POPE_{CG}$ were higher than those obtained for bio-polyols synthesised with organosolv lignin from *Eucalyptus globulus* [4]. This, together with the low functionality, the I_{OH}, and M_w, suggests that POPE and $POPE_{CG}$ bio-polyols could be more suitable for the synthesis of PU adhesives.

Differences with respect to our previous studies can be explained by the scale-up of the reaction and the type of vessel employed in each case. In fact, the vessel used in the scale-up was of round bottom flask type whereas in the previous studies it was of the test tube type, which makes more difficult the homogenisation of the sample. Therefore, although the I_{OH} and *f* of EOPE and $EOPE_{CG}$ bio-polyols were slightly higher than the required values, the bio-polyols were suitable for synthesising PU adhesives.

2.2. Lignin-based polyurethane adhesive characterisation

A total of six PU adhesives were synthesised, three with each of the bio-polyols (EOPE and $EOPE_{CG}$), following the procedure summarised in Table P4.2. Aliquots of the PUs were taken every 30 minutes, with the aim of

following the reaction, until the gel time was reached, and then they were analysed by ATR-FTIR. The ATR-FTIR spectra are shown in Figure P4.1 and the most characteristic bands are listed in Table P4.4.

Table P4.4. ATR-FTIR band assignments of PU spectra synthesised with EOPE and POPE bio-polyols

Wavenumber (cm^{-1})	Band assignment
3400	O-H stretching
3290	N-H stretching vibration of urethane groups
2970-2940-2870	CH stretching of CH3 and CH2
2270	Antisymetric stretching vibration of NCO
1730-1706	C=O stretching
1599	C-C stretching of the aromatic ring of MDI
1507	N-H vending vibration
1407	C-H stretching of the aromatic ring of MDI
1308	C-N stretching of urethane group
1225	C-N stretching of urethane group
1096	C-O-C stretching

As observed, in all cases, as the reaction progresses in time, the band assigned to the O-H stretching (3400 cm^{-1}) decreases as a consequence of the reaction between the NCO groups of MDI and OH groups of bio-polyols to create urethane (NHCO) groups. The creation of urethane groups was confirmed by the appearance of the peaks at 3290 cm^{-1}, related with the stretching vibration of N-H groups, 1730 cm^{-1} and 1706 cm^{-1} bands corresponding to the C=O stretching vibration and the N-H vending vibration at 1507 cm^{-1} [5]. These bands increased as the isocyanate groups were consumed to create urethane bonds. It is also observable the C-N stretching bands of urethane group at 1308 cm^{-1} and 1225 cm^{-1} [6]. The C-C and C-H absorptions bands which correspond to the stretching of the aromatic ring of the MDI are observed at 1599 cm^{-1} and 1407 cm^{-1} [7].

Two aspects are noteworthy; the first one is that surprisingly in the cured LPA_{EOPE} samples, isocyanate remains unconsumed in all cases, while in the LPA_{POPE} samples, the band corresponding to the NCO anti-symmetric vibration (2270 cm^{-1}) is not observed in the cured samples. The reason for this is probably that lignin from *Eucalyptus globulus* is more sterically hindered than lignin form *Pinus radiata*, since the former has more syringyl groups [8]. This unreacted isocyanate in LPA_{EOPE} samples, besides being toxic, could react with the OH of the beech veneer strip or the water adsorbed by wood to form covalent bonds increasing the shear strength, leading to undesired behaviour of the PU [9]. The second is that, as the reaction progresses, the contribution of the bands corresponding to the C=O groups which are related to the free urethanes (1730 cm^{-1}) and the one assigned to the urethane groups linked through hydrogen bonds (1709 cm^{-1}) [10] gradually changes.

Using ATR-FTIR spectra, the degree of separation and miscibility of the micro-phase of a PU can be determined [11]. In fact, analysing this area of the spectra corresponding to carbonyl stretching, the different C=O species present in PUs known as free C=O groups not associated by hydrogen bonds (free C=O and free C=O ester), H-bonded C=O in disordered hard segment (HS), H-bonded C=O in ordered HS and H-bonded C=O in disordered soft segment (SS), can be determined [12]. The analysis of the micro-phase separation is of interest because the mechanical properties of PUs, among others, depend to a large extent on it [13].

Through the deconvolution of the absorbance bands of C=O groups, the degree of micro-phase separation could be determined, the curve fitting of the different cured PUs samples was carried out through a Gaussian curve shape obtaining R^2 values above 0.999 in all cases and the spectra are shown in Figure P4.2. Table P4.5 summarised the theoretical hard segment (HS_t)

percentage of each PU calculated as indicated in **Appendix II**, as well as the percentages of the different C=O species, which were calculated by deconvolution of such bands in the ATR-FTIR spectra.

As expected, the higher the NCO:OH ratio, the higher the HS_t content, moreover the percentage of HS_t was similar for PUs with the same isocyanate to hydroxyl ratio. The trend of free urethane carbonyl groups in HS in the LPA_{EOPE} formulations was to decrease, although for the 2.5 the value was slightly lower than in 3.0. Consequently, the H-bonded urethane carbonyl groups in both disordered and ordered HS followed the opposite trend, i.e., they increased with increasing MDI content, except in formulation 2.5 which was the lowest, despite it showed H-bonded urethane carbonyl groups in Soft-Hard segment. On the other hand, LPA_{POPE} formulations showed the same behaviour as LPA_{EOPE}, i.e., the H-bonded urethane carbonyl groups in disordered and ordered HS decreased in formulation 2.5 which is the opposite to what would be expected, since as the HS increases, the H-bonded urethane C=O groups tends to increase [10].

According to the procedure described by Niemczyk et al., (2017) [14], the mass fraction of the hard and soft segments of a PU, as well as their degree of micro-mixing, can be determined. Thus, it is possible to determine different parameters such as the proportion of H-bonded C=O groups (X_{HB}), the maximum mass fraction of the rigid segment mixed in the soft phase (W_H), if assuming that all the H-bondend C=O groups are only found in the rigid domains, the weight fraction of the mixed phase (MP_W), the soft segment weight fraction (SS_W) and the hard segment weight fraction (HS_W). The equations for the calculation of these parameters are listed in **Appendix II**. In Table P4.6 the corresponding values of these parameters are indicated for each formulation.

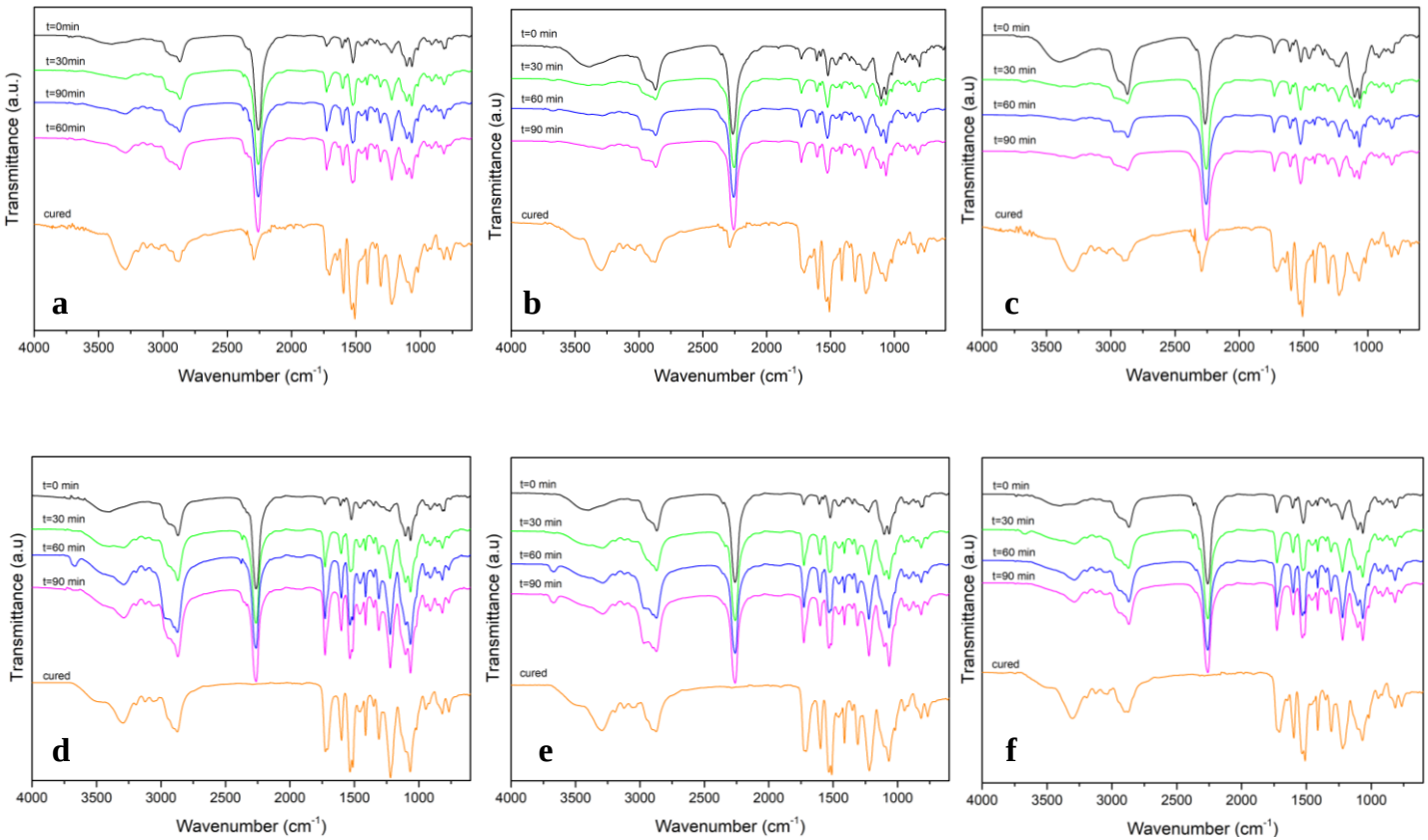

Figure P4.1. ATR-FTIR spectra of the LPA formulations at different reaction times and cured. a, b, and c are the 2.0, 2.5 and 3.0 LPA_{EOPE} formulations and d, e and f are the LPA_{POPE} equivalents

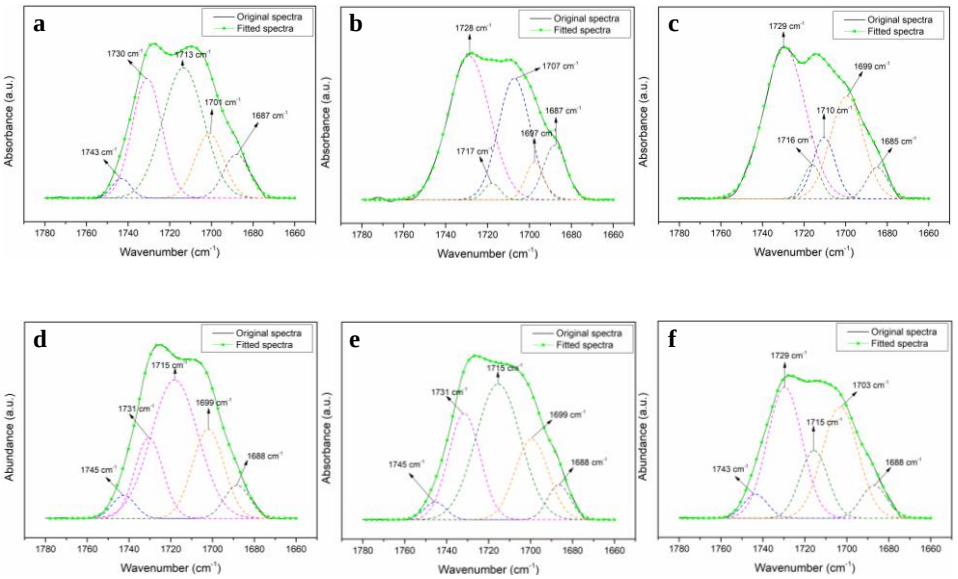

Figure P4.2. ATR-FTIR spectra in the absorbance region of the carbonyl groups of the different LPAs. a, b and c are the 2.0, 2.5 and 3.0 LPA_{EOPE} formulations and d, e and f are the LPA_{POPE} equivalents

Table P4.5. Percentages of C=O urethane species in cured LPAs

	NCO/OH	NCO (mol)	HS_t (%)	A	B	C	D	E	F
LPA_{EOPE}	2.0:1	2.00	33.60	3.01	29.02	43.76	---	15.02	9.19
	2.5:1	2.50	38.74	2.24	29.56	39.15	8.10	10.46	10.49
	3.0:1	3.00	43.15	2.59	46.59	20.16	---	25.70	4.64
LPA_{POPE}	2.0:1	2.00	34.33	4.10	17.43	50.29	---	21.67	6.51
	2.5:1	2.50	39.52	2.92	25.23	45.67	---	20.19	5.98
	3.0:1	3.00	43.95	2.76	38.83	26.36	---	27.05	5.00

A: 1745-1743 cm^{-1} Free C=O in Soft Segment (%)
B: 1732-1729 cm^{-1}: Carbonyl-carbonyl interactions in Soft Segment (%)
C: 1714-1713 cm^{-1}: Free urethane C=O in Hard Segment (%)
D: 1706 cm^{-1}: H-bonded C=O in Soft-Hard Segment (%)
E: 1701-1697 cm^{-1}: H bonded urethane C=O in disordered Hard Segment (%)
F: 1686-1688 cm^{-1}: H bonded urethane C=O in ordered Hard Segment (%)

Table P4.6. Relevant parameters estimated for the determination of microphase of different formulations

Sample	NCO:OH	*z*	X_{HB}	W_H	MP_W	SP_W	HS_W
LPA_{EOPE}	2.0:1	0.336	0.316	0.257	0.086	0.750	0.250
	2.5:1	0.387	0.308	0.304	0.118	0.730	0.270
	3.0:1	0.431	0.556	0.252	0.109	0.677	0.323
LPA_{POPE}	2.0:1	0.343	0.318	0.263	0.090	0.747	0.253
	2.5:1	0.395	0.323	0.307	0.121	0.726	0.274
	3.0:1	0.440	0.503	0.280	0.123	0.684	0.316

z is the HS_t fraction

According to the analysis of the data presented in Table P4.6, the mass fraction of the H-bonded urethane groups (X_{HB}) tended to increase with increasing the HS content except for LPA_{EOPE} 2.5 formulation which had the lowest value. Furthermore, in all cases the X_{HB} content was low. This could be explained by the cross-linked and sterically hindered nature of the lignobased bio-polyol. This unique chemical conformation may inhibit hydrogen bonding between the carbonyl group of the urethane groups of a rigid segment chain and the NH urethane groups of adjacent rigid segment chains [15].

When analysing the mass fraction of the rigid segment mixed in the soft phase (W_H), the same behaviour to X_{HB} was observed, i.e, it tends to increase with increasing the isocyanate content, therefore, the mass fraction of the mixed also increased. This was in agreement with the expected result, since increasing the MDI content in the mixture the degree of phase separation tends to be lower, in other words, the amount of hard segment mixed into the soft phase increases [14]. However, in the 3.0 formulations of both PUs, a decreasing behaviour was observed, thus in the case of LPA_{EOPE} the lowest amount of rigid segment mixed in the soft phase was observed, while in the case of LPA_{POPE} this formulation showed an intermediate value between

formulations 2.0 and 2.5. In general, LPA_{EOPE} W_H and MP_W values were slightly lower than those of LPA_{POPE}, i.e., the former exhibited higher phase separation or lower miscibility between the HS and the SS. An explanation for this may lie in the nature of the lignin used to synthesise the PUs. Thus, lignin from *Eucalyptus globulus* with a higher number of syringyl groups in its structure, presented a greater steric hindrance that increases phase separation and decreases the miscibility. This greater phase separation in LPA_{EOPE}, even if relatively small, could result in better mechanical properties of the PU [16].

The SS content predictably decreases with increasing HS content, which has a great influence on the final mechanical properties of the PU, since it is responsible for providing flexibility and mobility to the chains [17], so it is necessary to find a balance between the chain mobility offered by the SS and the stiffness conferred by HS. On the other hand, it should be noted that the theoretical value of HS content was higher than the calculated one, indicating that the presence of lignin as well as its origin affected to the HS formation.

The ABES testing was carried out to measure the bonding strength of the different PU adhesives formulation. Such tests are able to determine the tensile strength required to disrupt the adhesive bond and indicate the shear strength of an adhesive [6]. Figure P4.3a and 3b shows the shear strength test results of PUs synthesised with EOPE and POPE bio-polyols and employing different NCO:OH ratios.

At first glance, it is evident that there is a big difference between PUs synthesised with EOPE (Figure P4.3a) and those synthesised with POPE (Figure P4.3b). When using NCO:OH ratios of 2.0 and 2.5 othe PUs synthesised with the POPE bio-polyol reached lower shear strength values. On the contrary, when using a ratio of 3.0:1 the shear strength of the PU increased rapidly reaching a value of 4.08 (MPa) at pressing time of 120 s.

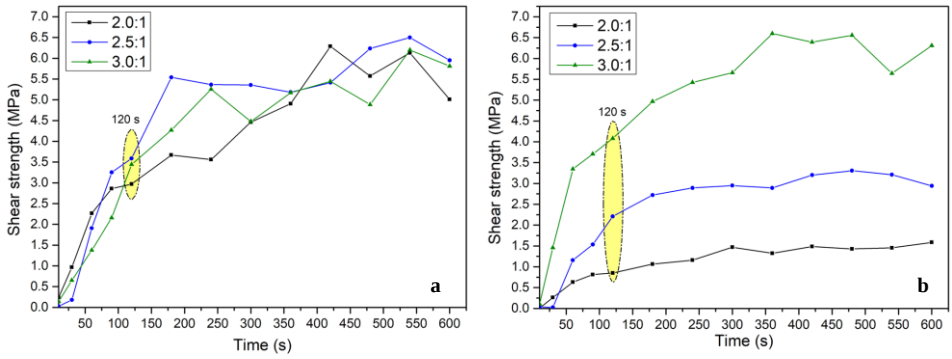

Figure P4.3. Shear strength of lignin-based polyurethane adhesives; (a) LPA_{EOPE}, (b) LPA_{POPE}

The shear strength continued increasing up to 5.66 MPa at 180 s and after this pressing time, the undesirable failure of the substrate occurred. From Figure P3.4a it can be noted that very similar high shear strength values were obtained regardless of the formulations used. This behaviour was probably caused by the unreacted isocyanate in these formulations, which interacted with the hydroxyl groups of the veneer strips to form additional covalent bonds that distorted the results. In addition, as with the PU formulated with POPE and a NCO:OH ratio of 3.0:1, at elevated pressing times, substrate failure occurred. Considering the values presented in Table P4.6, there was no significant difference in terms of HS_W and SS_W between the LPA_{EOPE} and LPA_{POPE} formulations, therefore, the previously mentioned unreacted isocyanate is the only explanation for the high results obtained with 2.0 and 2.5 LPA_{POPE} formulations.

Three typical stages were observed, caused by the behaviour of the adhesive in the curing process [18]. In the first stage, a delay in the development of bond strength is observed, which can be associated with energy loss due to water evaporation. The second zone is related to the chain elongation process and cross-linking between the chains. The third stage depends on the behaviour of the adhesive against temperature and humidity, so during this

stage the shear strength can increase or decrease depending on the nature of the adhesive [19]. This last stage is only visible in the 2.5 and 3.0 formulations of PUs synthesised with POPE.

Nevertheless, considering a pressing time of 120 s, which is a common pressing time in industry, it was observed that the highest shear strength value (3.58 MPa) was obtained with the 2.5:1 NCO:OH ratio in the PUs formulated with EOPE, while a value of 4.08 MPa was achieved in the PUs formulated with POPE using the 3.0:1 NCO:OH ratio. For this reason, this ratio was selected to formulate the PUs based on the bio-polyols synthesised using CG ($EOPE_{CG}$ and $POPE_{CG}$).

2.3. Characterisation of LPA employing bio-polyols formulated with CG

Employing the respective quantities of reagents summarised in Table P4.2, two PU adhesives were synthesised using the bio-polyols formulated with CG and NCO:OH ratio of 2.5:1, namely, LPA_{EOPECG} and LPA_{POPECG}. Finally, a comparison with the PU adhesives synthesised with the same NCO:OH ratio of the previous section was performed.

The ATR-FTIR spectra of both cured PU adhesives as well as the analysis of the region belonging to the carbonyl groups are represented in Figure P4.4 and Figure P4.5a and 5b, respectively. The spectra exhibit the same characteristic bands as those described above. It should be highlighted that also, in this case, isocyanate remains unreacted when the PU was formulated using the bio-polyol from *Eucalyptus globulus* lignin. Therefore, it can be confirmed that due to its higher steric hindrance, part of the isocyanate cannot react with the hydroxyl groups of the bio-polyol.

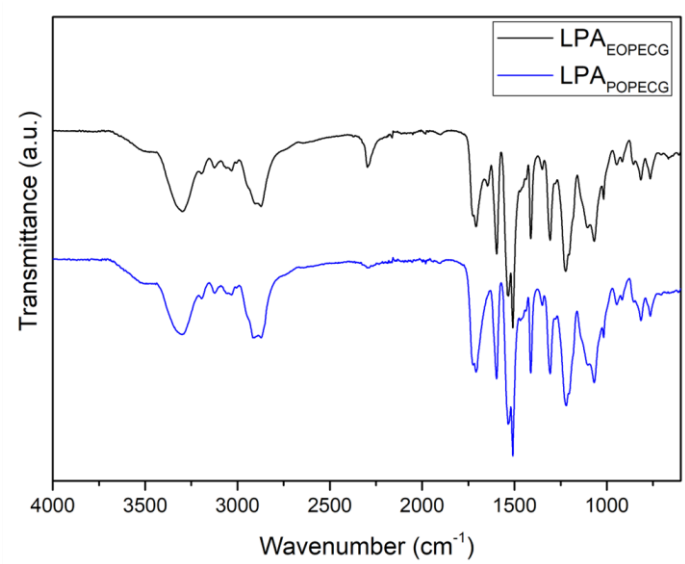

Figure P4.4. ATR-FTIR spectra of cured LPAs of LPA$_{EOPECG}$ and LPA$_{POPECG}$ samples

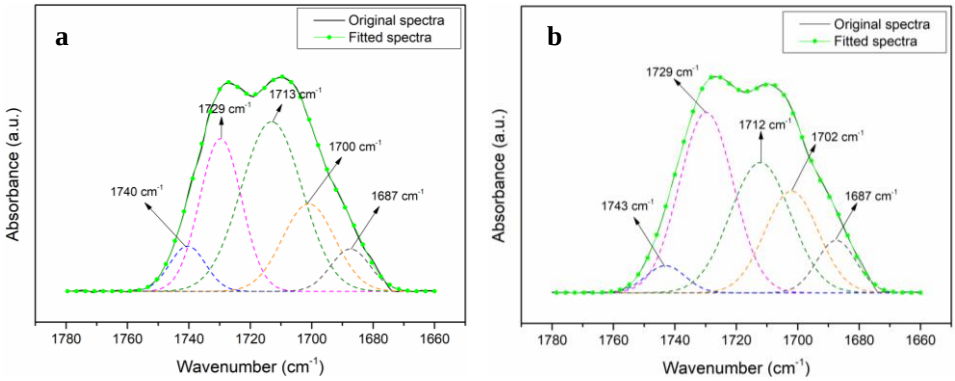

Figure P4.5. ATR-FTIR spectra of the absorbance region of the carbonyl groups of LPA$_{EOPECG}$ (a) and LPA$_{POPECG}$ (b) obtained through a Gaussian curve shape. The obtained R^2 values were above 0.999

From the deconvolution of the area corresponding to the carbonyl groups represented in Figures P4.5a and P4.5b, the X_{HB}, W_H, MP_W, SS_W and HS_W parameters were calculated and summarised in Table P4.7.

Compared to their respective homologues, for both PUs synthesised using the bio-polyol formulated with CG, the theoretical content of HS was lower. However, X_{HB} was higher in the case of LPA_{EOPECG}. Likewise, both W_H and MP_W were lower. This indicates that for this PUs there was a lower amount of HS mixed in the soft phase and therefore the segregation of the micro-phases was higher. Such behaviour could be explained by the higher molecular weight of the $EOPE_{CG}$ and $POPE_{CG}$ bio-polyols with respect to EOPE and POPE, which would allow the phase separation [20].

Table P4.7. Relevant parameters estimated for the determination of microphase separation in GC-formulated LPAs

Sample	NCO:OH	*z*	X_{HB}	W_H	MP_W	SP_W	HS_W
LPA_{EOPECG}	2.5:1	0.362	0.335	0.274	0.099	0.737	0.263
LPA_{POPECG}	2.5:1	0.346	0.303	0.269	0.093	0.747	0.253

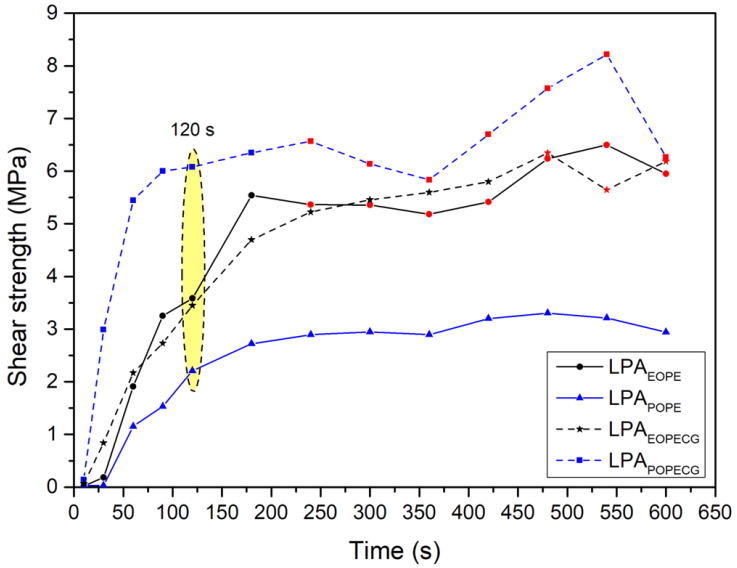

Figure P4.6. Shear strength of lignin-based polyurethane adhesives. The red point indicated the substrate failure

The shear strength of the LPA_{EOPECG} and LPA_{POPECG} adhesives were measured and compared with their counterparts LPA_{EOPE} and LPA_{POPE} in Figure P4.6. As

expected, the results obtained agreed with what was projected after studying the degree of microphase separation of PUs, since the mechanical properties of polyurethanes can be improved by increasing the microphase separation [13]. Thus, LPA_{POPECG} showed the best shear strength results (6.06 MPa) due to its lower weight fraction of the mixed phase. Nevertheless, as happened with LPA_{EOPE}, at pressing times higher than 180 s, substrate failure occurred. On the other hand, LPA_{EOPECG} with a shear strength value of 2.6 MPa behaved very similar to its homologue LPA_{EOPE} despite having a lower degree of phase separation, which may be a consequence of the unreacted isocyanate in both samples. The obtained shear strength values were in the range of those reported by other authors, such as Nacas et al., (2017) [9] who obtained a shear strength of 6.8 MPa using Kraft lignin and MDI with a NCO:OH ratio of 1.2:1. Magina et al., (2021) [6] used lignosulphonates together with MDI and different quantities of PEG200 to synthesise different wood adhesives. They concluded that the best formulation was the one with an NCO:OH ratio of 2.1:1 obtaining a shear strength value close to 3 MPa. Gouveia et al., (2020) [21] studied the effect of lignin hydroxypropylation by synthesising various PU wood adhesives using KL and hydroxypropylated KL with MDI and a NCO:OH ratio of 1.1:1. They concluded that the best shear strength value was obtained with unmodified lignin (4.5 MPa), while hydroxpropylation improved elasticity and tensile strength at the expense of shear strength. Vieira et al., (2022) [22] obtained a wood PU adhesive based on oxyalkylated Kraft lignin using a 1.3:1 ratio with a shear strength of 3.1 MPa.

The thermostability of the LPAs was studied through a thermogravimetric analysis. According to the DTG curves represented in Figure P4.7, the major weight loss of the samples took place between 225 °C and 450 °C. Regardless of the polyol used in the PU formulation, the degradation zones were the same although the maximum degradation temperatures varied slightly.

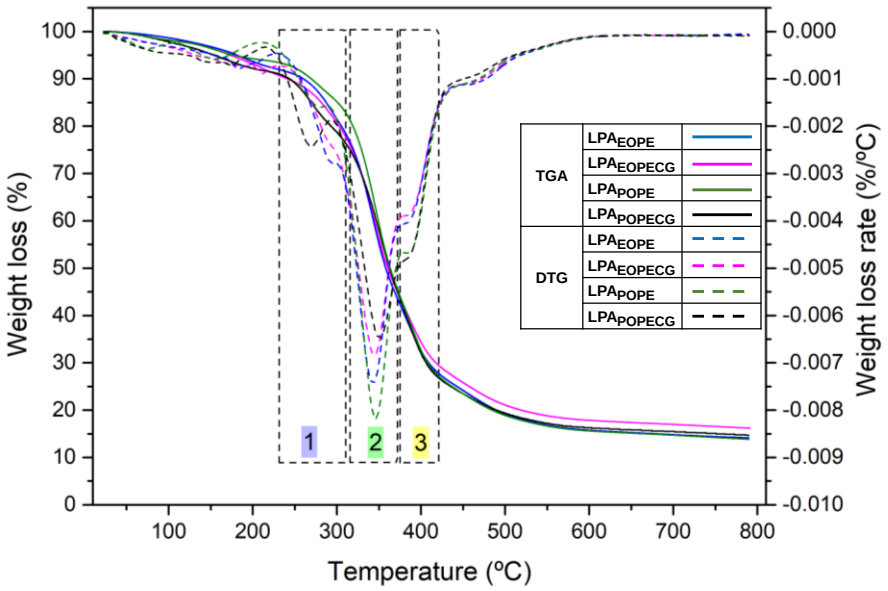

Figure P4.7. TGA and DTG curves of the different LPAs

The first degradation zone (225-310 °C) corresponds to the H-bonded urethane groups of the HS [23] and the cleavage of unstable ether linkages of lignin (β-O-4, α-O-4 and 4-O-5) [24]. The region with the highest mass loss, region 2, which is located between 310-375 °C, is associated with the degradation of the soft segment of the polyurethane [8]. The last mass loss area, region 3 (375-420 °C), is considered the degradation area of the diisocyanate and the aromatic rings of lignin [25]. A similar final residue was obtained for all PUs due to the presence of lignin in the samples. It can also be observed that the maximum degradation temperature at the first mass loss step was higher in LPA_{EOPE} and LPA_{EOPECG} than in LPA_{POPE} and LPA_{POPECG}, which means a higher stability of the formers. Generally, since the first degradation zone corresponds to the degradation of the H-bonded urethane groups, PUs with less amount of these, tend to be less stable, as less energy will be required to break them. However, this is not the case for LPA_{EOPE}, which despite having more H-bond urethane groups than LPA_{POPE} is more stable. Nevertheless, since the X_{HB} values were very similar in all cases, the

higher stability of the LPA_{EOPE} and LPA_{EOPECG} samples could be explained since, as mentioned above, in PUs with lignin, in this first degradation zone there is also degradation of ether linkages, which are more abundant in hardwoods such as *Eucalyptus globulus* than in softwood as *Pinus radiata* [26].

Using different heating rates (1, 2, 5 and 10 °C/min) and the isoconversional methods of OFW and KAS described in **Appendix II**, the activation energy (E_a) of each system was calculated. In addition, the average lifetime of the PUs was estimated through the OFW method, for which the pre-exponential factor A was determined. The calculation of both E_a and A was performed from the slope and the intercept of the plots of $\ln(\beta)$ and $\ln\left(\frac{\beta}{T_p^2}\right)$ versus 1000/Tp. In these graphs, the conversion rates from 5% to 90% for each system were ploted. FigureP4.8a, 8b, 8c and 8d showed the different TGA curves obtained with each heating rate for the different systems. In all cases, as expected, as the heating rate increases, the degradation curve shifted towards higher temperatures. The final residue of each PU was between 16.5-17 % (LPA_{EOPE}), 14-16 % (LPA_{EOPECG}), 13.9-15.8 % (LPA_{POPE}) and 11.8-13.8 % (LPA_{POPECG}).

From Figure P4.9, it could be concluded that the model was well selected since linear and parallel straight lines and very high correlation coefficients were obtained. Nevertheless, in the LPA_{POPECG} samples (Figure P4.9d and 4.9h), the line corresponding to the conversion of 0.9 was not properly fitted, so it was not considered for the calculation of the E_a and A.

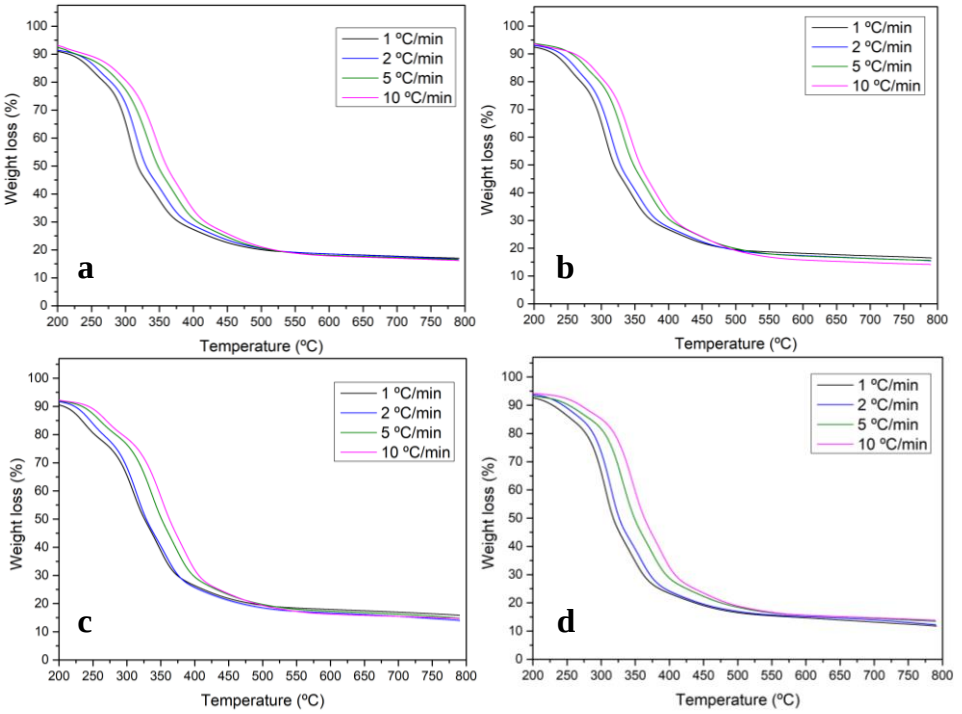

Figure P4.8. TGA curves at the different heating rates for LPA_{EOPE} (a), LPA_{EOPECG} (b), LPA_{POPE} (c) and LPA_{POPECG} (d)

According to the results obtained and outlined in Tables P4.8 and P4.9 and taking into account that the E_a is the impediment to the degradation process [27], the synthesised PUs will degrade in the following order from the slowest one to the fastest one for α=0.05: LPA_{EOPE} > LPA_{EOPECG} > LPA_{POPE} > LPA_{POPECG}. Due to the nature of the bio-polyols, different behaviour was observed in the decomposition reaction mechanism between PUs formulated with different bio-polyols as shown in Figure P4.10. The E_a follows the same trend for LPA_{EOPE} and LPA_{EOPECG}, both samples presented a high value at the beginning, which decreased to a minimum and then increased again. While in LPA_{POPE} and LPA_{POPECG}, the minimum E_a value was obtained at the beginning and then increased. However, in the case of LPA_{POPECG} the last two values tend to decrease because of the poor fitting.

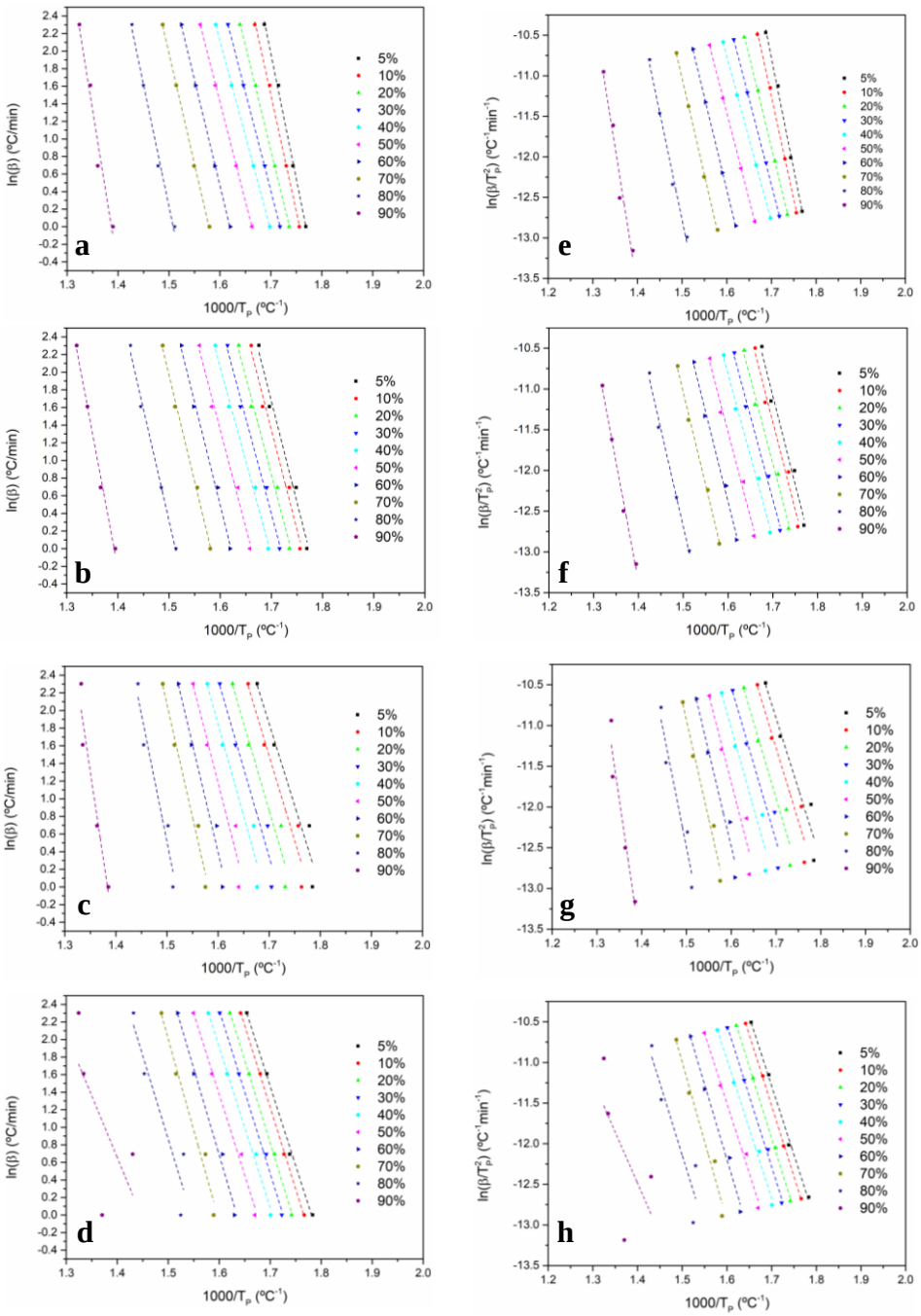

Figure P4.9. (a-d) OFW plots of ln(β) vs. $1000/T_P$ and (e-h) KAS plots of $\ln(\beta/T^2_P)$ vs. $1000/T_P$ for different conversion values. Where LPA_{EOPE} (a-e), LPA_{EOPECG} (b-f), LPA_{POPE} (c-g) and LPA_{POPECG} (d-h)

Table P4.8. Activation energies (E_a) (KJ/mol) and correlation coefficients of the linear regression of the PU samples for the decomposition obtained through the OFW method

	LPA_{EOPE}		LPA_{EOPECG}		LPA_{POPE}		LPA_{POPECG}	
α	R^2	E_a	R^2	E_a	R^2	E_a	R^2	E_a
0.05	0.9976	226.0	0.9830	180.8	0.9432	146.9	0.9970	143.4
0.1	0.9989	209.8	0.9849	179.0	0.9464	152.0	0.9995	154.9
0.2	0.9995	188.8	0.9899	174.4	0.9526	156.3	0.9992	157.1
0.3	0.9998	177.6	0.9923	171.1	0.9508	158.7	0.9972	154.8
0.4	0.9999	171.0	0.9920	168.7	0.9481	164.2	0.9947	152.2
0.5	0.9999	179.2	0.9893	175.4	0.9467	179.1	0.9919	153.4
0.6	0.9997	190.3	0.9926	184.0	0.9689	193.0	0.9900	164.0
0.7	0.9991	198.9	0.9964	190.3	0.9785	202.2	0.9762	172.9
0.8	0.9913	219.1	0.9939	199.6	0.9468	228.5	0.8829	158.8
0.9	0.9677	284.1	0.9929	243.4	0.9412	307.5	0.4439*	116.9

*Not considered for calculating the average

Table P4.9. Activation energies (E_a) (KJ/mol) and correlation coefficients of the linear regression of the PU samples for the decomposition obtained through the KAS method

	LPA_{EOPE}		LPA_{EOPECG}		LPA_{POPE}		LPA_{POPECG}	
α	R^2	E_a	R^2	E_a	R^2	E_a	R^2	E_a
0.05	0.9974	228.2	0.9811	180.5	0.9359	145.0	0.9967	141.2
0.1	0.9988	211.0	0.9832	178.6	0.9397	150.2	0.9994	145.1
0.2	0.9995	188.8	0.9887	173.6	0.9467	154.5	0.9990	147.2
0.3	0.9998	176.9	0.9914	170.0	0.9446	156.9	0.9968	144.8
0.4	0.9999	169.8	0.9910	167.4	0.9418	162.6	0.9938	142.1
0.5	0.9999	178.2	0.9880	174.2	0.9406	178.0	0.9906	143.0
0.6	0.9997	189.6	0.9917	183.0	0.9655	192.4	0.9885	153.4
0.7	0.9990	198.4	0.9960	189.3	0.9762	201.9	0.9730	162.1
0.8	0.9904	219.2	0.9932	198.6	0.9418	229.2	0.8671	147.6
0.9	0.9650	286.8	0.9922	243.8	0.9368	311.3	0.3914*	104.8

*Not considered for calculating the average

Consequently, the values of the preexponential factor (A) estimated with the OFW method and presented in Table P4.10, followed the same tendency. This factor is indicative of the collision frequency between molecules, i.e., it is an

indication of the availability of chemical groups which are susceptible to degradation [27]. Thus, the higher the value of A, the more difficult it is for the polymer to degrade. Therefore, LPA_{EOPE} and LPA_{EOPECG} polyurethanes remained more stable at 5% of conversion, while LPA_{POPE} and LPA_{POPECG} will degrade more easily at this conversion rate.

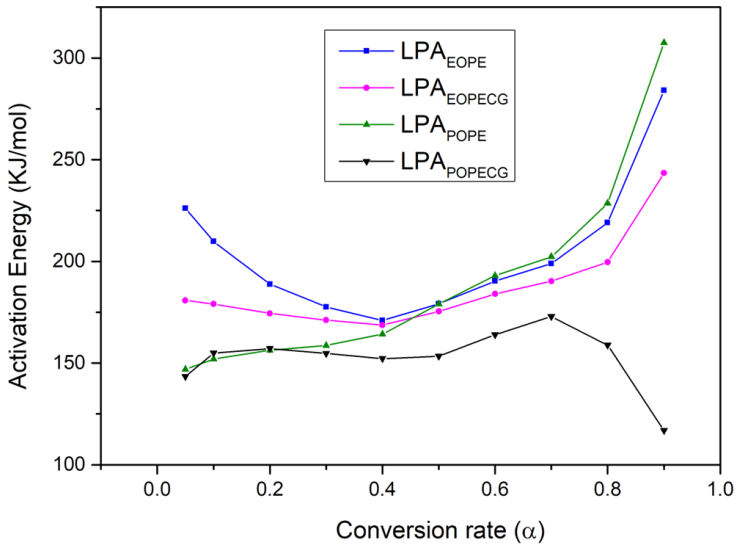

Figure P4.10. E_a calculated through OFW method vs. α

Table P4.10. Preexponential factor (A) of the PU samples for the decomposition obtained through the OFW method

	A (min^{-1})			
α	LPA_{EOPE}	LPA_{EOPECG}	LPA_{POPE}	LPA_{POPECG}
0.05	3.7E+18	9.7E+11	9.8E+08	6.6E+10
0.1	1.5E+17	2.1E+14	8.4E+11	2.3E+11
0.2	2.1E+15	1.0E+14	2.3E+12	5.0E+11
0.3	2.0E+14	5.2E+13	3.6E+12	3.5E+11
0.4	4.6E+13	2.8E+13	9.3E+12	2.1E+11
0.5	8.6E+13	6.9E+13	1.2E+14	2.0E+11
0.6	7.1E+14	2.1E+14	1.1E+15	9.7E+11
0.7	1.9E+15	3.5E+14	3.8E+15	3.1E+12
0.8	1.8E+16	5.4E+14	1.4E+17	1.1E+11
0.9	3.0E+17	6.9E+16	3.1E+21	2.3E+07

Finally, the lifetime of the synthesised PUs was evaluated, and the results are plotted in Figure P4.11. The determination of the lifetime of a material is of great interest in order to develop a specific product with the required specifications to perform the task for which it is conceived [28]. The estimation of the lifetime of the polymers can be determined employing the activation energies and the preexponential factors obtained through the Ozawa-Flynn-Wall method. Usually, the lifetime estimation is carried out for a 5% of weight loss or 5% conversion [29]. The obtained data must be treated prudently since they correspond to the degradation of PUs in an inert atmosphere, and therefore these values will vary in contact with an oxidising atmosphere, as the materials will degrade differently.

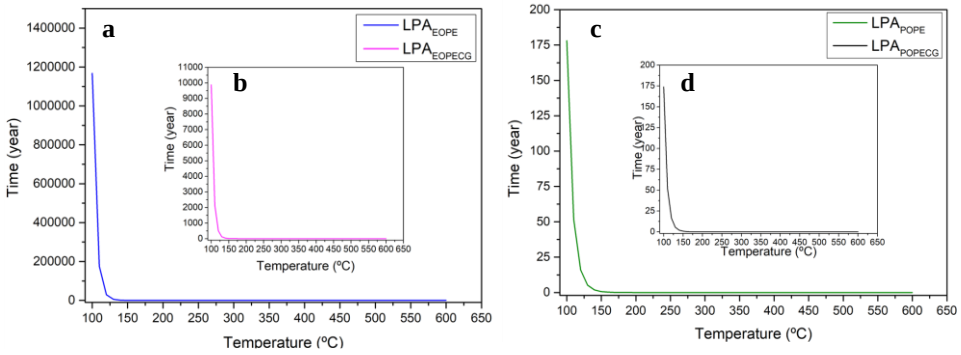

Figure P4.11. Estimated lifetime of LPA_{EOPE} (a), LPA_{EOPECG} (b), LPA_{POPE} (c) and LPA_{POPECG} (d)

As expected, the obtained results were consistent with the E_a values of the PUs. Consequently, the PU with the highest lifetime expectation was LPA_{EOPE}, followed by LPA_{EOPECG}, then LPA_{POPE} and finally LPA_{POPECG}. It should be noted that the difference between LPA_{EOPE} and LPA_{EOPECG} was very high because of the widely differing E_a values, while there was almost no difference between LPA_{POPE} and LPA_{POPECG}. Furthermore, it can be observed, that as the temperature increased, the degradation of the polymers was greatly accelerated in all cases.

3. CONCLUSIONS

This study demonstrated the applicability of a bio-polyols synthesised through the liquefaction process of lignin with polyhydric alcohols (PEG and Glycerol) by microwave irradiation in the formulation of PU adhesives. Moreover, the results indicate that it is possible to substitute commercial glycerol by a non-purified crude glycerol obtained from used vegetable oil. Based on the results, it was determined that the origin of the lignin had a great effect on the PUs. On the one hand, it was observed that when the bio-polyol derived from *Eucalyptus globulus* lignin was used, isocyanate remained unreacted in all cases, whereas with its counterpart derived from *Pinus radiata* lignin this was not the case due to the higher steric hindrance of the former. Furthermore, it was observed that due to the steric hindrance, the phase separation was higher in the PUs synthesised with EOPE bio-polyol regardless of the glycerol used. However, the origin of the glycerol also showed a significant influence on the microstructure since bio-polyols synthesised using CG showed higher molecular weights that favoured the phase separation. When studying the thermal degradation of the PUs it was found that the nature of the lignin also plays an important role, since despite having less H-bonded urethane groups in their structure, the PUs synthesised with EOPE proved to be more stable due to the higher amount of aryl ether bonds in their structure. Consequently, the estimated lifetime of the PUs at 5% degradation followed the same order LPA_{EOPE} > LPA_{EOPECG} > LPA_{POPE} > LPA_{POPECG}.

REFERENCES

[1] M. Ionescu, in: De Gruyter (Ed.), Polyols for Polyrethanes, Boston, Berlin, 2019, pp. 1–10.

[2] S. Hu, X. Luo, Y. Li, ChemSusChem 7(1) (2014) 66–72. 10.1002/cssc.201300760.

[3] Y.Y. Li, X. Luo, S. Hu, Bio-based Polyols and Polyurethanes, 2015, pp. 1–79.

[4] M. Ionescu, in: De Gruyter (Ed.), Polyols for Polyurethanes, Boston, Berlin, 2019, pp. 307–20.

[5] F. Ren, R. Zhou, F. Sun, H. Ma, Z. Zhou, W. Xu, RSC Adv. 7(47) (2017) 29779–85. 10.1039/c7ra04454b.

[6] S. Magina, N. Gama, L. Carvalho, A. Barros-Timmons, D.V. Evtuguin, Materials (Basel). 14(22) (2021) 1–18. 10.3390/ma14227072.

[7] M. Fuensanta, J.M. Martín-Martínez, Front. Mech. Eng. 6(June) (2020) 1–10. 10.3389/fmech.2020.00034.

[8] P. Cinelli, I. Anguillesi, A. Lazzeri, Eur. Polym. J. 49(6) (2013) 1174–84. 10.1016/j.eurpolymj.2013.04.005.

[9] A.M. Nacas, N.M. Ito, R.R.D. Sousa, M.A. Spinacé, D.J. Dos Santos, J. Adhes. 93(1–2) (2017) 18–29. 10.1080/00218464.2016.1177793.

[10] M. Fuensanta, J.M. Martín-Martínez, J. Adhes. Sci. Technol. 34(24) (2020) 2652–71. 10.1080/01694243.2020.1780774.

[11] Y. Liu, L. Liu, Y. Liang, J. Appl. Polym. Sci. 137(45) (2020) 1–9. 10.1002/app.49414.

[12] M. Fuensanta, J.M. Martín-Martínez, Polymers (Basel). 13(18) (2021). 10.3390/polym13183097.

[13] M. Gholami, V. Haddadi-Asl, I.S. Jouibari, J. Plast. Film Sheeting 38(4) (2022) 502–41. 10.1177/87560879221088939.

[14] A. Niemczyk, A. Piegat, Á. Sonseca Olalla, M. El Fray, Eur. Polym. J. 93(May) (2017) 182–91. 10.1016/j.eurpolymj.2017.05.046.

[15] X. Luo, A. Mohanty, M. Misra, Ind. Crops Prod. 47 (2013) 13–9. 10.1016/j.indcrop.2013.01.040.

[16] K. Kojio, S. Nozaki, A. Takahara, S. Yamasaki, J. Polym. Res. 27(6) (2020) 64–7. 10.1007/s10965-020-02090-9.

[17] S. Arévalo-Alquichire, M. Morales-Gonzalez, K. Navas-Gómez, L.E. Diaz, J.A. Gómez-Tejedor, M.A. Serrano, M.F. Valero, Polymers (Basel). 12(3) (2020). 10.3390/polym12030666.

[18] J.M.M. Ferra, M. Ohlmeyer, A.M. Mendes, M.R.N. Costa, L.H. Carvalho, F.D. Magalhes, Int. J. Adhes. Adhes. 31(3) (2011) 127–34. 10.1016/j.ijadhadh.2010.11.013.

[19] B.M. De Morais Lemos Esteves, L.P.V. Cruz-Lopes, A.P. Fernandes, J.M. Martins, I. De Jesus Domingos, J.V. Ferreira, S.H.F. Da Silva, J. Labidi, Wood Res. 64(1) (2019) 105–16.

[20] D.-K. Lee, H.-B. Tsai, R.-S. Tsai, P.H. Chen, Polym. Eng. Sci. 47(5) (2007) 695–701. 10.1002/pen.20742.

[21] J.R. Gouveia, L.D. Antonino, G.E.S. Garcia, L.B. Tavares, A.N.B. Santos, D.J. do. Santos, Https://Doi.Org/10.1080/00218464.2020.1784148

97(15) (2020) 1423–39. 10.1080/00218464.2020.1784148.

[22] F.R. Vieira, N. Gama, S. Magina, A. Barros-Timmons, D. V. Evtuguin, P.C.O.R. Pinto, Polymers (Basel). 14(23) (2022). 10.3390/polym14235305.

[23] J. D'Souza, R. Camargo, N. Yan, J. Appl. Polym. Sci. 131(16) (2014) 1–10. 10.1002/app.40599.

[24] C. Zhang, H. Wu, M.R.K. Kessler, Polymer (Guildf). 69(1) (2015) 52–7. 10.1016/j.polymer.2015.05.046.

[25] L.B. Tavares, C. V. Boas, G.R. Schleder, A.M. Nacas, D.S. Rosa, D.J. Santos, Express Polym. Lett. 10(11) (2016) 927–40. 10.3144/EXPRESSPOLYMLETT.2016.86.

[26] X. Erdocia, F. Hernández-ramos, A. Morales, N. Izaguirre, P.L. De Hoyos-martínez, J. Labidi, Lignin-Based Materials for Biomedical Applications, Elsevier Inc., 2021, pp. 61–104.

[27] N.L. Batista, M.L. Costa, K. Iha, E.C. Botelho, J. Thermoplast. Compos. Mater. 28(2) (2015) 265–74. 10.1177/0892705713484740.

[28] J.H. Flynn, J. Therm. Anal. Calorim. 44(2) (1995) 499–512. 10.1007/BF02636139.

[29] L. Núñez, F. Fraga, M.R. Núñez, M. Villanueva, J. Appl. Polym. Sci. 78(6) (2000) 1239–44. 10.1002/1097-4628(20001107)78:6<1239::aid-app90>3.0.co;2-

“If no mistake you have made, losing you are.

A different game you should play.”

Master Yoda

Publication V

Lignin-based non isocyanate polyurethane adhesives. Synthesis and determination of adhesion properties and thermal degradation kinetic

ABSTRACT

In this work, different non-isocyanate adhesives were synthesised through polycondensation reaction of a ligno-based bio-polyol with dimethyl carbonate (DMC) and hexamethylenediamine (HDMA). The bio-polyols were obtained in previous works (***Publication II and III***). The formulated NIPU adhesives called, LNA_{EOPE}, LNA_{EOPECG}, LNA_{POPE} and LNA_{POPECG} were characterised and subjected to shear strength test employing an ABES system with undesirable results. To improve the adhesion properties of NIPU adhesives, different amounts (5%, 15% and 25%) of (3-Aminopropyl) trimethoxysilane (APTMS) were added. The best result was obtained by adding 15% APTMS in all cases except for LNA_{EOPE}, in which the best results were obtained by adding 25% APTMS. A thermal degradation study of silanised NIPUs called $CLNA_{EOPE\text{-}25}$, $CLNA_{EOPECG\text{-}15}$, $CLNA_{POPE\text{-}15}$ and $CLNA_{POPECG\text{-}15}$ was carried out using OFW and KAS isoconversional methods. With them, the E_a, the pre-exponential factor A and an estimation of the lifetime of the polymers were determined.

1. MATERIALS AND METHODS

1.1. Materials

The raw materials, *Eucalyptus globulus* chips and *Pinus radiata*, as well as the used vegetable oil and chemicals employed in this work were obtained as described in s***ection 2.1*** of the **2nd PART.**

1.2. Lignin obtaining procedure

Lignins used in this work were obtained after the organosolv delignification process and the subsequent ultrasound treatment of the black liquor described in ***section 2.2*** of **2nd PART**. These lignins called EOUL (*Eucalyptus globulus* organosolv lignin) and POUL (*Pinus radiata* organosolv lignin) were characterised in ***Publication II***.

1.3. Crude glycerol obtaining procedure

CG was obtained by the transesterification reaction outlined in **section 2.4** of the **2nd PART**.

1.4. Lignin based bio-polyols

For this work, the same lignin-based bio-polyols that were employed and characterised in ***Publication IV*** were used. These bio-polyols were synthesised through liquefaction of the different organosolv lignins (EOUL and POUL) following the procedure that is described in ***section 2.3.1*** of the **2nd PART**.

Table P5.1 summarises the main parameters of these bio-polyols to facilitate the reading of this publication. The discussion about the characterisation of the bio-polyols is detailed in ***Publication IV***.

Table P5.1. Most relevant parameters of the bio-polyols synthesised in the ***Publication IV***

Sample	M_n	M_w	PI	I_{OH}	A_n	f
EOPE	739 ± 43	3934 ± 98	5.33 ± 0.18	330 ± 3	35 ± 0.36	4.16
POPE	707 ± 32	4079 ± 50	6.29 ± 0.92	182 ± 51	25 ± 0.00	2.29
$EOPE_{CG}$	852 ± 8	6644 ± 89	7.79 ± 0.18	284 ± 1	17 ± 0.24	4.29
$POPE_{CG}$	933 ± 85	11035 ± 1059	12.63 ±0.00	182 ± 30	20 ± 0.64	2.83

1.5. Synthesis of lignin based non-isocyanate polyurethane adhesives

Using the bio-polyols synthesised by the liquefaction process described in the previous section, called EOPE, $EOPE_{CG}$, POPE and $POPE_{CG}$, different lignin based non-isocyanate polyurethane adhesives (LNA) labelled as N_{EOPE}, N_{EOPECG}, N_{POPE} and N_{POPECG} were synthesised. The synthesis was performed following the procedure described in the ***section 2.6*** of the ***2nd PART***.

1.6. Characterisation of the obtained non-isocyanate polyurethane adhesives

The pH of the different NIPUs was determined using a digital pH meter "CRISON basic 20" at room temperature. The solids content of the NIPUs were calculated by weighing a certain amount of sample which was dried in an oven at 100°C for 24 hours and employing the formula presented in Equation P5.1. A triplicate of each sample was performed. The NIPUs without the silane coupling agent were cured in an oven for 24 hours at 120 °C and 150 °C.

$$Solid\ content\ (\%) = \frac{W_2}{W_1} \times 100 \qquad \text{Equation P5.1}$$

Where W_2 is the final weight (g) of the sample after 24 hours at 100 °C and W_1 is the initial weight (g) of the sample.

Then, the non-cured and cured NIPUs were characterised to determine the molecular weight distribution through GPC the chemical structure as well as

the microphase separation and miscibility through ATR-FTIR. The NIPUs with the 3-Aminopropyltrimethoxysilane coupling agent were cured at 120°C in an oven for 24 hours and characterised by ATR-FTIR and thermogravimetric analysis. The shear strength of the NIPUs with and without coupling agent was carried out at 120 °C through ABES. Such characterisations were performed according to the procedures described in **Appendix II.**

2. RESULTS AND DISCUSSION

2.1. Characterisation of the synthesised lignin based non-isocyanate polyurethane adhesives

In aqueous formulations it is important to obtain as high solids content as possible. This is because of the higher latent heat of evaporation of water than that of organic solvents, which hinders the drying process and therefore prevents such formulation from meeting the requirements of modern industry [1]. On the other hand, pH can affect the curing process and the adhesion performance of the resulted adhesives [2]. Table P5.2 summarised the solids contents as well as the pH obtained for each NIPU formulation according to the Equation P5.1.

Table P5.2. Solid content and pH of the different LNA formulation

Sample	Solid content (wt.%)	pH
LNA_{EOPE}	52.58 ± 0.43	11.54 ± 0.04
LNA_{EOPECG}	49.58 ± 0.24	11.47 ± 0.02
LNA_{POPE}	44.53 ± 0.30	11.57 ± 0.01
LNA_{POPECG}	45.20 ± 0.25	11.49 ± 0.03

The solid content as well as the pH of the synthesised NIPUs were within the range reported by other authors when synthesising NIPUs adhesives with lignin or tannins with DMC and HDMA. Thus, Saražin et al., (2021) [3]

obtained an organosolv lignin based NIPU adhesive with a solid content of 46% and a pH of 11. Likewise, Chen et al., (2022) [2] synthesised different NIPUs employing tannins and reacting them with DMC and HDMA and different concentrations of glycerol diglycidyl ether (GDE). When the concentration of the GDE was zero, the solids content of the obtained NIPU adhesive was 54.38% and the pH was 11.1, the latter decreased as the concentration of GDE increased. Despite this, the authors did not find significant differences in the adhesion properties of the NIPUs.

Employing the bio-polyols summarised in section 1.4 called EOPE, $EOPE_{CG}$, POPE and $POPE_{CG}$, four different LNAs were synthesised following the instructions described in section 1.5 and the different steps of the reaction were analysed through ATR-FTIR (Figure P5.1). In the first step of the reaction, the addition of DMC, the appearance of three characteristic DMC bands can be observed, viz. 1751 cm^{-1}, 1457-1452 cm^{-1} and 1284-1272 cm^{-1}, corresponding to stretching of C=O in the ester group, CH deformation in CH_3 and C-O stretching in the ester group of DMC [4]. The appearance of these characteristic bands indicates that the DMC reacted properly with the bio-polyols. In addition, the broad bands between 3423 cm^{-1} and 3401 cm^{-1} could be associated with the water in the medium in which the reaction was carried out.

In the second stage of the reaction, the hexamethylenediamine was added to form urethane groups through reaction with DMC. The formation of urethane groups could be confirmed by the appearance of three bands at wavenumbers 3360-3336 cm^{-1}, 1720-1686 cm^{-1} and 1531-1525 cm^{-1}. The first one (3360-3336 cm^{-1}), which appears as a small peak, since it was overlapped by the reaction water band, correspond to the N-H stretching vibration of urethane groups [4], carbonyl (C=O) groups belonging to free urethane groups (1730 cm^{-1}) and H-bonded urethane groups (1686 cm^{-1}) [5]

and the N-H vending vibration at 1531-1525 cm^{-1} [6]. In addition to urethane bonds, the reaction between HDMA and DMC could create urea bonds which are confirmed by the appearance of a peak between 1646-1636 cm^{-1} wavenumbers [7]. These groups that were created by the reaction between DMC and HDMA during the NIPU synthesis had a major importance on the morphology and final properties of the material. This is due, among other reasons, to their ability to form double H-bonds generating stronger interactions [8] and thus increasing the mechanical strength [9].

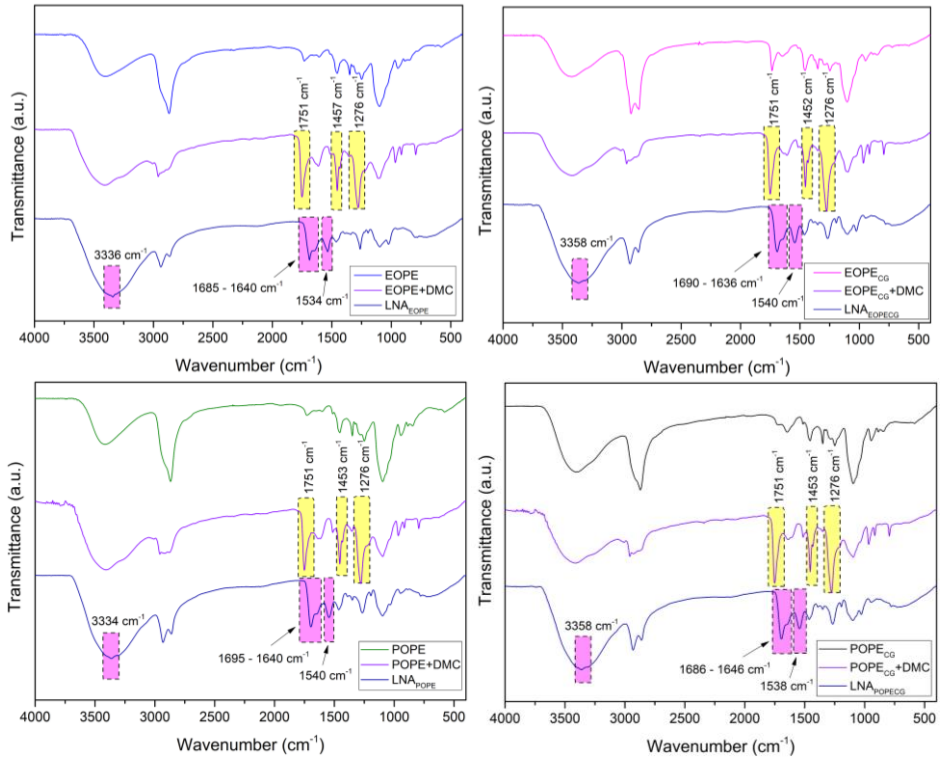

Figure P5.1. ATR-FTIR spectra of the different steps of the LNA reaction. a, b, c and d correspond to the LNAs formulated with EOPE, EOPECG, POPE and POPECG respectively.

Afterwards, the NIPUs were cured employing three different temperatures, i.e., 100 °C, 120 °C and 150 °C. To do so, the NIPUs were poured into an aluminium mould and placed in the oven at the above-mentioned temperatures for 24 hours. Then, the cured samples were analysed through

GPC to determine the variation of the molecular weight distribution (Figure P5.2), and through ATR-FTIR to analyse the chemical structure of the samples (Figure P5.3).

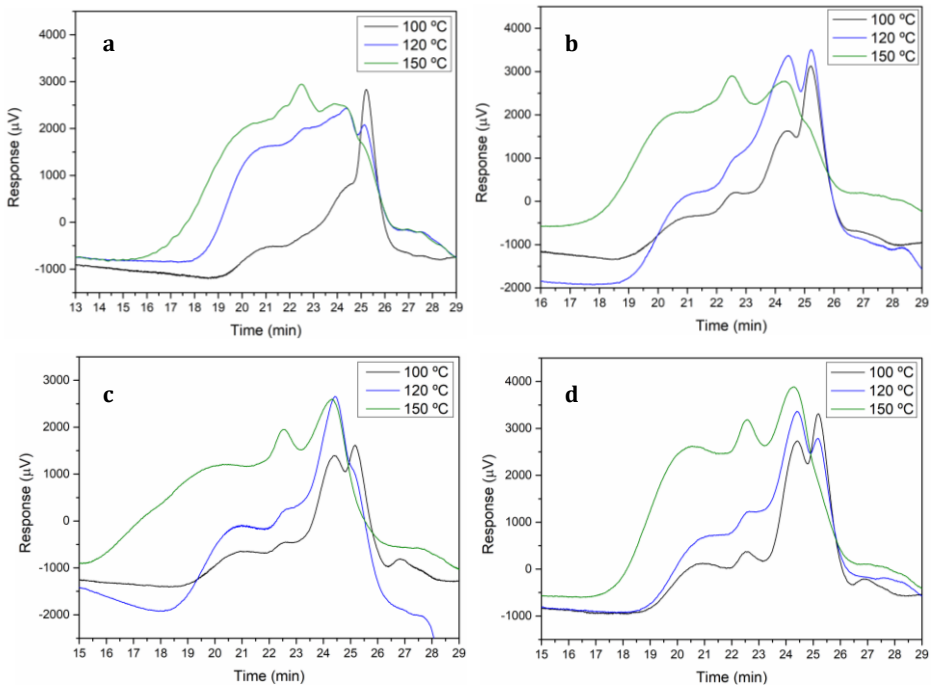

Figure P5.2. Molecular weight distribution of the synthesised LNAs

As shown in Figure P5.2, in all cases the chromatograms follow the same pattern. The samples cured at 100 °C showed four peaks, although the intensities vary depending on the samples. Those sample cured at 120 °C also presented four peaks, however the last one at 25.2 min lost intensity with respect to the previous peak at 24.3 min, and even almost disappeared in the case of LNA_{POPE}. For the samples cured at 150 °C, this peak disappeared or almost disappeared in all cases. This could be explained by the fact that the smaller unreacted molecules took part in the increasing polymerisation with increasing temperature. It is also remarkable that, except for LNA_{EOPE}, the first peak that corresponds to the higher molecular weight starts roughly at

the same retention time, which means that there is not much difference between the higher molecular weight fragments of the samples cured at 100 °C or 120 °C. However, as the curing temperature increased to 150 °C the retention time of this peak decreased remarkably in all cases, indicating that the molecular weights of the samples increased due to the higher degree of polymerisation. This increase in molecular weights is well reflected in Table P5.3 where the average molecular weights corresponding to the different retention times are listed.

Table P5.3. Average molecular weight (MW) (g/mol) of LNAs by retention time (min)

Sample	100 °C		120 °C		150 °C	
	R_T	M_w	R_T	M_w	R_T	M_w
LNA_{EOPE}	21.28	18025	21.27	29894	20.61	57316
	22.53	3270	22.75	4374	21.78	8473
	24.17	873	24.38	998	22.45	3165
	25.22	365	25.14	342	23.87	908
	-	-	-	-	25.01	368
LNA_{EOPECG}	21.67	20519	21.02	21901	20.69	39312
	22.71	4088	22.59	3458	21.93	8222
	24.46	889	24.45	872	22.52	3172
	25.22	365	25.23	352	24.34	876
	26.47	237	26.82	236	25.09	362
LNA_{POPE}	20.93	20291	20.98	23838	17.89	147950
	22.60	3667	22.60	3281	20.29	46757
	24.40	908	24.43	816	22.53	4992
	25.17	365	25.11	339	24.31	823
	26.82	239	-	-	-	-
LNA_{POPECG}	20.92	20957	21.22	21333	20.58	37083
	22.60	3324	22.64	3774	22.58	3730
	24.41	808	24.39	909	24.27	775
	25.18	364	25.18	354	-	-
	26.83	237	-	-	-	-

The chemical structure of LNAs cured at different temperatures is represented in Figure P5.3. It was evident that, as the LNAs were cured, the

water in the samples was evaporated revealing a sharp peak (3358-3302 cm^{-1}) associated to the N-H vibration band which was masked in the non-cured samples (Figure P5.1). It is noteworthy that, in general, all the bands related with urethane groups became wider as the curing temperature was increased. In addition, in all LNA samples, as the curing temperature increased, a band around wavenumber 3480 cm^{-1} belonging to free NH_2 appeared, which was indicative of micro-phase separation [10]. In addition, in the region corresponding to Amide I, the bands belonging to carbonyl urethane and urea groups (1740-1644 cm^{-1}) [11] (amplified in each figure) revealed that as the curing temperature increased, a shoulder towards lower wavenumbers appeared. Therefore, the microphase distribution varied as the curing temperature increased. However, this variation in the microphase structure was not very significant between the samples cured at 120 °C and 150 °C. On the other hand, H-bonded C-O around 1097 cm^{-1} [12], increased as well. Therefore, from both GPC and ATR-FTIR characterisation, it was evident that as the curing temperature went higher, cross-linking of the LNAs increased and therefore the H-bonded urethane groups increased generating different degrees of phase separation. However, in general, no major differences were observed between the samples cured at 120 °C and 150 °C, so it was decided to use the former for the adhesion test.

Prior to measure the shear strength, the micro-phase separation of the LNAs at 120 °C was studied, since the micro-phase separation of PUs, generated by the immiscibility between the HS and SS of the polymer, is determinant in the final properties of the PUs [13]. While the SS are responsible for providing the elastomeric behaviour, the HS provide stability as they behave as crosslinkers [14]. The degree of separation as well as the miscibility of the micro-phases of a PU can be determined by different techniques such as Nuclear magnetic resonance spectroscopy [15], Differential scanning

calorimetry [16], Dynamic thermomechanical analyser [17] Atomic force microscopy [18] and through ATR-FTIR [19] among others.

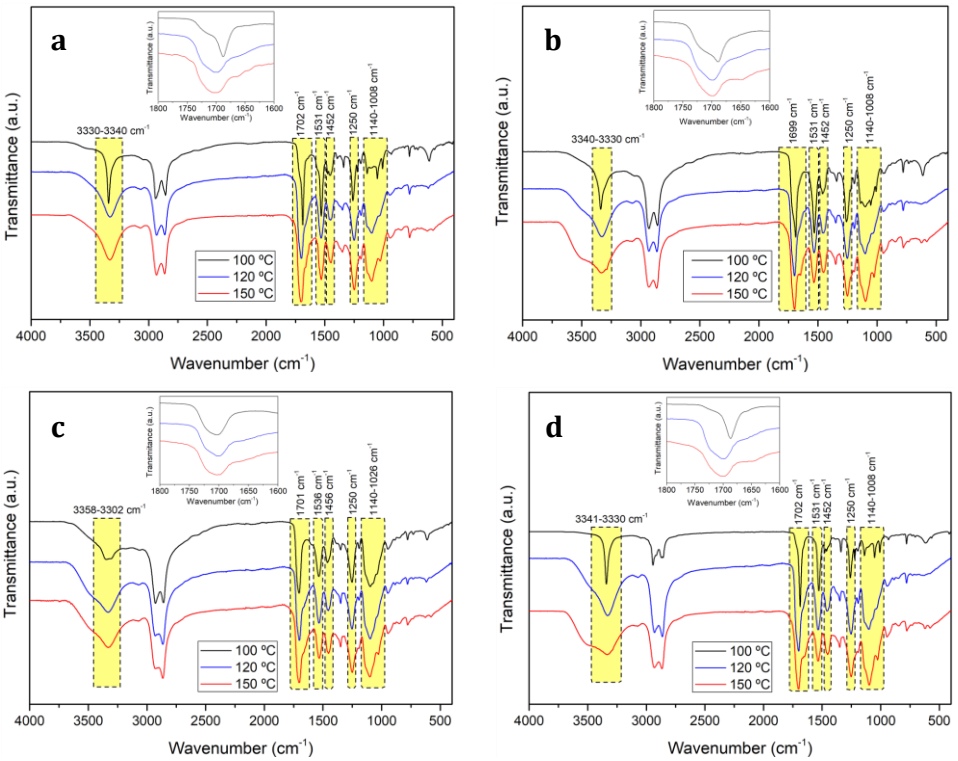

Figure P5.3. ATR-FTIR spectra of LNAs cured at different temperatures: a) LNA_{EOPE}; b) LNA_{EOPECG}; c) LNA_{POPE}; d) LNA_{POPE}

To analyse the microphase separation employing ATR-FTIR technology it is necessary to study the contribution of the different bands corresponding to the carbonyl groups of the PU, i.e., free C=O groups, H-bonded C=O in disordered and ordered HS and H-bonded C=O groups in disordered SS [5]. To carry out such analysis it is necessary to perform a deconvolution of the absorbance bands of the C=O groups. In addition, the H-bonded C=O groups (X_{HB}), the maximum mass fraction of the rigid segment mixed in the soft phase (W_H), the weight fraction of the mixed phase (MP_W), the soft segment weight fraction (SS_W) and the hard segment weight fraction (HS_W) could be calculated using the equations summarised in Appendix II.

In Table P5.4 the theoretical HS_t % of the different LNAs, determined as indicated in **Appendix II**, are shown, as well as the percentages of the different carbonyl and urea species which were calculated from the deconvolution of the bands at wavenumbers between 1750-1640 cm^{-1} of the ATR-FTIR spectrum depicted in Figure P5.4.

Table P5.4. Percentage of C=O urethane and urea species in cured LNAs

	T (ºC)	HSt (%)	A	B	C	D
LNA_{EOPE}	120	30.379	12.599	67.143	15.845	4.413
LNA_{EOPECG}	120	28.045	13.006	70.479	11.765	4.749
LNA_{POPE}	120	31.112	15.305	63.154	18.383	3.158
LNA_{POPECG}	120	26.581	15.717	64.995	17.171	2.117

A:1720-1714 cm^{-1} Free urethane C=O in Hard Segment
B:1702-1699 cm^{-1} H-bonded C=O urethane in disordered Hard Segment
C:1663-1660 cm^{-1} H-bonded urea in disordered Hard Segment
D:1644-1638 cm^{-1} H-bonded urea in ordered Hard Segment

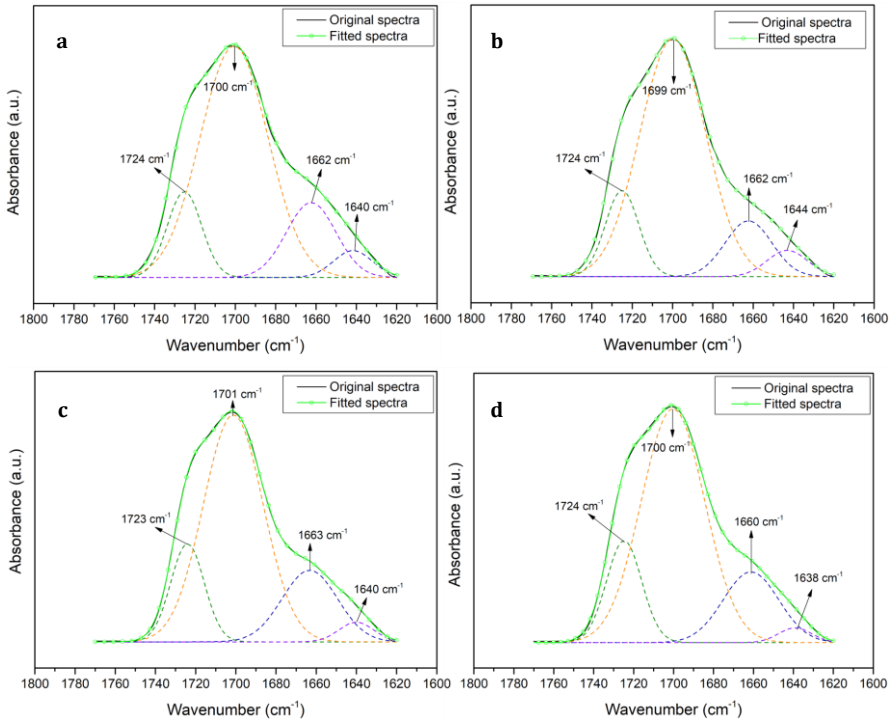

Figure P5.4. ATR-FTIR spectra of the absorbance region of the carbonyl group of the different LNAs cured at 120 °C. a) LNA_{EOPE}; b) LNA_{EOPECG}; c) LNA_{POPE}; d) LNA_{POPECG}

The spectra shown in Figure P5.4 were fitted through Gaussian method and a good fit was obtained with R^2 values which were above 0.999 in all cases. The groups involved in all cases were the same. In the LNA_{EOPE} and LNA_{POPE} samples the amount of free urethane C=O in HS was lower and consequently the amount of H-bonded C=O urethane in HS was higher. The presence of urea groups in all cases was noteworthy. These groups tend to increase phase separation compared to urethane groups mainly due to their higher polarity which affects the solubility, and the formation of double H-bonds among other considerations [8]. Using the results of the contribution of each group (Table P5.4), the X_{HB}, W_H, MP_W, SS_W and HS_W parameters were calculated (Table P5.5)

Table P5.5. Relevant parameter for the determination of microphase separation in LNAs

	T (°C)	z	X_{HB}	W_H	MP_W	SP_W	HS_W
LNA_{EOPE}	120	0.304	0.853	0.060	0.018	0.715	0.285
LNA_{POPE}	120	0.311	0.822	0.074	0.023	0.712	0.288
LNA_{EOPECG}	120	0.280	0.848	0.056	0.016	0.735	0.265
LNA_{POPECG}	120	0.266	0.817	0.062	0.017	0.751	0.249

z is the HS_t fraction

The mass fraction of H-bonded urethane or/and urea group (X_{HB}) in LNA_{EOPE} and LNA_{EOPECG} was very similar and the same for LNA_{POPE} and LNA_{POPECG}. However, the distribution of these H-bond urethane and/or urea groups was different. In general, the values of W_H and consequently MP_w were low in all cases, however, the samples LNA_{EOPECG} and LNA_{POPECG} showed a slightly lower phase miscibility than LNA_{EOPE} and $LNA_{POPE.}$

The tensile strength which is necessary to break the adhesive bonds of the LNA adhesive formulations were carried out employing an Automatic Bond Evaluation System (ABES) by measuring the shear strength. In Figure P5.5, the results of the shear strength test of the different LNAs are represented.

As mentioned above, a temperature of 120 °C was selected and different pressing times were used.

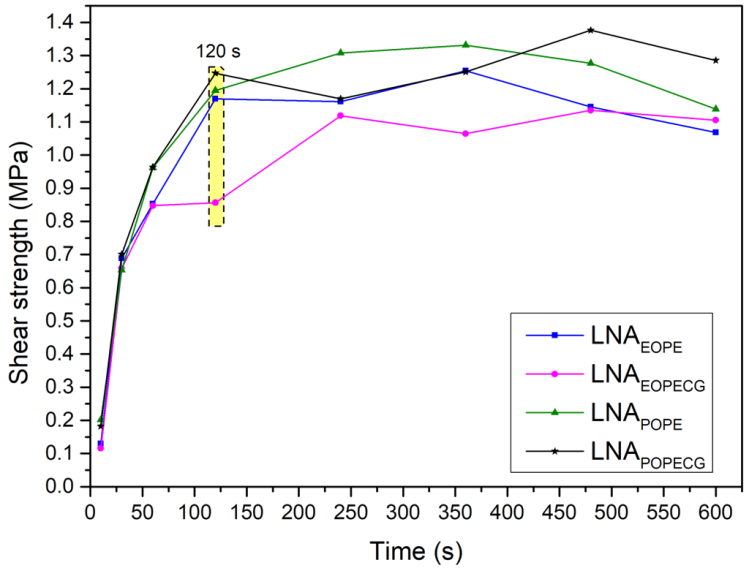

Figure P5.5. Shear strength of LNA adhesives

Analysis of the shear strength results revealed the usual behaviour of adhesive curing process in this type of test [20]. A first stage where a delay in the development of the bond strength is observed, which is related with the loss of energy caused by the evaporation of the water in the sample. The second zone, almost linear, corresponds to the process of elongation and crosslinking of the chains during the curing process [21]. The last stage is a zone where the shear strength can increase or decrease depending on the behaviour of the adhesive with respect to temperature and/or humidity [22]. Similar maximum values were obtained in all cases, although they were achieved at different retention times. Thus, the maximum shear strength for LNA_{EOPECG} and LNA_{POPECG} were obtained at a pressing time of 480 s, being the highest value for LNA_{POPECG} 1.38 MPa and 1.13 MPa for LNA_{POPECG}. On the other hand, the maximum shear strength values for LNA_{EOPE} and LNA_{POPE}

were 1.25 MPa and 1.33 MPa respectively and were reached at a pressing time of 360 s.

To improve both the adhesion and crosslinking properties of the NIPUs, a silane coupling agent (3-aminopropyltrimethoxysilane) (APTMS) was added. The silane coupling agent acts by hydrolysing rapidly in basic aqueous media forming silanol and methanol as residue. These hydrolysed molecules tend to condense with adjacent silanol molecules forming oligomers. Then the OH groups of the oligomers form H-bonds with the OH groups of the surface and finally during the curing process covalent bonds are formed, leaving the amino group free to form covalent bonds or physical interactions with other groups [23]. This amino group can interact via H-bonds with the NH groups of urethane and urea groups as well as with the amino-terminal groups of the NIPUs increasing the amount of H-bonded groups [4]. The coupling agent was added at different molar ratios (5, 15 and 25%) with respect the I_{OH} of the bio-polyols, assuming that all of them reacted to form urethane and urea bonds. Once the coupling agent was added, the samples were magnetically stirred for 24 hours, and then the shear strength was determined, and the results are represented in Figure P5.6. Additionally, to characterise them, the different LNAs with the silane coupling agent (CLNA) were cured at 120 °C employing an aluminium mould.

As expected, the higher the APTMS concentration, the higher the shear strength. Nevertheless, in the $CLNA_{POPECG}$ formulations, better results were obtained with an APTMS concentration of 15%. Thus, in $CLNA_{EOPE}$ formulation, the maximum shear strength value was obtained with the addition of 25% APTMS (3.90 MPa) and a pressing time of 300 s. At the same pressing time but with 15% APTMS the value was slightly lower (3.68 MPa) while with 5% the maximum value (2.25 MPa) was obtained at the maximum pressing time. In the $CLNA_{EOPECG}$ formulation a maximum value of 3.41 MPa

was reached at 25% APTMS (240 s) while adding 15 and 5% the maximum shear strength values, 2.70 MPa and 1.93 MPa, were achieved at 360 s.

The addition of 25% of APTMS in the $CLNA_{POPE}$ formulation reached a maximum shear strength value of 3.21 MPa at 600 s, 2.68 MPa at 480 s with the addition of 15% and 1.49 MPa at 360s with 5%. Finally, as mentioned above, for the $CLNA_{POPECG}$ formulation the highest values were obtained when 15% APTMS was added. In this case the maximum shear strength (3.50 MPa) was obtained at a pressing time of 240 s as in the formulation with 5% (2.46 MPa), while by adding 25% APTMS the maximum value (3.20 MPa) was attained at 480 s. Considering the pressing time used as a reference (120 s), it was observed that except for the $CLNA_{EOPE}$ formulation, an increase from 15% to 25% of APTMS would not be justified since very similar shear strength values were obtained.

These results were significantly lower than those obtained by Saražin et al., (2021) [3] using organosolv lignin to synthesise a NIPU adhesive. However, in this study an epoxy-based silane coupling agent was used, which can create C-N bonds with the amino-terminal groups facilitating the curing process; moreover, higher curing temperatures were used. Thus, they obtained a lignin based NIPU adhesive with a shear strength above 7 MPa adding 22% of coupling agent and using a curing temperature of 200 °C and 10 min of pressing time. Chen et al., (2022) [2] synthesised a NIPU wood adhesive by reacting mimosa tannins with DMC, HDMA and glycerol diglycidyl ether obtaining a maximum shear strength value around 1.4-1.5 MPa. Therefore, the following formulations were selected as optimal: $CLNA_{EOPE}$ with 25% of APTMS ($CLNA_{EOPE-25}$), $CLNA_{EOPE-15}$, $CLNA_{POPE-15}$ and $CLNA_{POPECG-15}$, in the latter three 15% APTMS was used.

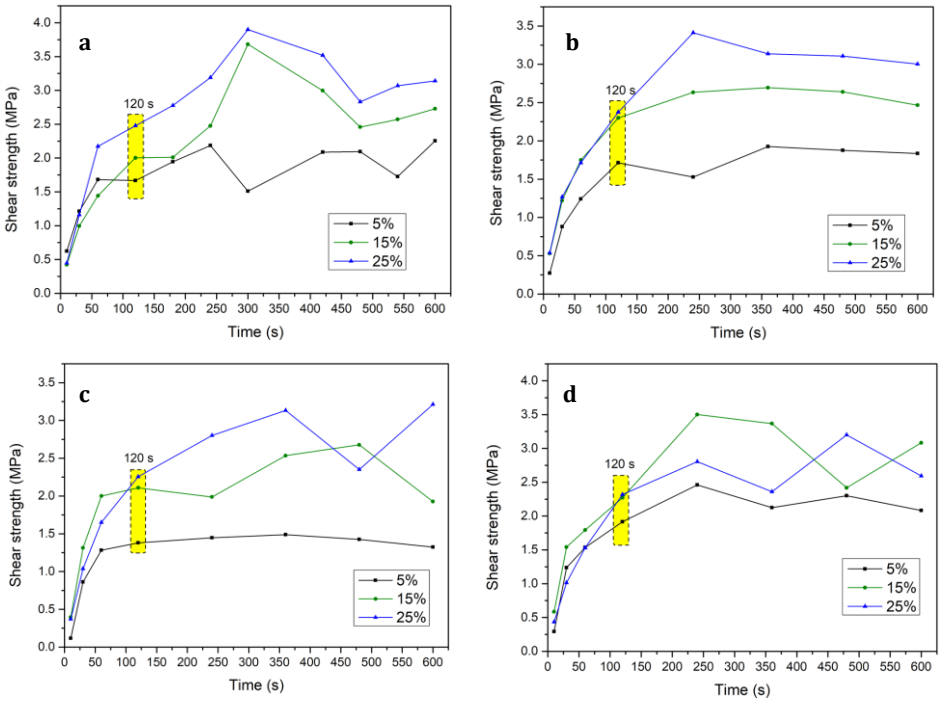

Figure P5.6. Shear strength of different CLNA. a) $CLNA_{EOPE}$; b) $CLNA_{EOPECG}$; c) $CLNA_{POPE}$; d) $CLNA_{POPECG}$

2.2. Characterisation of the synthesised lignin based non-isocyanate polyurethane adhesives with silane coupling agent

The optimised CLNA formulations were characterised through ATR-FTIR to determine their chemical structure as well as to analyse the microphase structure. In addition, through TGA, the thermal stability of the samples was studied and using the isoconversional methods of OFW and KAS, described in **Appendix II**, the *Ea*, *A* and a lifetime estimation of each system was determined. Unfortunately, in this case the molecular weight of the samples could not be determined as they were insoluble in the mobile phase used.

The chemical structure of CLNAs is compared with LNAs and the obtained ATR-FTIR spectra are shown in Figure P5.7. Few differences could be observed between the chemical structure of CLNA and LNA samples. However, there were some signals that indicated the incorporation of the

APTMS. One of them was the appearance, in all cases, of a signal at wavenumber 694 cm^{-1} corresponding to the C-Si-C vibration [24]. On the other hand, it was observed that the signal related to the H-bonded urea increased as a possible consequence of the reaction between the terminal carbonate groups and the amino groups of the APTMS. The band at 1100 cm^{-1} assigned to the Si-O-C bond [25] was more pronounced. In addition, around 805 cm^{-1} wavenumber a small band shoulder which was not visible in $CLNA_{POPE-15}$appeared. This band is related to the Si-O-Si deformation vibration [26] of the oligomers formed through the condensation of the APTMS molecules.

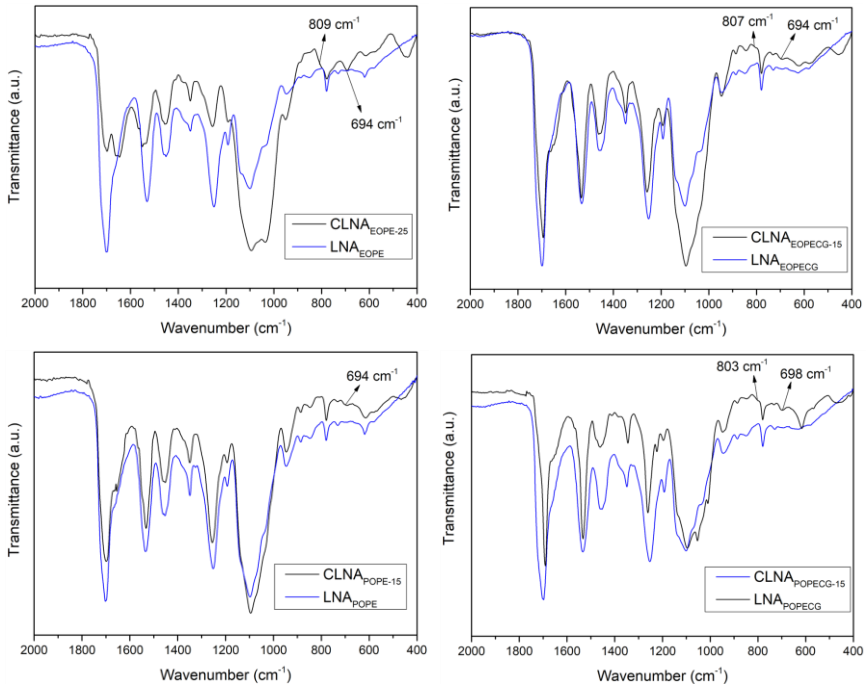

Figure P5.7. ATR-FTIR spectra of CLNA and LNA samples.

The analysis of the carbonyl region (1750-1640 cm^{-1}) is depicted in Figure P5.8. The spectra were fitted through Gaussian method and a good fit was obtained with R^2 values which were above 0.999 in all cases. In Table P5.6 the percentages of the carbonyl and urea species presented.

Table P5.6. Percentage of carbonyl and urea species in cured CLNAs

	T (°C)	HSt(%)	A	B	C	D
$CLNA_{EOPE-25}$	120	30.379	11.156	41.488	35.830	11.525
$CLNA_{EOPECG-15}$	120	28.045	17.608	52.516	15.493	14.382
$CLNA_{POPE-15}$	120	31.112	11.925	58.385	27.272	1.996
$CLNA_{POPECG-15}$	120	26.581	24.409	27.599	35.250	12.742

A:1723-1711 cm^{-1} Free urethane C=O in Hard Segment
B:1701-1691 cm^{-1} H-bonded C=O urethane in disordered Hard Segment
C:1675-1654 cm^{-1} H-bonded urea in disordered Hard Segment
D:1644-1630 cm^{-1} H-bonded urea in ordered Hard Segment

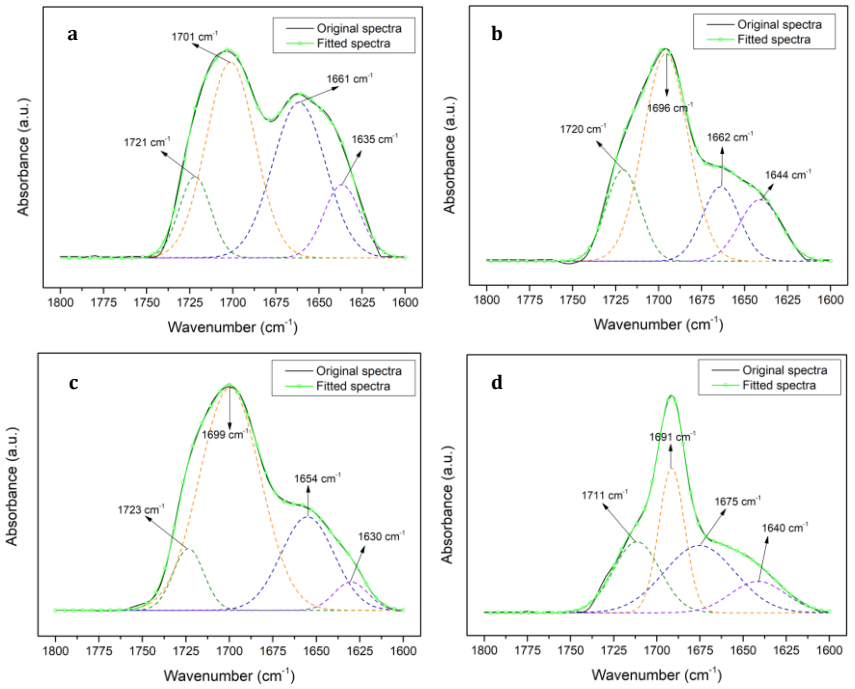

Figure P5.8. ATR-FTIR spectra of the absorbance region of the carbonyl group of the different CLNAs cured at 120 °C. a) $CLNA_{EOPE-25}$; b) $CLNA_{EOPECG-15}$; c) $CLNA_{POPE-15}$; d) $CLNA_{POPECG-15}$

When comparing the carbonyl and urea species of the samples with the APTMS coupling agent (Table P5.6 and Figure P5.7) and those obtained without the APTMS (Table P5.4 and Figure P5.4), is evident that the percentage of H-bonded urea group in both ordered and disordered HS increased considerably despite the decrease of the H-bonded urethane CO.

This could be because the H-bond between the urea groups were promoted by the addition of the coupling agent. On the one hand, the higher increase of H-bond urea group in the $CLNA_{EOPE-25}$ sample compared to the other samples was expected due to the higher amount of APTMS used. On the other hand, among the samples in which 15% of APTMS was used, the sample $CLNA_{POPECG-15}$ surprisingly showed a much higher increase than the other two, achieving a slightly higher amount of H-bond urea group than those obtained by $CLNA_{EOPE-25}$. It was also worth noting that the samples synthesised with CG showed an increase in free urethane groups.

Table P5.7. Relevant parameters for the determination of microphase separation in CLNs

	T (°C)	z	X_{HB}	W_H	MP_W	SP_W	HS_W
$CLNA_{EOPE-25}$	120	0.304	0.869	0.054	0.016	0.713	0.287
$CLNA_{EOPECG-15}$	120	0.280	0.796	0.074	0.021	0.740	0.260
$CLNA_{POPE-15}$	120	0.311	0.860	0.060	0.019	0.707	0.293
$CLNA_{POPECG-15}$	120	0.266	0.721	0.092	0.024	0.759	0.241

z is the HS_t fraction

Because of the decrease in H-bonded urethane CO groups in $CLNA_{EOPECG-15}$ and $CLNA_{POPECG-15}$, an increase in the miscibility between the microphases was observed. On the contrary, since both H-bonded urethane and urea groups increased in $CLNA_{EOPE-25}$ and $CLNA_{POPE-15}$ samples, the mass fraction of HS mixed in SS decreased slightly with respect to the samples without APTMS as can be seen in Table P5.7. This microphase configuration affected the adhesion behaviour of the samples. A greater phase separation between HS and SS usually improves the material behaviour, as was the case with sample $CLNA_{EOPE-25}$, which obtained the highest shear strength value. However, the second-best result was not obtained with $CLNA_{POPE-15}$, as expected, but was obtained with the sample with the least phase separation. Thus, $CLNA_{POPECG-15}$ with lower amount of APTMS obtained a maximum value only 0.4 MPa lower than the one obtained by $CLNA_{EOPE-25}$. Furthermore, this

value was obtained using a shorter pressing time. Therefore, it can be concluded that a higher amount of urea groups helped favourably in the adhesion properties of the synthesised NIPUs.

The thermal stability of the formulated CLNAs was studied through TGA. Figure P5.9 shows the TGA and DTG curves obtained for each sample, which indicates that there were three main degradation zones besides the moisture evaporation zone (30-120 °C).

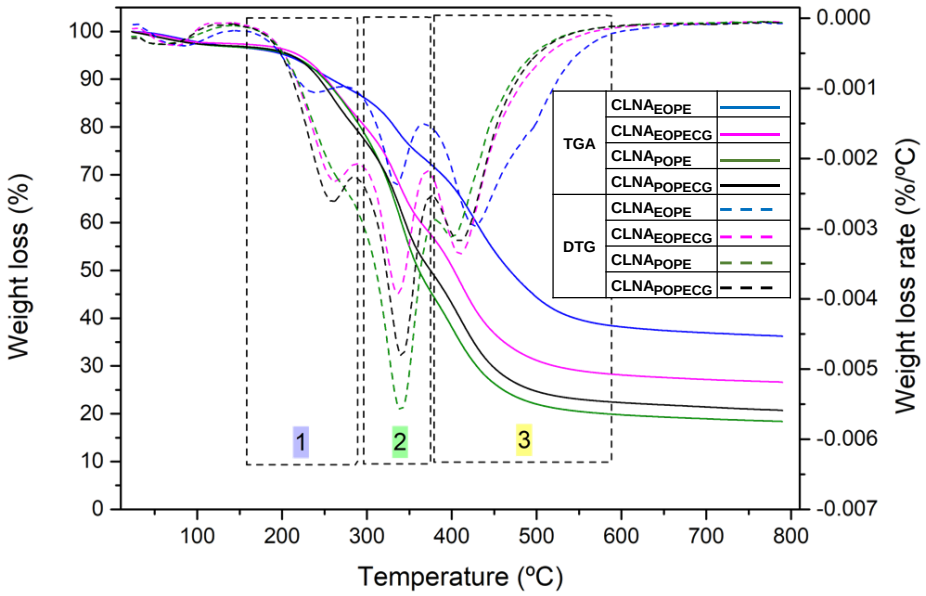

Figure P5. 9. TGA and DTG curves of the synthesised CLNAs

The first degradation zone (150-280 °C) is associated with the following events: the cleavage of H-bonded urethane and urea groups [27], the cleavage of unstable β-O-4, α-O-4 and 4-O-5 ether bonds of lignin [28] and the presence of unreacted HDMA [2], which boiling point is 204 ºC. The mass loss zone between 280-380 °C is related with the degradation of the soft segment [29] (bio-polyol) and it was the area with the highest mass loss, except in the case of $CLNA_{EOPE\text{-}25}$. The last degradation area (380-580 °C) is

attributed to the cleavage of covalent C-C [30], the aromatic rings of lignin [31] as well as the degradation of APTMS [32]. The degradation of the latter takes place in two stages, the first between 380-450 °C, corresponding to the intercalated silane and the second between 450-550 °C, belonging to grafted silane [33]. Depending on the sample and thus on the amount of APTMS used, the final residue was different. Therefore, an increase of APTMS was reflected in an increase in the final residue.

Employing OFW and KAS isoconversional methods, which are described in **Appendix II**, and using different heating rates (1, 2, 5 and 10 ºC/min) the E_a and the pre-exponential factor (A) of the synthesised CLNAs was calculated. Both, E_a and A, were calculated from the slope and intercept of the plots of $\ln(\beta)$ and $\ln\left(\frac{\beta}{T_p^2}\right)$ versus 1000/Tp where the conversion rates (α) from 5% to 90% for each system were plotted.

The most commonly used isoconversional method, since it is not necessary to know the reaction order, is the OFW method [34]. Nevertheless, a second method (KAS) was employed to validate the model. In both cases, a linear fit must be obtained for the model to be applicable [35]. In Figure P5.10 a-d and P5.10 e-f, the fitted plots of the CLNAs using OFW and KAS methods are outlined, and the obtained R^2 determination coefficients and E_a of each CLNA are summarised in Table P5.8 (OFW) and Table P5.9 (KAS). Through OFW methods the pre-exponential factor was obtained for every conversion rate to make an estimation of the half-life of the polymer. This estimation was carried out using the OFW method.

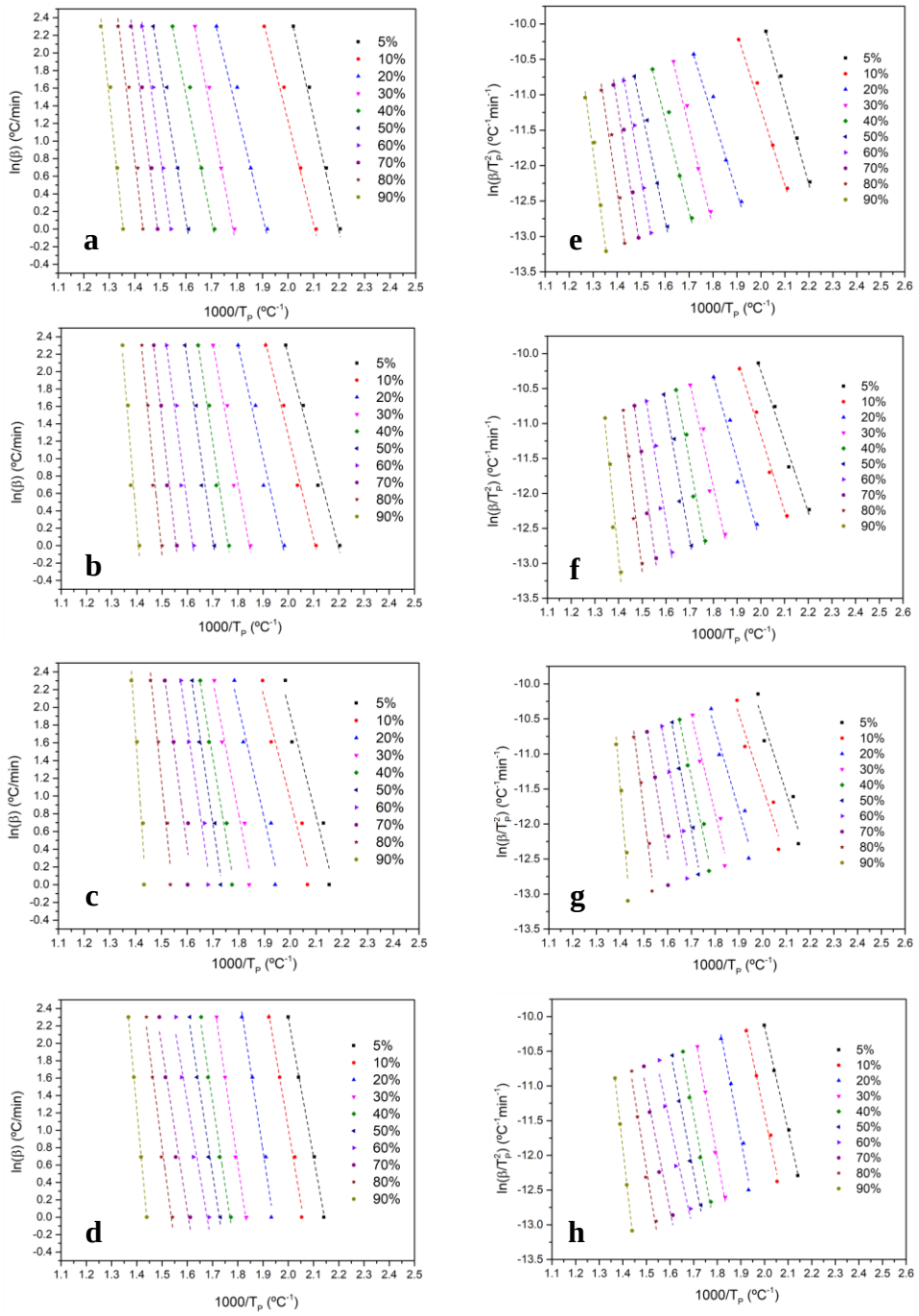

Figure P5.10. (a-d) OFW plots of ln(β) vs. 1000/T_P and (e-h) KAS plots of ln(β/T^2_P) vs. 1000/T_P for different conversion values of $CLNA_{EOPE-25}$ (a-e), $CLNA_{EOPECG-15}$ (b-f), $CLNA_{POPE-15}$ (c-g) and $CLNA_{POPECG-15}$(d-h)

As mentioned above, OFW and KAS methods must fit a linear regression, furthermore, as shown in Figure P5.10 the lines must follow a parallel trend to each other. Therefore, since both conditions are fulfilled, it can be concluded that the selected models were correct.

In addition, the R^2 determination coefficients reported in Tables P5.8 and P5.9 reveal a good fit of the regressions. Moreover, as it can be observed, the E_a values obtained by the two methods were very similar, which confirms the good selection of the methods.

The dependence of the E_a with respect to the conversion degree is different in each case as can be seen in Tables P5.8 and P5.9 and Figure P5.11. Thus, for a α of 5%, the sample $CLNA_{POPECG-15}$ showed the highest value, followed by $CLNA_{EOPE-25}$, $CLNA_{POPE-15}$ and $CLNA_{EOPECG-15}$.

Table P5.8. Activation energies (E_a) (KJ/mol) and correlation coefficients of the linear regression of the PU samples for the decomposition obtained through OFW method

	$CLNA_{EOPE-25}$		$CLNA_{EOPECG-15}$		$CLNA_{POPE-15}$		$CLNA_{POPECG-15}$	
α	R^2	E_a	R^2	E_a	R^2	E_a	R^2	E_a
0.05	0.998	100.1	0.9842	87.3	0.9413	90.7	0.9982	126.2
0.1	0.992	91.2	0.9877	93.9	0.9492	90.1	0.9909	142.6
0.2	0.983	93.9	0.9542	102.7	0.9487	99.4	0.9850	158.4
0.3	0.9918	120.3	0.9552	126.8	0.9589	118.6	0.9953	164.3
0.4	0.9823	113.5	0.9750	153.2	0.9792	137.0	0.9901	161.0
0.5	0.9908	134.2	0.9586	161.0	0.9840	154.3	0.9889	157.1
0.6	0.9903	161.0	0.9496	173.4	0.9692	157.1	0.9590	141.2
0.7	0.9832	173.3	0.9770	203.9	0.9134	173.4	0.9643	154.4
0.8	0.9731	183.7	0.9674	232.0	0.9697	223.8	0.9801	184.9
0.9	0.9806	211.0	0.9393	276.3	0.9451	341.8	0.9999	264.0

Table P5.9. Activation energies (E_a) (KJ/mol) and correlation coefficients of the linear regression of the PU samples for the decomposition obtained through KAS method

	$CLNA_{EOPE-25}$		$CLNA_{EOPECG-15}$		$CLNA_{POPE-15}$		$CLNA_{POPECG-15}$	
α	R^2	E_a	R^2	E_a	R^2	E_a	R^2	E_a
0.05	0.9976	97.4	0.9813	83.9	0.9308	87.4	0.9979	124.7
0.1	0.9902	86.6	0.9854	90.5	0.9395	86.4	0.9897	134.2
0.2	0.9791	89.7	0.9464	99.2	0.9393	95.6	0.9831	149.5
0.3	0.9904	116.8	0.9486	124.0	0.9523	115.4	0.9947	154.9
0.4	0.9786	109.2	0.9718	151.4	0.9761	134.5	0.9889	151.3
0.5	039891	130.3	0.9535	159.3	0.9819	152.4	0.9876	147.2
0.6	0.9888	158.1	0.9437	171.8	0.9651	155.1	0.9530	130.9
0.7	0.9807	170.7	0.9747	203.5	0.9034	171.7	0.9594	143.6
0.8	0.9694	181.2	0.9643	232.7	0.9666	224.3	0.9776	173.7
0.9	0.9781	209.3	0.9344	278.6	0.9415	347.8	0.9998	252.1

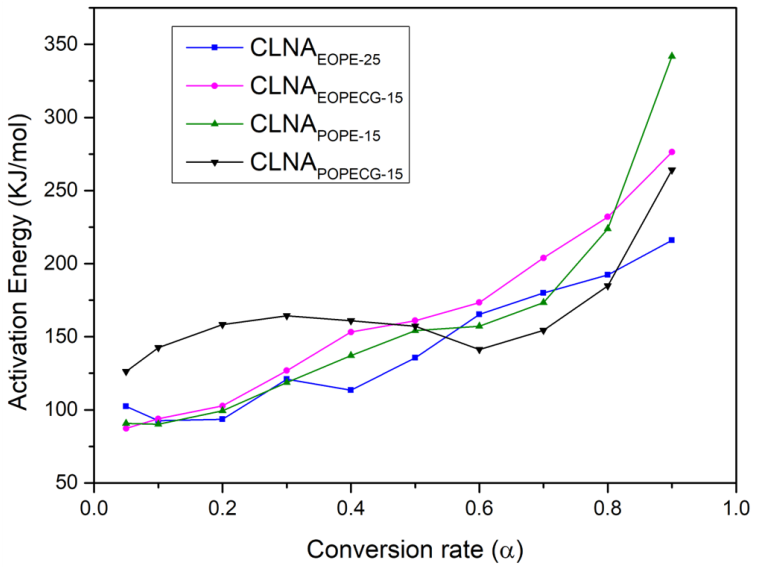

Figure P5.11. E_a vs. α of different CLNAs calculated with OFW method.

As the conversion degree increased, different behaviour was observed in the samples, in this way, the E_a of $CLNA_{EOPE-25}$ decreased at 10% of conversion and increased again until reach a maximum value of 211.0KJ/mol at 90% of conversion. The tendency for the $CLNA_{EOPECG-15}$ as well as for $CLNA_{POPE-15}$ was

to increase with the degree of conversion. Finally, E_a increased in $CLNA_{POPECG-15}$ until it reached a value of 161.0 KJ/mol at 40% of conversion, thereafter it decreased progressively up to 60% of conversion and increased again until it reached a final value of 264.0 KJ/mol. These different behaviours, as well as the differences in E_a with increasing the conversion rate, indicates that the decomposition process throughout the reaction did not follow the same reaction mechanism, as E_a is a function of α. This could be explained by the different nature of the bio-polyols, the different amount of H-bonded urethane and urea groups presented in the samples as well as the interaction of APTMS with them.

Furthermore, as can be seen at 5% degradation the highest E_a values corresponds to the samples with the highest content of H-bonded urea groups ($CLNA_{POPECG-15}$ and $CLNA_{EOPE-25}$), since the stability of the urea groups is greater than that of the urethane groups [36]. Therefore, the greater the urea groups, the greater the stability of the NIPU. On the other hand, comparing $CLNA_{EOPECG-15}$ and $CLNA_{POPE-15}$ samples with similar urea and urethane groups, it was observed that the obtained E_a values were very similar, though slightly lower for $CLNA_{EOPECG-15}$ due to the lower amount of H-bonded groups.

In Table P5.10 the A values calculated with OFW method are summarised. As this factor refers to the availability of chemical groups that would be susceptible to degrade [35], a higher value indicates a higher resistance to degradation.

Table P5.10. A (min^{-1}) of the CLNA samples obtained through OFW method

	A (min^{-1})			
α	$CLNA_{EOPE-15}$	$CLNA_{EOPECG-15}$	$CLNA_{POPE-15}$	$CLNA_{POPECG-15}$
0.05	1.2E+09	3.5E+07	6.2E+07	5.1E+11
0.1	7.7E+07	1.4E+08	4.2E+07	2.8E+12
0.2	3.3E+07	5.4E+08	1.9E+08	2.7E+13
0.3	3.5E+09	3.8E+10	6.2E+09	1.9E+13
0.4	3.8E+08	3.9E+12	1.7E+11	4.1E+12
0.5	6.8E+09	8.9E+12	3.9E+12	1.1E+12
0.6	4.5E+11	2.6E+13	3.9E+12	2.7E+10
0.7	2.0E+12	2.7E+15	3.2E+13	1.2E+11
0.8	5.0E+12	1.4E+17	1.1E+17	1.0E+13
0.9	1.0E+14	3.2E+19	1.2E+25	1.0E+18

As it was expected, the A values followed the same trend as the E_a values. As mentioned above, the pre-exponential factor is used to estimate the lifetime of the polymer through OFW method and is usually carried out at 5% of conversion [37]. Therefore, the polymers with the highest expected lifetime those with the highest A value at a α=5%, i.e., $CLNA_{POPECG-15}$ > $CLNA_{EOPE-25}$ > $CLNA_{POPE-15}$ > $CLNA_{EOPECG-15}$.

The lifetime versus temperature of the formulated CLNAs is represented in Figure P5.12.

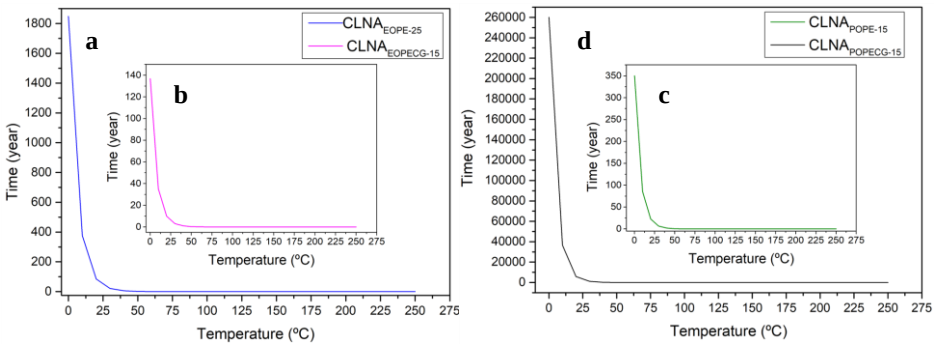

Figure P5.12. Lifetime estimation of a) $CLNA_{EOPE-25}$; b) $CLNA_{EOPECG-15}$; c) $CLNA_{POPE-15}$; d) $CLNA_{POPECG-15}$

Accordingly, with the higher values of A, the lifetime of the polymers was as follows from highest to lowest $CLNA_{POPECG-15}$ > $CLNA_{EOPE-25}$ > $CLNA_{POPE-15}$ > $CLNA_{EOPECG-15}$. In all cases the degradation of the CLNAs increases rapidly with increasing temperature. Thus, above 40ºC the lifetime decreases sharply from years to days in all cases except $CLNA_{POPECG-15}$. However, it should be noted that these results were obtained from degrading the CLNAs in an inert atmosphere (N_2) and that oxidising atmosphere the polymers will degrade differently.

3. CONCLUSIONS

Four different NIPU adhesives were synthesised, characterised, and subjected to adhesion test employing an ABES with poor results between 1.13-1.38 MPa. To improve the adhesion properties, a coupling agent (APTMS) was employed in different amounts and the optimal formulations ($CLNA_{EOPE-25}$, $CLNA_{EOPECG-15}$, $CLNA_{POPE-15}$ and $CLNA_{POPECG-15}$) were selected based on the shear strengths obtained at a pressing time of 120 s. A kinetic degradation study was carried out employing the isoconversional OFW and KAS methods and the E_a, A and half-life of the selected CLNAs were determined. From the obtained E_a values, it was concluded that the degradation mechanisms were different in each sample, leading to the following order of stability of the CLNAs: $CLNA_{POPECG-15}$ > $CLNA_{EOPE-25}$ > $CLNA_{POPE-15}$ > $CLNA_{EOPECG-15}$.

REFERENCES

[1] F. Zhang, X. Wei, Z. Xiao, J. Appl. Polym. Sci. 127(3) (2013) 1730–6. 10.1002/app.37763.

[2] X. Chen, A. Pizzi, E. Fredon, C. Gerardin, X. Zhou, B. Zhang, G. Du, Int. J. Adhes. Adhes. 112(September 2021) (2022) 103001. 10.1016/j.ijadhadh.2021.103001.

[3] J. Saražin, A. Pizzi, S. Amirou, D. Schmiedl, M. Šernek, J. Renew. Mater. 9(5) (2021) 881–907. 10.32604/jrm.2021.015047.

[4] F.J. Santiago-Medina, M.C. Basso, A. Pizzi, L. Delmotte, J. Renew. Mater. 6(4) (2018) 413–25. 10.7569/JRM.2017.634172.

[5] M. Fuensanta, J.M. Martín-Martínez, Polymers (Basel). 13(18) (2021). 10.3390/polym13183097.

[6] F. Ren, R. Zhou, F. Sun, H. Ma, Z. Zhou, W. Xu, RSC Adv. 7(47) (2017) 29779–85. 10.1039/c7ra04454b.

[7] N. Kébir, M. Benoit, C. Legrand, F. Burel, Eur. Polym. J. 96(August) (2017) 87–96. 10.1016/j.eurpolymj.2017.08.046.

[8] I. Yilgör, E. Yilgör, G.L. Wilkes, Polymer (Guildf). 58 (2015) A1–36. 10.1016/j.polymer.2014.12.014.

[9] S. Sakurai, Y. Okamoto, H. Sakaue, T. Nakamura, L. Banda, S. Nomura, J. Polym. Sci. Part B Polym. Phys. 38(13) (2000) 1716–28. 10.1002/1099-0488(20000701)38:13<1716::AID-POLB50>3.0.CO;2-X.

[10] H. Huang, H. Pang, J. Huang, P. Yu, J. Li, M. Lu, B. Liao, Constr. Build. Mater. 284 (2021) 122388. 10.1016/j.conbuildmat.2021.122388.

[11] Z. Shen, L. Zheng, C. Li, G. Liu, Y. Xiao, S. Wu, J. Liu, B. Zhang, Polymer (Guildf). 175(May) (2019) 186–94. 10.1016/j.polymer.2019.05.010.

[12] F. Dong, S. Maganty, S.J. Meschter, J. Cho, Prog. Org. Coatings 114(September 2017) (2018) 58–67. 10.1016/j.porgcoat.2017.09.018.

[13] V. Costa, A. Nohales, P. Félix, C. Guillem, D. Gutiérrez, C.M. Gõmez, J. Appl. Polym. Sci. 132(12) (2015) 1–10. 10.1002/app.41704.

[14] S. Arévalo-Alquichire, M. Morales-Gonzalez, K. Navas-Gómez, L.E. Diaz, J.A. Gómez-Tejedor, M.A. Serrano, M.F. Valero, Polymers (Basel). 12(3) (2020). 10.3390/polym12030666.

[15] S. D'Hollander, C.J. Gommes, R. Mens, P. Adriaensens, B. Goderis, F. Du Prez, J. Mater. Chem. 20(17) (2010) 3475–86. 10.1039/b923734h.

[16] J. Balko, B. Fernández-D'Arlas, E. Pöselt, R. Dabbous, A.J. Müller, T. Thurn-Albrecht, Macromolecules 50(19) (2017) 7672–80. 10.1021/acs.macromol.7b00871.

[17] J. Zhou, H. Li, X. Lu, Polym. Adv. Technol. 29(8) (2018) 2308–16. 10.1002/pat.4342.

[18] S. Abdollahi Baghban, M. Khorasani, G.M.M. Sadeghi, J. Appl. Polym. Sci. 135(46) (2018) 1–13. 10.1002/app.46744.

[19] A. Niemczyk, A. Piegat, Á. Sonseca Olalla, M. El Fray, Eur. Polym. J.

93(May) (2017) 182–91. 10.1016/j.eurpolymj.2017.05.046.

[20] B. Esteves, J. Martins, J. Martins, L. Cruz-Lopes, J. Vicente, I. Domingos, Maderas Cienc. y Tecnol. 17(2) (2015) 277–84. 10.4067/S0718-221X2015005000026.

[21] J.M.M. Ferra, M. Ohlmeyer, A.M. Mendes, M.R.N. Costa, L.H. Carvalho, F.D. Magalhes, Int. J. Adhes. Adhes. 31(3) (2011) 127–34. 10.1016/j.ijadhadh.2010.11.013.

[22] B.M. De Morais Lemos Esteves, L.P.V. Cruz-Lopes, A.P. Fernandes, J.M. Martins, I. De Jesus Domingos, J.V. Ferreira, S.H.F. Da Silva, J. Labidi, Wood Res. 64(1) (2019) 105–16.

[23] B. Arkles, Gelest, Inc. (2014) 1–76.

[24] S. Cichosz, A. Masek, Materials (Basel). 13(13) (2020) 1–19. 10.3390/ma13132901.

[25] A.A. Issa, A.S. Luyt, Polymers (Basel). 11(3) (2019). 10.3390/polym11030537.

[26] M. Baloch, M. Alberro, J. Labidi, Polymers (Basel). 13(4) (2021) 1–15. 10.3390/polym13040643.

[27] J. D'Souza, R. Camargo, N. Yan, J. Appl. Polym. Sci. 131(16) (2014) 1–10. 10.1002/app.40599.

[28] C. Zhang, H. Wu, M.R.K. Kessler, Polymer (Guildf). 69(1) (2015) 52–7. 10.1016/j.polymer.2015.05.046.

[29] P. Cinelli, I. Anguillesi, A. Lazzeri, Eur. Polym. J. 49(6) (2013) 1174–84.

10.1016/j.eurpolymj.2013.04.005.

[30] O.S.H. Santos, M. Coelho da Silva, V.R. Silva, W.N. Mussel, M.I. Yoshida, J. Hazard. Mater. 324 (2017) 406–13. 10.1016/j.jhazmat.2016.11.004.

[31] L.B. Tavares, C. V. Boas, G.R. Schleder, A.M. Nacas, D.S. Rosa, D.J. Santos, Express Polym. Lett. 10(11) (2016) 927–40. 10.3144/EXPRESSPOLYMLETT.2016.86.

[32] S. Thanomchat, K. Srikulkit, Adv. Mater. Sci. Eng. 2015 (2015). 10.1155/2015/741242.

[33] W. Shen, H.P. He, J. Zhu, P. Yuan, R.L. Frost, J. Colloid Interface Sci. 313(1) (2007) 268–73. 10.1016/j.jcis.2007.04.029.

[34] A. Singh, R. Kumar, P.K. Soni, V. Singh, J. Macromol. Sci. Part B Phys. 59(12) (2020) 775–95. 10.1080/00222348.2020.1802850.

[35] N.L. Batista, M.L. Costa, K. Iha, E.C. Botelho, J. Thermoplast. Compos. Mater. 28(2) (2015) 265–74. 10.1177/0892705713484740.

[36] Y. Yang, X. Cao, H. Luo, X. Cai, J. Polym. Res. 25(11) (2018). 10.1007/s10965-018-1634-z.

[37] L. Núñez, F. Fraga, M.R. Núñez, M. Villanueva, J. Appl. Polym. Sci. 78(6) (2000) 1239–44. 10.1002/1097-4628(20001107)78:6<1239::aid-app90>3.0.co;2-x.

4th PART

CONCLUSIONS AND FUTURE WORK

CONCLUSIONS

As a general conclusion, lignin from *Eucalyptus globulus* and *Pinus radiata* can be valorised to synthesise bio-polyols through microwave irradiation technology by using liquefaction reaction with PEG and Gly or CG. Furthermore, the process could be scalable without significant variations in the characteristics of the bio-polyols. The formulated polyurethane adhesives for wood application with isocyanate and without isocyanate showed high shear strength and high stability against degradation. Therefore, it was concluded that the synthesised wood adhesives could be an alternative to be considered in the wood industry.

In addition, the following specific conclusions were obtained for each Publication.

- **Publication I**: It was demonstrated the possibility to valorise the residual aqueous phase produced as residue during the lignin precipitation process to obtain bio-polyols. These bio-polyols exhibited low molecular weights and high I_{OH} values, characteristics that make them suitable for the manufacture of PUs. Nevertheless, due to the low yield obtained, no PUs were synthesised in this work.
- **Publication II**: By means of a Box Behnken experimental design and using the response surface methodology, the reaction conditions to synthesise different types of bio-polyols were optimised. The experimental design was carried out employing microwave radiation technology and showed a good fit achieving determination coefficients (R^2) above 0.97. In addition, the good fit of the model was confirmed by Fisher's F-test. Thus, using the lignins obtained in the ***Publication I***, bio-polyols with the required characteristics to formulate rigid and elastic PUs were obtained.

- **Publication III**: Using the reaction conditions optimised in ***Publication II***, and following the same methodology, it was determined that it is possible to substitute technical grade glycerol with an unrefined crude glycerol from used vegetable cooking oil in the lignin liquefaction process. However, some differences from those obtained in ***Publication II*** were observed, e.g., lower yields and lower I_{OH} due to the lower amount of glycerol in the sample. Nevertheless, despite these differences, the obtained bio-polyols exhibited the required characteristics for PU synthesis.
- **Publication IV**: In this work, a scale-up of the microwave liquefaction reaction was carried out, obtaining bio-polyols with very similar characteristics to those obtained in ***Publications II and III***, demonstrating that the scale-up is possible. Furthermore, the applicability of the bio-polyols by synthesising PU wood adhesives was demonstrated. It was concluded that the best results were obtained with a NCO:OH ratio of 2.5:1. On the other hand, it was found that the nature of the lignin affects the microstructure of the PUs, producing a greater phase separation when using bio-polyols synthesised with lignin from *Eucalyptus globulus*, due to its higher steric hindrance.
- **Publication V**: The synthesis of NIPUs wood adhesives by polycondensation reaction between lignin-based bio-polyols with DMC and HDMA was successful. However, the obtained shear strength values during the ABES test were unsatisfactory. Therefore, a silane-based coupling agent was employed to increase the crosslinking of the polymer and improve the shear strength values.

FUTURE WORKS

Some possible research routes are proposed below that could complement the work presented here.

- Synthesise of polyurethanes using the biopolyols obtained in ***Publication I*.**
- Synthesise of polyurethane foams employing the biopolyols optimised in ***Publication II***.
- A Lyfe Cycle Analysis (LCA) of the routes followed in this work.
- Substitution of the diamine used to produce the NIPUs in ***Publication V*** by a more environmentally friendly compound.

This party is Over

Mace Windu

LIST OF FIGURES & TABLES

FIGURES

Introduction

Figure I.1. a adapted from [19], b and c adapted from [17], d is courtesy of the Scripps Institution of Oceanography, University of California, San Diego [20]

Figure I.2. World virgin plastic production. Includes Thermoplastics, Polyurethanes, Thermosets, Elastomers, Adhesives, Coatings and Sealants and PP-fibers. Not Included PET, PA and Polyacryl-Fibers. Data obtained from [25]

Figure I.3. Plastic Post-Consumer Waste treatment in EU27+3. Adapted from [26]

Figure I.4. Addition reaction between hydroxyl and isocyanate group to form urethane group

Figure I.5. Primary structure of PU

Figure I.6. Secondary structure of PUs formed by HS and SS

Figure I.7. Schematic of the molecular structure of a PU synthesised by the one-shot method

Figure I.8. Scheme of the molecular structure of a PU synthesised by the prepolymer method

Figure I.9. Different synthesis routes to produce NIPUs

Figure I.10. Diagram with the different classification parameters of a biorefinery

Figure I.11. Representation of the structural constituents of the plant cell wall

Figure I.12. Structure of lignin molecule and the aromatics alcohols from which it is synthesised (Adapted from [87])

Figure I.13. Lignin phenolic units

Figure I.14. Liquid biofuels production capacities in Europe between 2000 and 2019. Data obtained from [116]

Figure I.15. Schematic explanation of the experimental procedure carried out

Methodology

Figure M.1. Scheme of the delignification process followed in this thesis

Figure M.2. Diagram for obtaining the bio-polyol in ***Publication I***

Figure M.3. Synthesis of the bio-polyols formulated in ***Publication II and III***

Figure M.4. Schematic diagram of the synthesis of LPA adhesives

Figure M.5. Procedure to synthesise LNA adhesives through polycondensation reaction between lignin-based bio-polyols with DMC and HDMA

Results and discussion

Publication I

Figure P1.1. ATR-FTIR spectra (a) and Fingerprint region of FTIR spectra (b) of EOP and POP

Figure P1.2. GC-MS chromatograms of EOP and POP

Figure P1.3. TGA and DTG thermograms of EOP and POP

Figure P1.4. Molecular weight distribution of EOP and POPE

Figure P1.5. Storage (G') and loss (G'') modulus (Pa) as a function of ω(rad/s) of EOP (a) and POP (b)

Figure P1.6. (a) Viscosity (η) VS shear rate (γ̇) and (b) Shear stress (τ) VS shear rate (γ̇) of EOP and POP

Publication II

Figure P2.1. Molecular weight distribution of organosolv lignins

Figure P2.2. Fingerprint región of ATR-FTIR spectra of non-ultrasonicated and ultrasonicated organosolv lignins

Figure P2.3. Response Surface for MW: *Eucalyptus globulus* (a, b, c); *Pinus radiata* (d, e, f)

Figure P2.4. Response Surface for I_{OH}: *Eucalyptus globulus* (a, b, c); *Pinus radiata* (d, e, f)

Figure P2.5. TGA thermograms and DTG curves of bio-polyols

Figure P2.6. Viscosity (η) VS shear rate ($\dot{\gamma}$) and (b) shear stress (τ) VS shear rate ($\dot{\gamma}$) of bio-polyols at optimum point

Publication III

Figure P3.1. GC-MS chromatogram of CG

Figure P3.2. ATR-FTIR spectra of commercial glycerol and crude glycerol

Figure P3.3. Molecular weight distribution of the liquefied bio-polyols

Figure P3.4. TGA thermograms and DTG curves of liquefied bio-polyols

Figure P3.5. Storage module (G') and loss module (G'') (Pa) as function of ω (rad/s) of bio-polyols

Figure P3.6. (a) Viscosity (η) as a function of shear rate (γ̇); (b) shear stress (τ) as a function of shear rate (γ̇)

Publication IV

Figure P4.1. ATR-FTIR spectra of the LPA formulations at different reaction times and cured. a, b and c are the 2.0, 2.5 and 3.0 LPA_{EOPE} formulations and d, e and f are the LPA_{POPE} equivalents

Figure P4.2. ATR-FTIR spectra in the absorbance region of the carbonyl groups of the different LPAs. a, b and c are the 2.0, 2.5 and 3.0 LPA_{EOPE} formulations and d, e and f are the LPA_{POPE} equivalents

Figure P4.3. Shear strength of lignin-based polyurethane adhesives; (a) LPA_{EOPE}, (b) LPA_{POPE}

Figure P4.4. ATR-FTIR spectra of cured LPAs of LPA_{EOPECG} and LPA_{POPECG} samples

Figure P4.5. ATR-FTIR spectra of the absorbance region of the carbonyl groups of LPA_{EOPECG} (a) and LPA_{POPECG} (b) obtained through a Gaussian curve shape. The obtained R^2 values were above 0.999

Figure P4.6. Shear strength of lignin-based polyurethane adhesives. The red point indicated the substrate failure

Figure P4.7. TGA and DTG curves of the different LPAs

Figure P4.8. TGA curves at the different heating rates for LPA_{EOPE} (a), LPA_{EOPECG} (b), LPA_{POPE} (c) and LPA_{POPECG} (d)

Figure P4.9. (a-d) OFW plots of ln(β) vs. $1000/T_P$ and (e-h) KAS plots of $\ln(\beta/T^2_P)$ vs. $1000/T_P$ for different conversion values. Where LPA_{EOPE} (a-e), LPA_{EOPECG} (b-f), LPA_{POPE} (c-g) and LPA_{POPECG} (d-h)

Figure P4.10. E_a calculated through OFW method vs. α

Figure P4.11. Estimated lifetime of LPA_{EOPE} (a), LPA_{EOPECG} (b), LPA_{POPE} (c) and LPA_{POPECG} (d)

Publication V

Figure P5.1. ATR-FTIR spectra of the different steps of the LNA reaction. a, b, c and d correspond to the LNAs formulated with EOPE, $EOPE_{CG}$, POPE and $POPE_{CG}$ respectively

Figure P5.2. Molecular weight distribution of the synthesised LNAs

Figure P5.3. ATR-FTIR spectra of LNAs cured at different temperatures: a) LNA_{EOPE}; b) LNA_{EOPECG}; c) LNA_{POPE}; d) LNA_{POPECG}

Figure P5.4. ATR-FTIR spectra of the absorbance region of the carbonyl group of the different LNAs cured at 120 °C. a) LNA_{EOPE}; b) LNA_{EOPECG}; c) LNA_{POPE}; d) LNA_{POPECG}

Figure P5.5. Shear strength of LNA adhesives

Figure P5.6. Shear strength of different CLNA. a) $CLNA_{EOPE}$; b) $CLNA_{EOPECG}$; c) $CLNA_{POPE}$; d) $CLNA_{POPECG}$

Figure P5.7. ATR-FTIR spectra of CLNA and LNA samples

Figure P5.8. ATR-FTIR spectra of the absorbance region of the carbonyl group of the different CLNAs cured at 120 °C. a) $CLNA_{EOPE\text{-}25}$; b) $CLNA_{EOPECG\text{-}15}$; c) $CLNA_{POPE\text{-}15}$; d) $CLNA_{POPECG\text{-}15}$

Figure P5.9. TGA and DTG curves of the synthesised CLNAs

Figure P5.10. (a-d) OFW plots of ln(β) vs. $1000/T_P$ and (e-h) KAS plots of $\ln(\beta/T^2_P)$ vs. $1000/T_P$ for different conversion values of $CLNA_{EOPE-25}$ (a-e), $CLNA_{EOPECG-15}$ (b-f), $CLNA_{POPE-15}$ (c-g) and $CLNA_{POPECG-15}$(d-h)

Figure P5.11. E_a vs. α of different CLNAs calculated with OFW method

Figure P5.12. Lifetime estimation of a) $CLNA_{EOPE-25}$; b) $CLNA_{EOPECG-15}$; c) $CLNA_{POPE-15}$; d) $CLNA_{POPECG-15}$

TABLES

Introduction

Table I.1. Main Pu types based on the different existing criteria

Table I.2. Chemical composition of different lignocellulosic biomass types (Adapted from [67]

Table I.3. Percentage (%wt.) of functional groups in lignin [95]

Methodology

Table M.1. Commercial chemical compounds employed in the thesis

Table M.2. Reaction conditions of organosolv delignification processes

Table M.3. Characterisation techniques employed in Publications

Results and discussion

Publication I

Table P1.1. Characterisation of the black liquors

Table P1.2. Identification of the compounds from EOP and POP observed in CG-MS chromatograms

Table P1.3. M_w (g/mol), M_n (g/mol) and PI of EOP and POP

Table P1.4. A_n, I_{OH} and f of EOP and POP

Table P1.5. Power-Law linear functions based on the rheological data from EOP and POP

Publication II

Table P2.1. Experimental design involved in the study

Table P2.2. Mw (g/mol), Mn (g/mol) and PDI of organosolv lignins and ultrasonicated organosolv lignins

Table P2.3. Independent normalised (Norm.) and not normalised (Not norm.) variables, Cat (%wt.) (X_1); Temperature (°C) (X_2) and PEG/Gly (w/w) (X_3), together with the dependent variables, average molecular weight (Y_{Mw}) (g/mol) and hydroxyl number (Y_{IOH}) (mgKOH/g), of the Box-Behnken experimental design

Table P2.4. Regression coefficient plus their statistical parameters

Table P2.5. Not-normalised and normalised values of the optimal points

Table P2.6. Theoretical values of M_w and corrected I_{OH} predicted by the software and experimental values at optimum conditions

Table P2.7. Mn (g/mol), PDI (Mw/Mn), An (mg KOH/g), f and yield (%) of bio-polyols at optimum conditions

Table P2.8. Main degradation stages on TGA-DTG analysis

Table P2.9. Power-Law Linear functions based on the rheological data from bio-polyol samples

Publication III

Table P3.1. Liquefaction reaction conditions optimised in ***Publication II***

Table P3.2. M_W, $I_{OH,}$ A_n, f, Equivalent Weight of polyol (EW) and yield of bio-polyols

Table P3.3. Interval temperature (T_{int}) and maximum degradation temperature (T_m) in °C of degradation stages of the TGA-DTG curves for the analysed bio-polyols

Table P3.4. Power-Law linear functions based on the rheological data obtained from the studied bio-polyols

Table P3.5. Different studies of lignocellulosic biomass and lignin liquefaction employing commercial or crude glycerol

Publication IV

Table P4.1. Liquefaction reaction conditions optimised in ***Publication II***

Table P4.2. Recipe used for the synthesis of LPAs

Table P4.3. Characterisation of bio-polyols employed to synthesise PUs

Table P4.4. ATR-FTIR band assignments of PU spectra synthesised with EOPE and POPE bio-polyols

Table P4.5. Percentages of carbonyl species in cured LPAs

Table P4.6. Relevant parameters estimated for the determination of microphase of different formulations

Table P4.7. Relevant parameters estimated for the determination of microphase separation in GC-formulated LPAs

Table P4.8. Activation energies (E_a) (KJ/mol) and correlation coefficients of the linear regression of the PU samples for the decomposition obtained through the OFW method

Table P4.9. Activation energies (E_a) (KJ/mol) and correlation coefficients of the linear regression of the PU samples for the decomposition obtained through the KAS method

Table P4.10. Preexponential factor (A) of the PU samples for the decomposition obtained through the OFW method

Publication V

Table P5.1. Most relevant parameters of the bio-polyols synthesised in the ***Publication IV***

Table P5.2. Solid content and pH of the different LNA formulation

Table P5.3. Average molecular weight (M_W) (g/mol) of LNAs by retention time (min)

Table P5.4. Percentage of carbonyl and urea species in cured LNAs

Table P5.5. Percentage of carbonyl and urea species in cured LNAs

Table P5.6. Percentage of carbonyl and urea species in cured CLNAs

Table P5.7. Relevant parameters for the determination of microphase separation in CLNAs

Table P5.8. Activation energies (E_a) (KJ/mol) and correlation coefficients of the linear regression of the PU samples for the decomposition obtained through OFW method

Table P5.9 Activation energies (E_a) (KJ/mol) and correlation coefficients of the linear regression of the PU samples for the decomposition obtained through KAS method

Table P5.10. A (min^{-1}) of the CLNA samples obtained through OFW method

APPENDIX II

- Table A.1. Different tests and equipments used for the rheological characterisation of bio-polyols synthesised in ***Publications I, II and III***

APPENDIX

APPENDIX I. Procedure for black liquor characterisation

I. pH determination

The pH of *Eucalyptus globulus* and *Pinus radiata* organosolv black liquors was determined using a digital pH meter "CRISON basic 20" at room temperature. All measurements were carried out in triplicate.

II. Density determination

The density of the black liquors was measured gravimetrically by weighing a known volume of the black liquor. A pre-weighed, moisture-free volumetric flask was employed for this purpose. Triplicate measurements were carried out.

III. Total Dissolved Solids (TDS)

The determination of TDS in organosolv black liquors was performed in accordance with the procedure described in the LAP-012 standard of the National Renewable Energy Laboratory (NREL). This procedure consists of 5.0 ± 0.01 g of the black liquors were weighted in a pre-weighed and moisture-free crucible. Then, the crucibles were introduced into an oven at 105 ± 3 °C for 24 h. Afterwards, the crucibles were cooled in a desiccator and weighed until a constant weight was obtained. Finally, the TDS calculation was carried out using the Equation A.I.1.

$$TDS\ (\%) = \frac{(m_f - m_i)}{m} \times 100 \qquad \text{Equation A.I.1}$$

where m_f is the weight (g) of the crucible with the sample after 24 h in the oven, m_i is the weight of the dry crucible (g) and m is the weight of the initial black liquor sample.

IV. Inorganic and Organic Matter (IM, OM)

The IM of the black liquors was determined using an adapted procedure of the TAPPI T-211 om-93 standard.

The crucible with the dry sample used in to calculate the TDS were burned in an oven at 525 °C for 3h. Then, the crucible was cooled in a desiccator and weighted until constant weight. The IM was determined using the Equation A.I.2.

$$IM\ (\%) = \frac{(m_f - m_i)}{m} \times 100 \qquad \text{Equation A.I.2}$$

where m_f is the weight (g) of the crucible with the burned sample, m_i is the weight of the dry crucible (g) and m is the weight of the initial black liquor sample.

The OM was calculated as the difference between TDS and IM (Equation A.I.3).

$$OM\ (\%) = TDS(\%) - IM(\%) \qquad \text{Equation A.I.3}$$

V. Lignin content

The lignin fraction dissolved in the black liquors was gravimetrically determined.

Firstly, the lignin was precipitated from black liquors and filtered as described in ***section 2.2*** of the ***2nd PART.*** Afterwards, the solid lignin was dried in an oven at 50 ± 2°C. After drying, it was cooled in a desiccator and weighted until the weight was constant. The lignin concentration was determined employing the Equation A.I.4.

$$Lignin\ content\ (\%) = \frac{(m_f - m_i)}{(V \times \rho)} \times 100 \qquad \text{Equation A.I.4}$$

where m_f is the weight (g) of the dried filter with lignin, m_i is the weight of the dry filter (g), V is the liquid volume (mL) and ρ is the density of the liquid fraction (g/mL).

APPENDIX II. Procedure for bio-polyols and polyurethane characterisation

I. Chemical composition

The chemical composition of the bio-polyol which was obtained in ***Publication I*** was determined through Gas chromatography-Mass spectrometry analysis (GC-MS). The sample was dissolved in HPLC grade ethyl acetate in a metric flask. Then, the solution was injected into GC-MS instrument consisting of an Agilent GC (7890A) and a MS (5975C inert MSD with Triple-Axis Detector. The equipped capillary column was a HP-5MS ((5%Phenyl)-methylpolysiloxane, 30m x 0.25mm) and Helium was used as gas carrier. The temperature program started at 50 °C; then, the temperature was increased to 120 °C at 8 °C/min and kept for 5 min. After that, the temperature was raised to 280 °C at 8°C/min, this temperature was held for 10 min, finally the temperature was increased at 10°C/min to the final temperature of 300°C and maintained for 2 min. The calibration was carried out employing pure compounds provided by Sigma-Aldrich, viz. phenol, ortho, meta and para cresol, guaiacol, catechol, 3-methylcatechol, 4-methylcatechol, 4-ethylcatechol, 3-methoxycatechol, syringol, 4-hydroxybenzaldehyde, acetovanillone, veratrole, 4-hydroxybenzoic acid, 4-hydroxy-3-methoxyphenylacetone, vanillin, vanillic acid, syringaldehyde, 3,5-dimethoxy-4-hydroxyacetophenone and syringic acid.

II. Chemical structure

The chemical structure of the bio-polyols obtained in ***Publication I***, as well as the lignin samples of ***Publication II*** and PUs and NIPUs of ***Publications IV and VI***, were analysed through Attenuated Total Reflection-Fourier Transformed Infrared Spectroscopy (ATR-FTIR). A PerkinElmer Spectrum Two FTIR Spectrometer equipped with a Universal Attenuated Total

Reflectance accessory provided with an internal reflection diamond crystal was used. The scans (20) were collected in transmission mode with a resolution of 4 cm^{-1} from 4000-600 cm^{-1}.

Through ATR-FTIR spectra, the degree of separation and miscibility of the micro-phases of PUs were determined. The weight fraction of H-bonded urethane groups (X_{HB}) was determined by the Equation A.II.1.

$$X_{HB} = \frac{A_{Hb}}{K\prime A_{Fc} + A_{Hb}} \qquad \text{Equation A.II.1}$$

Where X_{HB} is the weight fraction of H-bonded urethane and urea groups, A_{Hb} is the absorbance of the H-bonded C=O urethane groups (1708-1704 cm^{-1}, 1697-1694 cm^{-1} and 1688-1686 cm^{-1}) and urea groups (1675-1654 cm^{-1} and 1644-1630 cm^{-1}), A_{Fc} is the absorbance of free urethane C=O groups (1730-1728 cm^{-1}) and the constant value K' which is the extinction coefficient between H-bonded and free urethane C=O.

The maximum mass fraction of the rigid segment mixed in the soft phase (W_H) was estimated using the Equation A.II.2.

$$W_H = \frac{(1 - X_{HB}) \times z}{[(1 - X_{HB}) \times z + (1 - z)]} \qquad \text{Equation A.II.2}$$

Where z is the theoretical Hard Segment (HS_t) fraction which was calculated with the Equation A.II.3.1 for MDI based PUs and Equation A.II.3.2 for NIPUs.

$$HS_t\ \% = \frac{nM_{MDI}}{(n+1)M_{MDI} + \bar{M}_{nPolyol}} \times 100 \qquad \text{Equation A.II.3.1}$$

$$HS_t\ \% = \frac{nM_{DMC} + nM_{HDMA}}{(n+1)M_{DMC+}\ (n+1)M_{HDMA} + \bar{M}_{nPolyol}} \times 100 \qquad \text{Equation A.II.3.2}$$

Where M_{MDI}, M_{DMC} and M_{HDMA} are the molecular weights of the MDI diisocyanate, DMC and HDMA, $M_{nPolyol}$ is the average number molecular weight of the bio-polyol (g/mol) and n is the number of mols.

The weight fraction of the mixed phase (MP_W), the soft segment weight fraction (SS_W) and the hard segment weight fraction (HS_W) was calculated through the Equations A.II.4, A.II.5 and A.II.6.

$$MP_W = z \times W_H \qquad \text{Equation A.II.4}$$

$$SS_w = MP_W + (1 - z) \qquad \text{Equation A.II.5}$$

$$HS_w = 1 - SS_W \qquad \text{Equation A.II.6}$$

III. Molecular weight distribution

The molecular weight distribution of lignin and bio-polyols samples was analysed to determine de molecular weight average (M_w) and molecular number average (M_n) as well as the polydispersity index (PI), expressed as (M_w/M_n), through Gel Permeation Chromatography (GPC). A Jasco chromatograph equipped with a LC Netll/ADC interface, two Varian Polymer Laboratories PolarGel-M (300 mm x 7.5 mm) columns in series, and a RI-2031 Plus refractive index detector was employed. N,N-dimethylformamide (DMF) with 0.1% of lithium bromide was used as mobile phase employing a flow rate of 700 mm^3/min and a temperature of 40 °C. Polystyrene standards, provided by Sigma Aldrich, with molecular weight from 266 to 70000 g/mol were used for the calibration curve.

IV. Elemental analysis

The elemental analysis was carried out employing a Leco TruSpec micro elemental analyser at 1050 °C. Both carrier gas (pure Helium 3X) and test gas

(extra pure Oxygen 4X) were supplied by Nippon Gases. The calibration was performed using Leco Sulfamethazine (C=51.78%; H=5.07%; S=11.5%). Triplicate assays were performed using 2 mg of sample.

V. Hydroxyl number (I_{OH}) and acid number (A_n) determination

The I_{OH} and the A_n, both defined as mg KOH/g of sample, of bio-polyols obtained in ***Publications I, II and III*** were determined using the ASTM D4274 [1] and ASTM D974 [2] standards methods, respectively.

To carry out the measurement of the I_{OH} trough the ASTM D4274 standard method 0.5-1 g of each bio-polyol was dissolved in 25 mL of a phthalation reagent formed by 115g of phthalic anhydride dissolved in 700 mL of pyridine. The solution was heated for 1 h at 115°C under reflux and constant stirring. When the reaction was finished, 50 mL of pyridine was poured through the condenser. Finally, the final solution was back titrated using a 0.5 M NaOH dissolution. The I_{OH} was calculated employing the Equation A.II.7.

$$I_{OH} = \frac{(B-A)\times M \times 56.1}{w} + A_n \qquad \text{Equation A.II.7}$$

Where B and A are the NaOH solution (mL) required for the titration of the blank and bio-polyol solutions, respectively. M is the NaOH molarity; W is the sample (g) and A_n is the acidic number of the sample.

For the determination of the A_n of the samples, 0.4 g of each bio-polyols was dissolved in 50 mL of a dissolution composed by 1,4-dioxane:water (4:1 v/v) and then back titrated with a 0.1 M KOH solution in ethanol. The A_n was determined using the Equation A.II.8.

$$A_n = \frac{(C-B)\times M \times 56.1}{w} \qquad \text{Equation A.II.8}$$

Where C is the volume (mL) which was necessary for the titration of the KOH solution, B is the titration volume (mL) of the blank solution, M is the molarity of KOH dissolution, and w is the weight (g) of the bio-polyol to be analysed.

Due to the dark colour of the lignin derived bio-polyols, it was not possible to perform a classical titration using phenolphthalein as indicator in the titration. Therefore, a potentiometric titration was carried out employing an Automatic 888 titrator (Titrando Metrohm) and Tiamo 2.5 software.

VI. Rheological behaviour

The rheological behaviour of the bio-polyols (***Publications I, II and II***) was studied by both oscillatory and rotational rheological test. The former was carried out to determine the storage modulus (G') and loss modulus (G''), while the latter were used to study the viscosity (η) and shear stress (τ) as a function of the shear rate ($\dot{\gamma}$).

The measurements were carried out using a Haake viscotester IQ (Thermo Fisher Scientific) and a Rhemometric Scientific Advanced Rheometric Expansion System (ARES) as shown in Table A.II.1. Test were performed at room temperature and the geometry used varied depending on the analysed bio-polyol.

Thus, in ***Publication I***, for the measurement of both modulus and viscosity a parallel plate geometry with a diameter of 25 mm and 35 mm was employed respectively. The oscillatory test was carried out using a frequency sweep from 0.1 to 100 rad·s^{-1} at a fixed strain of 10%. For the rotational test a shear rate sweep from 0.02 to 120 s^{-1} was used.

Table A.II.1. Different tests and equipments used for the rheological characterisation of bio-polyols synthesised in ***Publications I, II and III***

	Rheometer			
	ARES		HAAKE	
Publication	Oscillatory	Rotational	Oscillatory	Rotational
I	√	x	x	√
II and III	x	x	√	√

In ***Publications II and III***, both modulus and viscosity determinations were carried out using a coaxial cylinders geometry (CC 25 DIN/Ti adapter) with a piston radius of 12.54mm and a ring gap of 1 mm. In both cases the conditions employed in ***Publication I*** were used.

The rotational test parameters were adjusted to the Power-Law equation (Equation A.II.9).

$$\tau = \kappa \cdot \dot{\gamma}^{n} \qquad \text{Equation A.II.9}$$

Where both n and κ are adjustment parameters which depend on the nature of the fluid and the measurement conditions and have been called consistency index (κ) and flow index (n). The former is related to the apparent viscosity of the fluid at a shear rate of $1s^{-1}$, presenting higher values as the viscosity of the sample increased [3], whereas the latter indicates the fluid's behaviour. Thus, the fluid is Newtonian if n=1, pseudoplastic when n<1 and dilatant for n>1.

VII. Thermogravimetric analysis (TGA)

Thermogravimetric analysis of bio-polyols (***Publications I, II and III***), and PU and NIPUs (***Publications IV and V***) was performed employing a TGA/SDTA RSI analyser 851 (Mettler Toledo). For the analysis of the samples

3-5 mg of bio-polyols were heated, under N_2 atmosphere (10 mL· min^{-1}), from 25 °C to 800 °C using a heating rate of 10 °C·min^{-1}.

VIII. Thermal degradation kinetic and lifetime estimation

To obtain the thermal degradation kinetic as well as the lifetime estimation of the PUs and NIPUs of ***Publications IV and V***, the same TGA and procedure described in the previous point was employed. However, in this case, four different heating rates were used (1, 2, 5 and 10 °C·min^{-1}). For the determination of the activation energy (E_a) two different methods were selected, namely, Ozawa-Flynn-Wall [4] (Equation A.II.10) and Kissinger-Akahira-Sunose [5] (Equation A.II.11).

Where β is the heating rate, T_p is the peak exothermic temperature at a certain heating rate. E_a is the activation energy, A is the pre-exponential factor, R is the universal gas constant and $f(\alpha)$ is a function determined by the mechanism.

$$\ln(\beta) = ln\left(\frac{AE_a}{Rf(\alpha)}\right) - 5.331 - 1.052\frac{E_a}{RT_p} \qquad \text{Equation A.II.10}$$

$$\ln\left(\frac{\beta}{T_p^2}\right) = ln\left(\frac{AR}{E_a}\right) - \frac{E_a}{RT_p} \qquad \text{Equation A.II.11}$$

In both cases, the activation energy (E_a) and the preexponential factor (A)can be obtained from the slop and the intercept of the plots of $\ln(\beta)$ and $\ln\left(\frac{\beta}{T_p^2}\right)$ versus $1/T_p$.

The lifetime estimation of PUs and NIPUs were determined using the Ozawa's method and was calculated using the Equation A.II.12.

$$\ln t = \frac{E}{RT} + \ln\left[-\frac{\ln(1-\alpha)}{A}\right] \qquad \text{Equation A.II.12}$$

IX. Adhesion test of PUs and NIPUs with ABES

The adhesion test of PU and NIPU adhesives (***Publication IV and V***) was assessed using an automated bonding evaluation system (ABES, Crovallis, OR, USA) at the Department of Wood Engineering, Polytechnic Institute of Viseu. Tests were carried out with beech (*Fagus sylvatica)* veneer strip with dimensions of 117 mm x 20 mm and 0.5mm thickness. 10 mg of the adhesive was applied and distributed over 5 mm of the edge of the beech veneer to cover a bonding area of 100 mm^2. Then, the wood strip with adhesive and one without adhesive were placed in the ABES and tested at different pressing times at 120 °C.

REFERENCES

[1] S.T. Methods, Test 08(Reapproved 2010) (2000) 3–6. 10.1520/D4671-05.2.

[2] ASTM, i (2013) 1–7. 10.1520/D0974-12.2.

[3] D. Chimene, C.W. Peak, J.L. Gentry, J.K. Carrow, L.M. Cross, E. Mondragon, G.B. Cardoso, R. Kaunas, A.K. Gaharwar, ACS Appl. Mater. Interfaces 10(12) (2018) 9957–68. 10.1021/acsami.7b19808.

[4] T. Ozawa, Bull. Chem. Soc. Jpn. 38(11) (1695) 1881–6. 10.1246/bcsj.38.1881.

[5] S. Vyazovkin, Molecules 25(12) (2020). 10.3390/molecules25122813.

APPENDIX III. Publications & Conferences

Contributions included in this thesis

The following publications are directly related to the thesis presented here.

Publication 0:

Book chapter.

Biorefinery: A Sustainable Approach for the Production of Biomaterials, Biochemicals and Biofuels. **(Under edition)**

Title: Current Approaches for Polyurethane Production from Lignin.

Authors: **Fabio Hernández-Ramos**, Pedro L. de Hoyos-Martínez, Sebastián Barriga, Xabier Erdocia and Jalel Labidi

Publication I:

Paper in Scientific Journal.

Renewable Biopolyol from Residual Aqueous Phase Resulting after Lignin Precipitation **(Published)**

Journal: ACS Sustainable Chemistry & Engineering. https://dx.doi.org/10.1021/acssuschemeng.0c09357

Authors: Fabio Hernández-Ramos, María González Alriols, Tamara Calvo-Correas, Jalel Labidi and Xabier Erdocia.

Publication II:

Paper in Scientific Journal.

Organosolv lignin-based bio-polyols for polyurethane production: Process optimisation through response surface methodology. **(Under revision)**

Appendix III

Journal: Industrial Crops & Products.

Authors: **Fabio Hernández-Ramos**, Vincent Novi, María González Alriols, Jalel Labidi and Xabier Erdocia

Publication III:

Paper in Scientific Journal.

Valorisation of crude glycerol in the production of liquefied lignin bio-polyols for polyurethane formulations. **(In process)**

Authors: **Fabio Hernández-Ramos**, María González Alriols, M. Mirari Antxustegi, Jalel Labidi and Xabier Erdocia

Publication IV:

Paper in Scientific Journal.

Synthesis, characterisation, and thermal degradation kinetic of lignin-based polyurethane wood adhesives. **(In process)**

Authors: **Fabio Hernández-Ramos**, Jalel Labidi, Xabier Erdocia and Bruno Esteves

Publication V:

Paper in Scientific Journal.

Lignin-based non isocyanate polyurethane adhesives. Synthesis and determination of adhesion properties and thermal degradation kinetic. **(In process)**

Authors: Fabio Hernández-Ramos, Jalel Labidi, Xabier Erdocia and Bruno Esteves

Contributions not included in this thesis

During this thesis different book chapters as well as scientific publications not directly related to the work presented here have been collaborated on.

Book Chapters:

Erdocia, X., **Hernández-Ramos, F.**, Morales, A., Labidi, J., 2021. Lignin depolymerization for monomers production by sustainable processes, Micro and Nanolignin in Aqueous Dispersions and Polymers: Interactions, Properties, and Applications. https://doi.org/10.1016/B978-0-12-823702-1.00005-0

Erdocia, X., **Hernández-ramos, F.**, Morales, A., Izaguirre, N., Hoyos-martínez, P.L. De, Labidi, J., 2021. Lignin extraction and isolation methods, in: Lignin-Based Materials for Biomedical Applications. Elsevier Inc., pp. 61–104. https://doi.org/10.1016/c2019-0-01345-3

Fernández-Rodríguez, J., Erdocia, X., **Hernández-Ramos, F.**, Alriols, M.G., Labidi, J., 2019. Lignin Separation and Fractionation by Ultrafiltration, in: Separation of Functional Molecules in Food by Membrane Technology. pp. 229–265. https://doi.org/10.1016/b978-0-12-815056-6.00007-3

Fernández-Rodríguez, J., Alriols, M.G., **Ramos, F.H.**, Labidi, J., 2018. Energetic assessment of lignin extraction processes by simulation, Computer Aided Chemical Engineering. Elsevier Masson SAS. https://doi.org/10.1016/B978-0-444-64235-6.50268-0

Appendix III

Scientific Journals:

Gómez-Cruz, I., Romero, I., Contreras, M. del M., Labidi, J., **Hernández-Ramos, F.**, Roseiro, L.B., Duarte, L.C., Castro, E., Carvalheiro, F., 2022. Combined Extraction and Ethanol Organosolv Fractionation of Exhausted Olive Pomace for Bioactive Compounds. Adv. Sustain. Syst. 6. https://doi.org/10.1002/adsu.202100361

Egüés, I., **Hernandez-Ramos, F.**, Rivilla, I., Labidi, J., 2021. Optimization of ultrasound assisted extraction of bioactive compounds from apple pomace. Molecules 26. https://doi.org/10.3390/molecules26133783

Fernández-Marín, R., **Hernández-Ramos, F.**, Salaberria, A.M., Andrés, M.Á., Labidi, J., Fernandes, S.C.M., 2021. Eco-friendly isolation and characterization of nanochitin from different origins by microwave irradiation: Optimization using response surface methodology. Int. J. Biol. Macromol. 186, 218–226. https://doi.org/10.1016/j.ijbiomac.2021.07.048

Rajhi, I., **Hernandez-Ramos, F.**, Abderrabba, M., Dhia, M.T. Ben, Ayadi, S., Labidi, J., 2021. Antioxidant, antifungal and phytochemical investigations of capparis spinosa L. Agric. 11. https://doi.org/10.3390/agriculture11101025

Sillero, L., Morales, A., Fernández-Marín, R., **Hernández-Ramos, F.**, Davila, I., Erdocia, X., Labidi, J., 2021. Study of different extraction methods of bioactive molecules from different tree species. Chem. Eng. Trans. 86, 31–36. https://doi.org/10.3303/CET2186006

Sillero, L., Morales, A., Fernández-Marín, R., **Hernández-Ramos, F.**, Dávila, I., Erdocia, X., Labidi, J., 2021. Life Cycle Assessment of various biorefinery approaches for the valorisation of almond shells. Sustain. Prod. Consum. 28, 749–759. https://doi.org/10.1016/j.spc.2021.07.004

Fernández-Rodríguez, J., Erdocia, X., **Hernández-Ramos, F.**, Gordobil, O., González Alriols, M., Labidi, J., 2020. Direct lignin depolymerization process from sulfur-free black liquors. Fuel Process. Technol. 197, 106201. https://doi.org/10.1016/j.fuproc.2019.106201

Hernández-Ramos, F., Fernández-Rodríguez, J., Alriols, M.G., Labidi, J., Erdocia, X., 2020. Study of a renewable capping agent addition in lignin base catalyzed depolymerization process. Fuel 280, 118524. https://doi.org/10.1016/j.fuel.2020.118524

Morales, A., **Hernández-Ramos, F.**, Sillero, L., Fernández-Marín, R., Dávila, I., Gullón, P., Erdocia, X., Labidi, J., 2020. Multiproduct biorefinery based on almond shells: Impact of the delignification stage on the manufacture of valuable products. Bioresour. Technol. 315. https://doi.org/10.1016/j.biortech.2020.123896

Sepperer, T., **Hernandez-Ramos, F.**, Labidi, J., Oostingh, G.J., Bogner, B., Petutschnigg, A., Tondi, G., 2019. Purification of industrial tannin extract through simple solid-liquid extractions. Ind. Crops Prod. 139, 111502. https://doi.org/10.1016/j.indcrop.2019.111502

Hernandez, F., Erdocia, X., Labidi, J., 2018. Phenolic monomers production by the direct depolymerization of lignin contained in Kraft black liquor in the presence of metal catalyst. Chem. Eng. Trans. 70, 1597–1602. https://doi.org/10.3303/CET1870267

Appendix III

Contributions to conferences

BIOPOL 2022 (14th to 16th November, Alicante - Spain): **Fabio Hernández-Ramos**, María González Alriols, Jalel Labidi, Xabier Erdocia; *Lignin Based Polyurethane* adhesives (Oral comunication)

SUSTENG 2022 (31st Aug – 4th Sep 2022, Rethymno, Crete, Greece): **F. Hernández-Ramos**, M. Gonzalez Alriols, J. Labidi, X. Erdocia; *Valorisation of crude glycerol in the production of liquefied lignin biopolyols* (Oral comunication)

MZT 2021 (November 29-30, Bilbao – Spain): **F. Hernández-Ramos**, L. Sillero, A. Morales, R. Fernández-Marín, I. Dávila, X. Erdocia: *Euskal baso eta nekazaritza industrietatik eratorritako biomasaren prozesaketa goi-mailako bio-findegi batean* (Oral comunication)

BIORESTEC 2021 (May 17-19, Garda – Italy): **Fabio Hernández-Ramos**, María González Alriols, Jalel Labidi, Xabier Erdocia; *Polyol from residual aqueous phase resulting after the precipitation of lignin* (Poster)

PRES 2018 (25-29 Aug, Prague, Czech Republic): **F. Hernández**, X. Erdocia, J. Labidi; *Phenolic monomers production by the direct depolymerization of lignin contained in Kraft black liquor in the presence of metal catalyst* (Poster)

I must not fear. Fear is the mind-killer. Fear is the little-death that brings total obliteration. I will face my fear. I will permit it to pass over me and through me. And when it has gone past I will turn the inner eye to see its path. Where the fear has gone there will be nothing. Only I will remain.

Litany of Bene Gesserit against fear

Frank Herbert, Dune

Due to a more environmentally conscious society and increasingly restrictive laws, biomass valorisation is a promising alternative to produce biofuels and chemicals which are historically derived from the petrochemical industry. Among the different types of biomass that are available, lignocellulosic biomass is the most attractive one as it is considered as an abundant, cheap and environmentally friendly resource.

Among the different components of lignocellulosic biomass, lignin is, due to its phenolic nature and its high functionality, an ideal candidate for the development of biofuels and biobased chemicals and materials. Moreover, lignin is an available and cheap product, as it is generated as a byproduct from pulp & paper industry. Some of the materials that can be synthesised from lignin include plastics, membranes, hydrogels, polyols and polyurethanes.

eman ta zabal zazu

Universidad del País Vasco

Euskal Herriko Unibertsitatea

This thesis has been carried out with the financial support from the Spanish Government and Basque Government

BioRP

Biorefinery Processes Research Group